Pattern analysis, dimensionality reduction and hypothesis testing in high-dimensional data from animal studies with small sample sizes

Dissertation
zur Erlangung des Grades
Doktor der Naturwissenschaften

Am Fachbereich Biologie
der Johannes Gutenberg-Universität Mainz

Hristo Todorov
geb. am 24.05.1990 in Sliven, Bulgarien

Mainz, 2020

Table of contents

Abstract

Experimental animal studies are typically associated with small sample sizes due to ethical and practical limitations. However, such research projects often generate high-dimensional data sets where the number of response variables is much greater than the number of observations. This leads to several challenges with respect to the choice of an appropriate statistical method.

The current research project focused on exploratory and inferential analysis of multidimensional data sets from animal experiments with small group sizes. A systematic comparison of univariate and multivariate hypothesis testing methods using Monte Carlo simulations revealed that multivariate techniques offer no real benefit in terms of power compared to univariate statistics. The well-known dimensionality reduction technique, principal component analysis (PCA) was demonstrated to capture dominant patterns in transcriptomic data successfully. However, PCA was outperformed by ordination methods which take group assignment into account in terms of sensitivity to detect treatment effects using simulated data. In contrast, multicollinearity combined with small sample sizes was associated with high false positive rate when not handled correctly by the multivariate statistical method. Additionally, microbiome studies based on amplicon sequencing of the 16S rRNA gene were presented as a special case requiring more flexible ordination and hypothesis testing techniques.

Taken together, this thesis demonstrates that harnessing the full potential of multidimensional data is a challenging task which requires applying appropriate statistical methods. A profound understanding of the strengths and limitations of the alternative strategies is necessary in order to model the complex nature of multivariate data and in turn draw correct inferences.

Zusammenfassung

Tierversuche sind aufgrund ethischer und praktischer Einschränkungen typischerweise mit kleinen Strichprobengrößen verbunden. Solche Forschungsprojekte erzeugen jedoch oft hochdimensionale Datensätze, bei denen die Anzahl der abhängigen Variablen um einiges größer ist als die Anzahl der Beobachtungen. Dies führt zu erheblichen Herausforderungen bei der Wahl einer geeigneten statistischen Methode.

Die vorliegende Forschungsarbeit beschäftigte sich mit der explorativen und inferentiellen Analyse mehrdimensionaler Datensätze aus Tierversuchen mit kleinen Stichproben. Ein systematischer Vergleich von univariaten und multivariaten statistischen Methoden mit Hilfe von Monte-Carlo-Simulationen ergab, dass multivariate Techniken im Vergleich zu univariaten Statistiken keinen nützlichen Vorteil in Bezug auf die Teststärke bieten. Die Hauptkomponentenanalyse (PCA), die eine gängige Methode der Dimensionsreduktion ist, konnte dominante Muster in transkriptomischen Daten erfolgreich erfassen. Jedoch wiesen Ordinationsverfahren, die die Gruppenzuordnung berücksichtigen, eine höhere Sensitivität bei der Detektion von Behandlungseffekten unter Verwendung simulierter Daten auf. Im Gegensatz dazu führte Multikollinearität in Kombination mit kleinen Stichprobengrößen zu einer hohen Falsch-Positiv-Rate, wenn sie von der multivariaten statistischen Methode nicht korrekt berücksichtigt wurde. Zusätzlich wurden Mikrobiomstudien, die auf der Sequenzierung des 16S-rRNA-Gens basieren, als Sonderfall vorgestellt, bei der flexiblere Methoden zur Dimensionsreduktion und zum Testen von statistischen Hypothesen angewendet werden müssen.

Zusammengenommen zeigt die vorliegende Forschungsarbeit, dass die Nutzung des vollen Potenzials mehrdimensionaler Datensätze eine herausfordernde Aufgabe ist, die die Anwendung geeigneter statistischer Methoden erfordert. Ein tiefgreifendes Verständnis der Stärken und Grenzen der alternativen Strategien ist notwendig, um die Komplexität multivariater Daten zu modellieren und wiederum korrekte Schlussfolgerungen zu ziehen.

Introduction

Animal experiments usually recruit a limited number of subjects due to ethical considerations and practical limitations. In contrast, the number of endpoints which are analyzed often exceeds the number of observations by several orders of magnitude, which is especially true in the analysis of omics data [Manzoni et al., 2016]. Each variable produces its own dimension which results in high-dimensional data sets which follow complex correlation structures. Due to this multivariate nature of the data, different statistical testing methods can be employed for the analysis of the response variables. One option is to perform a series of univariate tests, which requires adjustments to the p-values due to multiple testing [Bender and Lange, 2001, Chen et al., 2017]. The other option is to use multivariate hypothesis testing methods, which are able to account for the correlation in the data and control for the family wise error rate by reducing the number of tests [Tabachnik and Fidell, 2014]. Since animal studies are often underpowered due to small sample sizes [Button et al., 2013, Sena et al., 2010], it is of great relevance to investigate if univariate or multivariate methods offer an advantage in terms of power to detect group differences.

In this line of thought, some fields of research such as neurotrauma have already proposed applying multivariate statistics to create composite outcome measures which can then be used for hypothesis testing (e.g. [Ferguson et al., 2011, Nielson et al., 2015, Ferguson et al., 2013]). However, it is important to systematically investigate how multivariate statistics perform in terms of type I and type II error rates compared to univariate methods. This can be achieved through simulation studies which can formally evaluate if the statistical method correctly retains or rejects a null or an alternative hypothesis.

Prior to formal hypothesis testing, however, it is often crucial to obtain a better understanding of general patterns of the data and identify important features. Exploratory analysis of high-dimensional data sets requires multivariate statistical techniques that are able to capture relevant patterns in the data and adequately represent them in reduced Euclidean space using 2- or 3-dimensional diagrams. This process is referred to as dimensionality reduction or ordination in reduced space

[Borcard et al., 2011, Legendre and Legendre, 2003]. In very general terms, ordination methods are based on the extraction of eigenvectors of an association matrix. These eigenvectors serve as axes of a new co-ordinate system onto which the data points are projected in reduced space. A successful ordination procedure accounts for a large proportion of the dispersion in the data. Additionally, it preserves the distance relationship between the objects to a high degree such that objects that are close to each other in the original hyper-ellipsoid also appear close to each other in the ordination diagram [Legendre and Legendre, 2003].

Principal component analysis (PCA) represents the best-known and most widely applied dimensionality reduction technique [Ringnér, 2008]. The method is based on spectral decomposition of a covariance or correlation matrix by simultaneously preserving the Euclidean distance between the data points. PCA can be applied to most quantitative or semi-quantitative variables, however, in certain cases, Euclidean distance is not the optimal strategy for describing the relationship between the objects of interest. Alternative ordination techniques can handle different distance or dissimilarity measures. For instance, principal coordinate analysis (PCoA), which is also known as classical multidimensional scaling (MDS), can be applied with any distance/dissimilarity matrix. Non-metric multidimensional scaling (NMDS) is a non-parametric method based on ranks obtained from any distance measure. Another example is correspondence analysis (CA), which preserves the χ^2-distance between the input objects.

Ordination techniques can be divided into two groups - unconstrained and constrained (canonical) - depending on how they handle labeling of the input data. Unconstrained methods are directly applied on the data matrix without considering external information such as group assignment. Association to grouping factors can be investigated descriptively once the ordination has been performed. In contrast, constrained methods relate a matrix of dependent variables Y to a matrix of explanatory variables X. For instance, redundancy analysis (RDA) [Legendre and Legendre, 2003] and canonical correspondence analysis (CCA) [Braak, 1986] are the constrained versions of PCA and CA, respectively. These dimensionality reduction techniques first use regression to produce a set of fitted values $\hat{y}$ for the response variables. The fitted values are then used in the ordination procedure. This also allows formally testing the hypothesis if the explanatory variables significantly impact the ordination. Discriminant analysis (DA) is a conceptually different constrained ordination method that treats the labeling of the data as the dependent variable and a set of quantitative measures as the explanatory variables. While DA can in fact be used for dimensionality reduction and ordination, the goal is often actually to classify new observations to a certain group by training a model on existing data. Alternative versions of DA include linear

discriminant analysis (LDA) and partial least squares discriminant analysis (PLS-DA). PLS-DA is also referred to as projection to latent structures discriminant analysis.
An overview of different unconstrained and constrained methods and the distance or dissimilarity measure they are based on is presented in Table 1.1. A comprehensive review of dimensionality reduction techniques and their application to omics data is provided by Meng et al. [2016].

Table 1.1: **Overview of unconstrained and constrained ordination techniques and the respective distance measures they preserve**

Unconstrained method	**Distance preserved**	**Constrained method**
Principal component analysis (PCA)	Euclidean distance	Redundancy analysis (RDA)
Principal coordinate analysis (PCoA) / Multidimensional scaling (MDS)	Any distance / dissimilarity	Canonical analysis of principal coordinates (CAP) / Distance-based redundancy analysis (dbRDA)
Correspondence analysis (CA)	χ^2-distance	Canonical correspondence analysis (CCA)
Detrended correspondence analysis (DCA)	χ^2-distance	Detrended canonical correspondence analysis (DCCA)
Non-metric multidimensional scaling (NMDS)	Any distance / dissimilarity	
	Diversity indices	Double principal coordinate analysis (DPCoA)
	Mahalanobis distance	Linear discriminant analysis (LDA)
	Mahalanobis distance	Partial least squares discriminant analysis (PLS-DA)

Microbiome studies as a special case for ordination and dimensionality reduction

Recently, studying the composition of intestinal bacteria has gained tremendous popularity as there have been multiple reports of associations between impairments in gut microbiome homeostasis and diseases such as obesity and type II diabetes [Cani et al., 2008, Turnbaugh et al., 2006, Cani et al., 2009], inflammatory bowel disease [Henke et al., 2019, Joossens et al., Hall et al., 2017], but also cognitive impairments [Buffington et al., 2016, Unger et al., 2016, Vogt et al., 2017, Zhuang et al., 2018]. Usually, amplicon sequencing of the 16S rRNA marker gene is employed to study the bacterial composition of biological samples under different experimental conditions [Morgan and Huttenhower, 2012]. The downstream analysis, i.e. the annotation of the findings and the investigation of the biological relevance, is based on matrices containing the absolute abundance of bacterial taxonomic units. These data present an interesting case with respect to ordination and dimensionality reduction since bacterial abundance matrices are sparse, meaning that they contain a great number of zeros [Paulson et al., 2013]. The absence of a bacterial taxonomic unit might be either due to a true biological or experimental effect or a consequence of methodological issues such as under-sampling or low sequencing depth. Incorrect handling of zero entries in the abundance matrix will very likely lead to spurious conclusions. For instance, two samples might appear more similar to each other simply because they have a lot of zero entries in the abundance matrix if the Euclidean distance is applied in an ordination procedure [Legendre and Legendre, 2003, Borcard et al., 2011]. Furthermore, the Euclidean distance gives a stronger weight to more abundant bacteria due to the squared term. Many ecologically more meaningful distance or dissimilarity measures exist. Ordination methods which can handle this broader range of distance or dissimilarity indices and should therefore be applied in microbiome studies include PCoA/MDS and its canonical equivalents constrained analysis of principal coordinates (CAP) and distance based RDA (dbRDA); CA and its canonical version CCA; NMDS and double PCoA [Pavoine et al., 2004].

Aims and structure of the thesis

The current cumulative thesis had three major aims which are addressed in the respective publications as detailed below:

- The first aim of the thesis was to provide a user-fIriendly and comprehensive overview of the theoretical aspects of PCA, which is the most widely used dimensionality reduction technique. This aim is addressed in the publication

presented in section 2.1. Apart from elaborating on the mathematical procedure of calculating the principal components, this publication also details the statistical application and interpretation of PCA. In particular, an applied example using transcriptomic data demonstrates how this ordination technique can be employed to detect gene expression patterns and how they are associated with experimental factors.

- The second aim of the thesis was to investigate if multivariate statistical techniques might offer an advantage over univariate techniques for detecting treatment effects in controlled animal studies with small samples. This aim is addressed in the publication presented in section 2.2. The power and type I error rate of alternative multivariate and univariate hypothesis testing methods were evaluated using Monte Carlo simulations by manipulating the sample and effect size as well as the distribution and variance of the response variables. Additionally, the sensitivity and specificity of the dimensionality reduction techniques PCA, RDA, PLS-DA and LDA to detect treatment effect patterns without formal hypothesis testing were compared. The simulations were based on a real traumatic brain injury study in rats in order to closely mimic realistic experimental conditions.

- The final and major aim of the thesis was to provide practical examples of applying ordination techniques and statistical testing methods in the special case of microbiome studies using 16S rRNA sequencing data. This aim is addressed in the publications included in sections 2.3 and 2.4. The first publication examined the impact of α-linolenic acid (ALA)-rich diet on the composition of small intestinal microbiota in mice. The second publication focused on the chronic and acute effects of amyloid-β exposure on commensal bacteria in wild type or Alzheimer's disease model mice (5xFAD). Canonical ordination techniques using distance/similarity measures appropriate for ecological data were employed to investigate the β-diversity between different experimental groups. Permutation-based analysis of variance was then applied to test if the experimental conditions significantly impacted microbiota composition. The challenging issue of testing differential abundance of individual bacterial taxonomic units was tackled by calculating log2-fold changes of bacterial abundance assuming a negative binomial distribution. To this end, the statistical procedure implemented by the DESeq2 R package was applied.

Publications

2.1 Principal components analysis: theory and application to gene expression data analysis

Authors: **Hristo Todorov**; David Fournier; Susanne Gerber.
This article is published in *Genomics and Computational Biology*, [S.l.], v. 4, n. 2, p. e100041, jan. 2018. ISSN 2365-7154.
doi: https://doi.org/10.18547/gcb.2018.vol4.iss2.e100041.

My contributions to this article are listed in section 4.2 Contributions to individual publications.

Review

Principal Components Analysis: Theory and Application to Gene Expression Data Analysis

Hristo Todorov[1,2], David Fournier[1], Susanne Gerber[1,*],

[1]Computational Systems Genetics, Faculty of Biology, Institute for Developmental Biology and Neurobiology (IDN) and Center for Computational Sciences in Mainz, Johannes Gutenberg-University Mainz, 55128, Germany
[2]Fresenius Kabi Deutschland GmbH, Else-Kröner-Str. 1, 61352, Bad Homburg, Germany

*Correspondence: Staudinger Weg 9, Mainz, 55128, Germany; sugerber@uni-mainz.de

Received 2017-10-27; Accepted 2018-01-12

ABSTRACT

Advances in computational power have enabled research to generate significant amounts of data related to complex biological problems. Consequently, applying appropriate data analysis techniques has become paramount to tackle this complexity. However, theoretical understanding of statistical methods is necessary to ensure that the correct method is used and that sound inferences are made based on the analysis. In this article, we elaborate on the theory behind principal components analysis (PCA), which has become a favoured multivariate statistical tool in the field of omics-data analysis. We discuss the necessary prerequisites and steps to produce statistically valid results and provide guidelines for interpreting the output. Using PCA on gene expression data from a mouse experiment, we demonstrate that the main distinctive pattern in the data is associated with the transgenic mouse line and is not related to the mouse gender. A weaker association of the pattern with the genotype was also identified.

KEYWORDS

Principal components analysis; gene expression; exploratory data analysis

INTRODUCTION

Research in the field of computational biology often requires measuring a huge number of variables simultaneously. This makes exploratory data analysis challenging since visualization techniques are optimal only in two- or three-dimensional space. On the other hand, if variables are analyzed individually, important associations may be ignored or some calculations may be redundant due to overlapping variance [1].

Principal components analysis (PCA) is a statistical technique applied to complex data sets aiming at reducing the dimensionality of the data while simultaneously retaining the maximum amount of variance. Dimensionality reduction is achieved by creating a set of new variables called principal components (PC) which are linear combinations of the original variables. Usually, a small number of components are sufficient to capture most of the variability of the data set. Exploratory data analysis can then be applied to a subset of principal components rather than analyzing the larger number of initial variables. Herewith, the complexity of the analysis can be reduced.

Furthermore, PCA can be applied to investigating the relationship among the original variables. Principal components identify subsets of variables which are correlated with each other, thereby possibly uncovering meaningful patterns in the original data. Such patterns might easily be overlooked if multivariate techniques are not used, since a large number of variables usually prohibits the systematic investigation of all possible pairwise interactions or interactions of higher order, respectively. PCA may also facilitate uncovering underlying processes in the data set. In this context, principal components can be perceived as latent variables which cannot be directly measured. Latent processes are considered to be responsible for the correlations between the observed variables [1].

BASIC PRINCIPLES OF PCA

The input for PCA is a data matrix **X**, in which the columns represent different variables and the rows correspond to values measured on the variables. For simplicity, consider the example in Table 1 which includes measurements on two variables. 100 data points (corresponding to different individuals) for each of the variables were generated using a bivariate normal distribution with a mean of 30 and 15, respectively, variances 10 and 2, respectively, and a Pearson correlation coefficient equal to 0.67 using the *mvrnorm()* R function. The maximal number of components in PCA is equal to the number of variables or the number of observations, whichever is smaller. Therefore, a maximum of two components can be extracted using the data in Table 1. The principal components are linear combinations of the original variables, i.e. a weighted sum of the input variables:

$$PC1 = w_{1,1}Var1 + w_{1,2}Var2$$
$$PC2 = w_{2,1}Var1 + w_{2,2}Var2$$

where $\mathbf{w_{i,j}}$ is a weighting coefficient. Importantly, the first principal component (PC1) points in the direction of the largest variance in the data set (Figure 1a). PC2 is orthogonal to PC1 and shows the direction of the

Subject	Var1	Var2
1	35.19	16.45
2	26.83	13.89
3	32.79	16.2
4	30.82	15.15
5	25.96	13.42
6	28.09	15.5
7	28.86	13.51
8	30.06	12.51
9	29.31	13.62
10	34.2	15.16

Table 1: Simulated data set including two variables. 100 data points were sampled from a random bivariate normal distribution with means 30 and 15, variances 10 and 2 and a Pearson correlation coefficient equal to 0.67 for var1 and var2 with the help of the *mvrnorm()* R function. Scores for 10 random subjects are shown.

second greatest variance, and so forth, until the maximal number of components is reached. As PC1 usually captures the majority of variance, the original (potentially high-dimensional) data can be projected on a subset of a few essential principal components only, while higher dimensions can be discarded without a major loss of information. In our simplified example (see Figure 1b, 1c), PC1 already captured 83.5% of the original variance, therefore PC2 can be neglected. Methods for selecting the appropriate number of components are discussed below. Furthermore, the R script used to generate the tables and figures is provided with the article (Supplementary File 1).

ASSUMPTIONS OF PCA

Several prerequisites need to be met to produce meaningful results with PCA. Firstly, the input data need to be continuous, real-valued variables measured on an interval or ratio scale because standard PCA investigates patterns of covariance/correlation, which only makes sense for such variables. Appropriate methods for discrete variables measured on an interval scale such as integers or categorical variables include among others correspondence analysis [2], multiple correspondence analysis [2, 3] or non-metric multidimensional scaling [2]. However, these techniques will not be discussed in the context of this article. Secondly, covariance/correlation measures require that the relationship between each pair of variables is linear. If non-linear relationships are detected, appropriate data transformation techniques (e.g. logarithmic transformation) should be considered. Screening for outliers should be performed prior to the analysis, since outliers can affect the size of the covariance/correlation and thus distort the results. Finally, a sufficiently large sample size is needed to obtain more accurate estimates for the covariance/correlation population parameters, which leads to more robust PCA results [1].

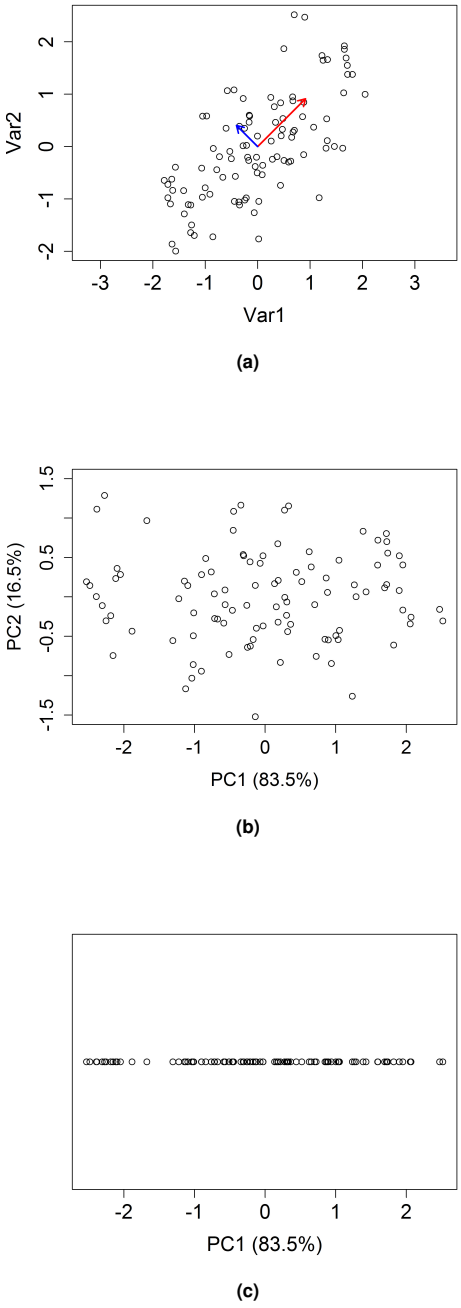

Figure 1: Basic principles of PCA. (a) Scatter plot of the standardized variables shown in Table 1. Variables were standardized by subtracting the respective mean from each value and dividing the result by the standard deviation. The red arrow represents the direction of the largest variance of the multivariate Gaussian distribution derived from the data. The blue arrow captures the direction of the second largest variance orthogonal to the first vector. (b) A scatter plot of the two variables projected on the first and second principal components. The amount of variance accounted for by each component is given in brackets. (c) Dimension reduction in this example can be achieved by retaining only the first principal component. Since PC1 captures 83.5% of the variance in the original data, discarding PC2 does not lead to a major loss of information.

EXTRACTION OF PRINCIPAL COMPONENTS

The main step of PCA is the computation of the weighting coefficients that are needed to create the linear combinations of the original variables. The different possible approaches are all based on the principles of low-rank matrix factorization, i.e. on decomposing a matrix into a product of matrices of a smaller rank/dimension. A common approach uses the covariance matrix **S** of the original variables to extract the principal components. **S** is a symmetric matrix whose off-diagonal elements correspond to the covariance between pairs of variables in a data set. The entries in the main diagonal represent the variance of a variable. In a procedure called eigendecomposition, **S** can be represented in the following way:

$$S = V_S L_S V_S^T$$

with $\mathbf{V_S}$ being the matrix of the normalized eigenvectors **v** of **S**. $\mathbf{L_S}$ is a diagonal matrix containing the corresponding eigenvalues and $\mathbf{V_S}^T$ the transpose of $\mathbf{V_S}$. Note that the eigenvector **v** of a square matrix **M** has the following property:

$$Mv = \lambda v$$

where λ is the corresponding eigenvalue. The eigenvectors of **S** are orthogonal to each other and the eigenvalues are non-negative.

The eigenvectors of the covariance matrix **S** are then used as weighting coefficients to calculate the principal component scores:

$$F = XV_S$$

where **X** is the matrix of mean-centered data and **F** is a matrix whose columns contain the principal components. From a statistical point of view each principal component can be regarded as a new variable which can be used for statistical tests or data visualization. Therefore, every subject from the original data set has a specific value measured on each principal component, also called a principal component score. The first eigenvector $\mathbf{v_1}$, corresponding to the largest eigenvalue λ_1, is used to calculate the first principal component. This procedure produces principal components with a mean equal to 0 and a variance equal to the corresponding eigenvalue. The sum of all eigenvalues is equal to the total variance in the original data matrix **X**. Since the first eigenvalue is the largest, the first principal component accounts for the biggest amount of variability in the original data.

An alternative approach of calculating the principal components is to use the eigenvectors of the correlation matrix **R** as weighting coefficients. Recall that **R** is a symmetric matrix whose off-diagonal elements represent the Pearson correlation coefficients between pairs of variables in a data set. The entries in the main diagonal are all equal to 1 because they correspond to the correlation of a variable with itself. This strategy is recommended when input variables are measured on different scales (otherwise variables with a larger scale dominate the size of the covariance). Component scores are calculated by multiplying the standardized data matrix **X** with the matrix $\mathbf{V_R}$ containing the eigenvectors of the correlation matrix **R**.

Finally, extraction of principal components may be facilitated by performing singular value decomposition of the original data matrix **X**:

$$X = UDV^T$$

where **U** is a matrix of the so-called left singular vectors, **D** is a diagonal matrix of singular values and **V** contains the right side singular vectors [4]. Singular value decomposition is performed either on the mean centered (each column has a mean of 0) or the standardized data matrix, respectively, where each column has a mean of 0 and a variance of 1. If the mean-centered matrix is used, the matrix **V** (i.e. the right singular vectors) is equal to the eigenvectors of the covariance matrix **S**. If, however, the standardized data matrix is used, then the right singular vectors correspond to the eigenvectors of the correlation matrix **R**. In both cases, the right singular vectors are used as weighting coefficients to calculate the principal component scores from the original variables.

In order to show a more detailed example of PCA, we extended the data shown in Table 1 with two additional variables. The new variables were sampled from a bivariate normal distribution with means 110 and 135, variances 20 and 33 and Pearson correlation coefficient 0.856. Since the scale of the variables was not specified, PCA was performed by singular value decomposition on the standardized data using the *prcomp()* R function. This produces identical results to performing eigendecomposition of the correlation matrix because *prcomp()* automatically rescales the singular values to the eigenvalues and reports the square root of the eigenvalues as standard deviation of the principal components. However, singular value decomposition is preferred due to numerical stability. The eigenvectors and the corresponding eigenvalues from our analysis on the simulated data set are shown in Table 2. This example demonstrates important characteristics of PCA, namely that the maximal number of components is equal to the number of original variables and that the first component accounts for the largest variance in the data.

Eigenvectors			
$\mathbf{V_1}$	$\mathbf{V_2}$	$\mathbf{V_3}$	$\mathbf{V_4}$
-0.3	0.64	-0.7	-0.12
-0.28	0.65	0.71	0.04
-0.66	-0.25	-0.07	0.71
-0.63	-0.33	0.09	-0.7
Eigenvalues (% variance captured)			
1.90	1.63	0.33	0.14
(48%)	(41%)	(8%)	(3%)

Table 2: PCA analysis on simulated data. For this example, the simulated data set in Table 1 was extended by two additional variables sampled from a bivariate normal distribution with means 110 and 135, variances 20 and 33 and Pearson correlation coefficient 0.856. PCA was then performed by singular value decomposition of the standardized data matrix (each variable with a mean of 0 and standard deviation of 1) using the *prcomp()* R function. The right singular vectors $\mathbf{V_1}$ to $\mathbf{V_4}$ which are equal to the eigenvectors of the correlation matrix were used as weighting coefficients to calculate the principal components. The corresponding eigenvalue and the percentage of variance captured by each component (calculated by dividing each eigenvalue by the sum of all eigenvalues) are included.

PRINCIPAL COMPONENTS SELECTION

A major issue in PCA is to decide on how many components to retain in order to still keep a sufficient amount of variance but, at the same time, to achieve a substantial reduction in dimensionality. One possibility is to define a threshold (e.g. a certain percentage of the original variability) and keep as many principal components as necessary to exceed this threshold. Another option is to keep only principal components with a corresponding eigenvalue equal to or greater than 1, the so called Kaiser criterion. This, however, is only applicable if PCA is performed by eigendecomposition of **R** or singular value decomposition of the standardized data matrix **X**. In this case, each original variable has a variance of 1. Therefore, only components which account for more variability than a single variable are meaningful and should be retained.

The probably most popular approach is the Scree plot [5], where the principal components are plotted on the x-axis in descending order against their corresponding eigenvalues. This leads to a decreasing function showing the variance explained by each PC. This plot often shows a clear crease (the so-called "elbow") separating the 'most important' components from the 'least important' components. All components to the right of the break point can be discarded. The disadvantage of this method is the visual inspection of the Scree plot - a subjective way to identify the correct number of principal components. Furthermore, in some practical applications, it might be difficult to determine the cut-off point where the slope of the line which goes through the eigenvalues changes the most.

A more sophisticated technique is parallel analysis [6]. Here, PCA is performed on a simulated data set with as many variables and cases as there are in the original data set. Averaged eigenvalues from the simulated data are compared to the eigenvalues obtained from the real data. Components from the real data with eigenvalues lower than the eigenvalues for the simulated data are discarded. Parallel analysis offers a more objective way to assess the appropriate number of components to keep. Therefore, it can be more useful than the Scree test in many real-world applications of PCA.

We applied the Scree test and parallel analysis on our example of PCA on the small simulated data set (Figure 2). Both techniques indicated that two components are meaningful, therefore the third and fourth principal components can be discarded.

INTERPRETATION OF PRINCIPAL COMPONENTS

Principal components are interpreted based on the original variables which "load" on them. Loadings correspond to correlations or covariances between the original variables and principal components. Variable loadings are stored in a loading matrix, **A**, which is produced by multiplying the matrix of the eigenvectors with a diagonal matrix containing the square root of the corresponding eigenvalues:

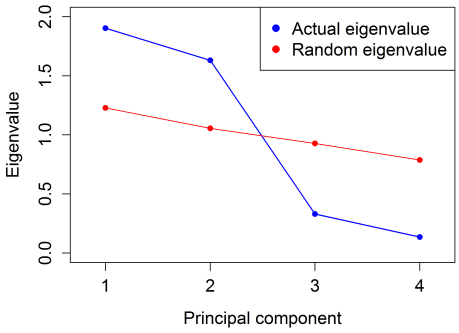

Figure 2: Scree plot and parallel analysis of PCA. Results from the Scree test and parallel analysis for PCA performed on the simulated data set with four variables and 100 cases are shown. The blue line shows the actual eigenvalues obtained from the PCA analysis. The dramatic slope change between the second and third principal components indicates that only the two first components are the most meaningful and so should be retained. The red line shows random eigenvalues generated with parallel analysis. Only the first and the second actual eigenvalues are larger than the random eigenvalues which indicates that only two principal components should be retained.

$$A = V\sqrt{L}$$

The entries in **A** are dependent on the technique used for extracting the components. If extraction is based on singular value decomposition of the matrix of mean-centered data or on eigendecompositon of the covariance matrix, then unstandardized loadings represent the covariance between mean-centered variables and standardized component scores. However, if eigendecomposition of the correlation matrix is performed, then standardized loadings are produced. These loadings represent correlations between the original variables and component scores. Standardized loadings are easier to interpret, since they always range from -1 to 1 and are independent of the scale used. A threshold is usually defined and only variables with loadings above this threshold are considered. A common rule of thumb suggests to only consider standardized loadings exceeding 0.45 (since this corresponds to 20% shared variance between the original variable and the principal component) [1].

The loading matrix for the PCA performed on our simulated data set with four variables is shown in Table 3. Since we used singular value decomposition of the standardized data matrix **X**, loadings represent correlations between principal components and original variables. PCA managed to capture the structural pattern of high correlation between var1 and var2 and between var3 and var4, respectively, in our simulated data.

VISUALIZATION OF RESULTS

PCA results are usually graphically represented by two- or three-dimensional dot plots of scores on the first few principal components. Each point represents

	PC1	PC2
Var1	0	0.82
Var2	0	0.83
Var3	-0.91	0
Var4	-0.87	0

Table 3: Standardized loading matrix. The loading matrix is based on our PCA analysis of simulated data including 4 variables and 100 cases (see Table 1 and Table 2). Loadings on the retained first two PC (see Figure 2) represent correlations between the original variables and the principal components. Loadings below 0.45 were set to 0 to ease interpretation. The loading matrix reveals a structural pattern in the original data. Var3 and var4 both load significantly on PC1 whereas var1 and var2 load significantly on PC2, thus indicating an association between var1 and var2 on the one hand and between var3 and var4 on the other.

a subject of the original data set and the coordinates correspond to the specific value measured for this subject on the corresponding principal component. While a scatter plot of scores on PC1 against PC2 is the most common (Figure 3), it is important to test different combinations since multivariate patterns might emerge based on other components.

AN EXAMPLE OF PCA ON GENE EXPRESSION DATA

In order to show a practical example of PCA applied to genomic data, we analyzed gene expression data from brain tissue samples obtained from a transgenic mouse model and wild-type controls (GEO identifier: GSE47029). The study by Maung and colleagues tested whether genetic ablation of the CCR5 chemokine receptor impacts brain damage induced by HIV envelope protein gp120 in two transgenic mouse lines [7]. The input data matrix included 225 samples and 33503 features.

Gene expression levels have been shown to be heteroscedastic, meaning that their variance changes depending on mean expression level. Usually, genes with lower expression levels are associated with higher variability across different measurements [8]. The Poisson distribution which is often applied to modelling count data tends to underestimate the variance in gene expression data [8]. In contrast, the negative binomial (NB) distribution has been shown to provide a good fit when modelling differential gene expression [9]. The NB model assumes that an observation has a population mean μ and variance $\sigma^2 = \mu + \phi\mu^2$, where ϕ is the so-called dispersion parameter [9]. To account for the heteroscedasticity of the input data, we estimated the dispersion parameter for each gene with the help of the *DESeq* R package. Afterwards, we applied the *varianceStabilizingTransformation()* function to the input data in order to produce a data matrix in which expression levels are homoscedastic. Finally, we extracted the principal components from the transformed data using the *plotPCA()* function. The *plotPCA()* function internally calls on *prcomp()*, meaning that PCA was performed by singular value decomposition of the matrix of mean centered, variance stabilized gene expression data. With default settings *plotPCA()* extracts the components using only the top 500 most variable genes. Therefore, the input data matrix for the example shown here consisted of 225 rows (samples) and 500 columns (genes).

PCA identified two distinct clusters in the data separated based on scores on the first principal component (Figure 3). Different colouring schemes were applied to investigate if the separation was associated with a specific factor. This analysis revealed that the two clusters correspond to mouse line 1 and 2 (Figure 3a), suggesting an overall differential gene expression between the two transgenic mouse lines. Maung et al., who conducted the study the data were obtained from, reported an increased gp120 RNA expression in animals from line 2 compared to line 1. Furthermore, an up-regulation associated with gp120 was observed for six genes (CCR5, CCL2, CCL3, CCL4, CXCL10 and C4b) in mouse line 2 relative to line 1. These findings are in agreement with the two distinct clusters corresponding to both mouse lines revealed by our PCA (Figure 3a).

No differences could be determined based on gender (Figure 3b), however a certain discrimination associated with genotype was present based on scores on the second principal component (Figure 3c). Notably, Maung and colleagues identified a core common set of genes for the gp120+ genotype in mouse line 1 and line 2 which were differentially expressed in the presence or absence of the CCR5 receptor. The multivariate genotype pattern which we observed within both clusters corresponding to mouse line 1 and 2 is very similar and might therefore mainly relate to the core set of genes identified by Maung et al. A detailed inspection of the loading matrix could provide even more insights into which specific genes are differentially expressed based on genotype.

PC1 and PC2 together only accounted for 24.03% of the total variance which means that additional components are important and may be associated with multivariate patterns. However, our goal here is not to provide a complete analysis of the gene expression data set, but more to demonstrate how PCA can be applied to this type of data for exploratory purposes. Since a multivariate pattern already emerged based on PC1 and PC2, we did not further evaluate the remaining components.

The R script used to perform the PCA analysis on gene expression data is included in Supplementary File 2.

ACKNOWLEDGEMENTS

The work of SG and DF was funded by the Center for Computational Sciences in Mainz (CSM). The work of HT was funded by Fresenius Kabi Deutschland GmbH.

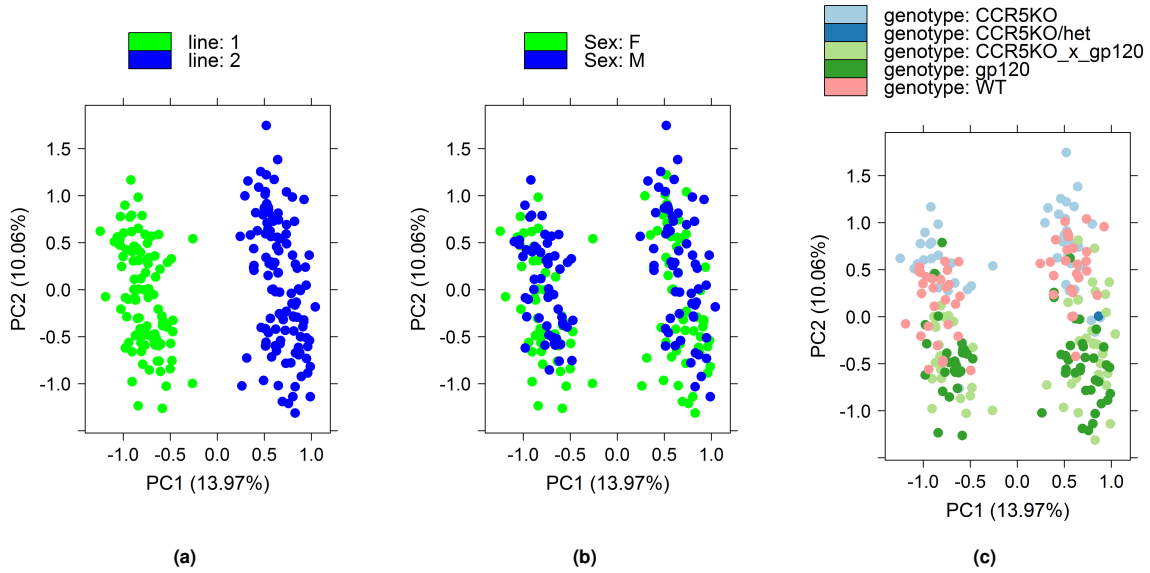

Figure 3: PCA analysis on gene expression data. PCA was performed on transformed gene expression data from a mouse model. PCA identified two distinct clusters in the data separated along the first principal component. Different colouring schemes revealed that clustering was associated with the mouse line (a). Gender was not associated with a pattern in the data (b), but genotype revealed a gradient of discrimination along the second principal component (c). The amount of variance in percent accounted for by each PC is included in brackets.

AUTHOR CONTRIBUTIONS

HT drafted the manuscript and performed the analysis on the simulated data. DF performed the analysis on the gene expression data and reviewed the manuscript. SG initiated the study, contributed to interpreting the results and editing the manuscript. All authors read and approved the final manuscript.

CONFLICT OF INTEREST

The authors declare no conflict of interests.

SUPPLEMENTARY DATA

High resolution figure files, together with supplementary items listed below, are available at Genomics and Computational Biology online.

Supplementary File 1. R script for simulated data; File: simdataPCA.R. This file includes the R script used to generate the simulated data and perform the example PCA.

Supplementary File 2. R script for gene expression data; File: expressionPCA.R. This file includes the R script used to process the gene expression data and perform PCA.

ABBREVIATIONS

F : female

GEO : gene expression omnibus

gp120 : envelope glycoprotein gp120

HIV : human immunodeficiency virus

M : male

NB : negative binomial

PCA : principal components analysis

PC : principal component

WT : wild type

REFERENCES

1. Tabachnik BG, Fidell LS. Principal components and factor analysis. In: **Using multivariate statistics**. 6th ed. Pearson Education, Ltd; 2014. p. 659–729.
2. Legendre P, Legendre L. Ordination in reduced space. In: **Numerical Ecology**. 2nd ed. Elsevier Science B.V.; 1998. p. 387–480.
3. Sourial N, Wolfson C, Zhu B, Quail J, Fletcher J, Karunananthan S, et al. **Correspondence analysis is a useful tool to uncover the relationships among categorical variables**. Journal of Clinical Epidemiology. 2010;63(6):638 – 646. doi:10.1016/j.jclinepi.2009.08.008.
4. Trefethen LN, Bau D. **Numerical linear algebra**. 1st ed. Society for industrial and applied mathematics; 1997.
5. Cattell RB. **The Scree test for the number of factors**. Multivariate Behavioral Research. 1966;1(2):245–276. doi:10.1207/s15327906mbr0102_10.
6. Horn JL. **A rationale and test for the number of factors in factor analysis**. Psychometrika. 1965;30(2):179–185. doi:10.1007/BF02289447.
7. Maung R, Hoefer MM, Sanchez AB, Sejbuk NE, Medders KE, Desai MK, et al. **CCR5 Knockout Prevents Neuronal Injury and Behavioral Impairment Induced in a Transgenic Mouse Model by a CXCR4-Using HIV-1 Glycoprotein 120**. The Journal of Immunology. 2014;193(4):1895–1910. doi:10.4049/jimmunol.1302915.
8. Anders S, McCarthy D, Chen Y, Okoniewski M, Smyth G, Huber W,

et al. **Count-based differential expression analysis of RNA sequencing data using R and Bioconductor**. Nature Protocols. 2013;8(9):1765–1786. doi:10.1038/nprot.2013.099.

9. Anders S, Huber W. **Differential expression analysis for sequence count data**. Genome Biology. 2010;11(10):R106. doi:10.1186/gb-2010-11-10-r106.

2.2 Applying univariate vs. multivariate statistics to investigate therapeutic efficacy in (pre)clinical trials: A Monte Carlo simulation study on the example of a controlled preclinical neurotrauma trial.

Authors: **Hristo Todorov**; Emily Searle-White; Susanne Gerber
This article is published in *PLOS ONE*, 2020, 15(3):e0230798.
doi: https://doi.org/10.1371/journal.pone.0230798

My contributions to this article are listed in section 4.2 Contributions to individual publications.

PLOS ONE

RESEARCH ARTICLE

Applying univariate vs. multivariate statistics to investigate therapeutic efficacy in (pre)clinical trials: A Monte Carlo simulation study on the example of a controlled preclinical neurotrauma trial

Hristo Todorov[1,2], **Emily Searle-White**[3], **Susanne Gerber**[1]*

1 Faculty of Biology, Institute for Developmental Biology and Neurobiology, Johannes Gutenberg-University Mainz, Mainz, Germany, **2** Fresenius Kabi Deutschland GmbH, Oberursel, Germany, **3** Institute of Mathematics, Johannes Gutenberg-University Mainz, Mainz, Germany

* sugerber@uni-mainz.de

Citation: Todorov H, Searle-White E, Gerber S (2020) Applying univariate vs. multivariate statistics to investigate therapeutic efficacy in (pre)clinical trials: A Monte Carlo simulation study on the example of a controlled preclinical neurotrauma trial. PLoS ONE 15(3): e0230798. https://doi.org/10.1371/journal.pone.0230798

Editor: Marco Bonizzoni, The University of Alabama, UNITED STATES

Received: June 6, 2019

Accepted: March 9, 2020

Published: March 26, 2020

Peer Review History: PLOS recognizes the benefits of transparency in the peer review process; therefore, we enable the publication of all of the content of peer review and author responses alongside final, published articles. The editorial history of this article is available here: https://doi.org/10.1371/journal.pone.0230798

Data Availability Statement: All relevant data are within the manuscript and its Supporting Information files.

Abstract

Background

Small sample sizes combined with multiple correlated endpoints pose a major challenge in the statistical analysis of preclinical neurotrauma studies. The standard approach of applying univariate tests on individual response variables has the advantage of simplicity of interpretation, but it fails to account for the covariance/correlation in the data. In contrast, multivariate statistical techniques might more adequately capture the multi-dimensional pathophysiological pattern of neurotrauma and therefore provide increased sensitivity to detect treatment effects.

Results

We systematically evaluated the performance of univariate ANOVA, Welch's ANOVA and linear mixed effects models versus the multivariate techniques, ANOVA on principal component scores and MANOVA tests by manipulating factors such as sample and effect size, normality and homogeneity of variance in computer simulations. Linear mixed effects models demonstrated the highest power when variance between groups was equal or variance ratio was 1:2. In contrast, Welch's ANOVA outperformed the remaining methods with extreme variance heterogeneity. However, power only reached acceptable levels of 80% in the case of large simulated effect sizes and at least 20 measurements per group or moderate effects with at least 40 replicates per group. In addition, we evaluated the capacity of the ordination techniques, principal component analysis (PCA), redundancy analysis (RDA), linear discriminant analysis (LDA), and partial least squares discriminant analysis (PLS-DA) to capture patterns of treatment effects without formal hypothesis testing. While LDA suffered from a high false positive rate due to multicollinearity, PCA, RDA, and PLS-DA were robust and PLS-DA outperformed PCA and RDA in capturing a true treatment effect pattern.

Funding: The work of HT was funded by Fresenius Kabi Deutschland GmbH. This does not alter our adherence to PLOS ONE policies on sharing data and materials. The work of SG was partly supported by the CRC 1193. ESW was supported by Center for Computational Sciences in Mainz (CSM). The funder provided support in the form of salaries for author HT, but did not have any additional role in the study design, data collection and analysis, decision to publish, or preparation of the manuscript. This does not alter our adherence to PLOS ONE policies on sharing data and materials. The specific roles of all authors are articulated in the 'author contributions' section.

Competing interests: The work of HT was funded by Fresenius Kabi Deutschland GmbH. This does not alter our adherence to PLOS ONE policies on sharing data and materials. The work of SG was partly supported by the CRC 1193.

Conclusions

Multivariate tests do not provide an appreciable increase in power compared to univariate techniques to detect group differences in preclinical studies. However, PLS-DA seems to be a useful ordination technique to explore treatment effect patterns without formal hypothesis testing.

Introduction

The aim of controlled preclinical studies is usually to investigate the therapeutic potential of a chemical or biological agent, or a certain type of intervention. For this purpose, animals are randomized to a control group and a number of treatment groups in a manner similar to clinical trials. For quantitative endpoints, treatment effects are evaluated by assessing mean differences between control and intervention groups. In an effort to obtain as much information as possible with minimal cost of life, usually multiple endpoints are included in the trial [1], which is further motivated by the fact that the optimal efficacy endpoint for a specific disease might not be known. In this context, the null hypothesis of no treatment effect (H_0) can be rejected in two ways. The standard approach consists of performing independent univariate tests on each variable separately. However, this strategy might lead to an inflated family-wise error rate. In addition, different endpoints are usually correlated, implying that preclinical trials are multi-dimensional in nature. Consequently, the second approach is to use a multivariate technique, which accounts for the covariance/correlation structure of the data. H_0 is usually tested on some kind of linear combination of the original variables. Due to the increased complexity of analysis and interpretation of results in this case, such an approach has found limited use in preclinical research so far.

A number of studies have highlighted the potential benefits of multivariate techniques in the context of preclinical trials [2] and more specifically animal neurotrauma models [3–7]. Traumatic or ischemic events to the central nervous system such as stroke, spinal cord or traumatic brain injury are followed by a multi-faceted pathophysiology which manifests on molecular, histological and functional levels [8–11]. Individual biological mechanisms that are disrupted by or result from the neurotrauma such as apoptosis [12, 13], neuroinflammation [14–18], oxidative stress [18–20] and plasticity alterations [21, 22] have provided therapeutic targets in animal models. However, translation of candidate therapies to humans continues to be mostly unsuccessful [23–26]. Many studies indicate that individual biological processes interact together in determining functional outcome, which is why multivariate measures might capture the complex disease pattern more successfully and therefore detect therapeutic intervention efficacy with increased sensitivity [3, 4]. However, no solid proof of the superiority of multivariate methods beyond these theoretical considerations has been ascertained so far.

The aim of our current study was to obtain empirical evidence as to whether univariate or multivariate statistical techniques are better suited for detecting treatment effects in preclinical neurotrauma studies. For this purpose, we performed simulations under a broad range of conditions while simultaneously trying to mimic realistic experimental conditions as closely as possible. We investigated the empirical type I error rate as well as empirical power of several competing techniques and evaluated factors which impact their performance.

Methods

Simulation procedure

We performed a Monte Carlo study using the statistical software R [27] and following recommendations of Burton et al. for the design of simulation studies [28]. Artificial data were based

on a real study in a rat model of traumatic brain injury. In the preclinical trial, twenty animals per group received either vehicle control or a therapeutic agent. Functional outcome was evaluated based on 6 different endpoints including 20-point neuro-score, limb placing score, lesion and edema volume, and T2 lesion in the ipsilateral and contralateral hemisphere. All variables were measured repeatedly on three time points, therefore resulting in a data matrix with 18 columns. In order to obtain more general estimates of the mean vector and covariance matrix for subsequent simulations, a non-parametric bootstrap procedure was applied using the data from the saline control group from the *in vivo* study. Since two animals from this group were excluded from the study, the resampling procedure was conducted with the available 18 animals. 10,000 samples were drawn from the original data with replacement and the average mean vector and covariance matrix were then calculated. In order to retain the covariance structure of the data, complete rows of the data matrix (corresponding to all measurements from a single animal) were always sampled as a 18x1-dimensional vector. The *nearPD* R function was then employed to force the calculated dispersion matrix to be positive definite. The resulting mean vector and covariance matrix were used as parameters for multivariate distributions, from which data for subsequent simulations were sampled (see S1 Appendix of Tables 1 and 2). We generated one control group and three treatment groups under each scenario, which corresponds to a typical preclinical trial design where increasing doses of a therapeutic agent are tested against a control treatment.

Simulation factors

Sample size. We performed simulations with 5, 10, 15 and 20 measurements per treatment group to investigate the impact of sample size. These values were selected to represent realistic group sizes commonly encountered in preclinical trials. Additionally, we performed simulations with 30, 40 and 50 replicates per group to investigate the effect of a larger sample size beyond those typical for animal studies. In the course of this study we use the terms measurements, subjects and replicates per group interchangeably.

Effect size. Treatment effects were based on Cohen's d with values set to 0, 0.2, 0.5 and 0.8 corresponding to no effects, small, moderate and large statistical effect sizes relative to the control group, respectively [29]. We chose Cohen's d because this standardized statistical measure of effect size is independent of the scale of the original variables. The population mean values for the treatment groups were then calculated using the formula $\mu_1 = \mu_0 \pm s^* d$, where μ_0 corresponds to the population mean of the respective variable in the control group and s signifies the standard deviation of both groups in case of equal variance or the average standard deviation in case of unequal variance. We performed simulations with no treatment effects in all groups to investigate empirical type I error rate. Additionally, we investigated empirical power by simulating either large, moderate or small effects in the treatment groups relative to the control group.

Distribution of dependent variables. The dependent variables were simulated to follow a multivariate normal distribution to comply with the assumptions of the investigated methods. Additionally, we employed the multivariate lognormal distribution and the multivariate gamma distribution in order to investigate the impact of departures from normality. The multivariate gamma distribution was modelled using its shape parameter α and its rate parameter β. These parameters were derived from the target mean and variance values using the following relationships: $\mu = \alpha/\beta$ and $\sigma^2 = \alpha/\beta^2$, where μ and σ^2 correspond to the mean and variance of the gamma distribution, respectively. Since we wanted to simulate specific values for the mean and variance, we used the following equations to obtain the shape and rate parameter of

the gamma distribution: $\alpha = \mu^2/\sigma^2$ and $\beta = \mu/\sigma^2$. The correlation matrix used for the simulation of multivariate data sets is shown in S1 Appendix of Table 2.

Variance. Parametric univariate methods to detect mean differences assume that variance in all groups is equal, which in the multivariate case extends to the assumption of homogeneity of covariance matrices [30]. Therefore we first performed simulations with all groups having equal variance. Then we simulated treatment groups having variance twice or 5 times higher than the variance in the control group. This allowed us to investigate the impact of increasing variance heterogeneity.

Factors were crossed to produce 252 different simulation scenarios with 1000 replicate data sets generated under each combination of simulation conditions.

Methods to detect treatment effects

Univariate statistics. The univariate approach of investigating treatment differences between groups consisted of a series of independent analysis of variance (ANOVA) tests on each outcome variable separately. Furthermore, we applied Welch's ANOVA as implemented in the *oneway.test* R function, which does not assume equal variance between groups [31]. In order to take the repeated measures nature of the input data into account, we also performed linear mixed effects tests for each endpoint. Since we did not simulate an interaction between treatment effect and time, we only included the main effects in the mixed effects model without an interaction term. We rejected H_0 of no treatment effect if the main effect for the treatment factor was significant.

Multivariate statistics. The first multivariate strategy we investigated was performing ANOVA tests on principal component (PC) scores obtained from the original variables. We used eigen decomposition of the population correlation matrix in order to calculate the PCs, which is the preferred approach when variables are measured on different scales [30, 32]. Based on the Kaiser criterion, we only retained components whose corresponding eigenvalue was greater than one [33]. Component scores were obtained by multiplying the standardized data matrix of original variables with the eigenvectors of the population correlation matrix [32].

The second multivariate technique consisted of a series of multivariate analysis of variance (MANOVA) tests on each study variable with repeated measures. Each repeated measure was considered a separate dependent variable for the respective MANOVA. Thus, we performed 6 MANOVA tests, each of which included the three repeated measures of one endpoint as the dependent variables. The significance of the MANOVA tests was evaluated using four different statistics which are commonly provided by statistical software such as R, SAS or SPSS: Wilks' lambda [34], Lawley-Hotelling trace [35], Pillai's trace [36] and Roy's largest root [37].

In all cases, H_0 was rejected when the p-value from the omnibus test was less than 0.05; no specific contrasts or post hoc analyses were considered. Different techniques were evaluated based on the empirical type I error rate or on empirical power. Empirical type I error rate was defined as the number of significant statistical tests divided by the total number of tests when no treatment effects were simulated. Empirical power was defined as the number of significant tests divided by the total number of tests in the cases when treatment effects were simulated.

Multivariate dimensionality reduction techniques for pattern analysis

In addition to formally comparing the type I error rate and power of univariate and multivariate statistics, we also investigated if ordination techniques might be useful to detect patterns of treatment effects in multi-dimensional preclinical data sets. We focused on methods that perform ordination and dimensionality reduction based on Euclidean distances and are therefore suitable for quantitative and semi-quantitative data. First, we applied PCA, linear discriminant

analysis (LDA), redundancy analysis (RDA), and partial least squares discriminant analysis (PLS-DA) on 1000 simulated data sets with 5 measurements per group and no treatment effects. We plotted the first versus the second multivariate dimension and visually inspected the plots. If the 95% confidence ellipse around the control group did not overlap with the confidence ellipses around the data points for the treatment groups, we considered that the ordination method falsely captured a treatment effect pattern in the data. Next, we examined the sensitivity of the ordination methods to detect true treatment effect patterns by simulating 1000 data sets with 5 measurements per group and huge treatment effects (Cohen's d = 2.0). We used this effect size as we did not observe a difference between groups when smaller effect sizes were simulated. We considered that the respective method correctly accounted for a treatment effect pattern in the data if the 95% confidence ellipse around the control group did not overlap with the confidence ellipses around the simulated treatment groups.

Finally, we provide an applied example of combining dimensionality reduction techniques with formal hypothesis testing using one simulated data set with 5 measurements per group and treatment effects on only half of all the variables.

Results

Competing multivariate statistics

Prior to investigating the performance of univariate and multivariate techniques, we examined the four MANOVA test statistics in order to identify the most appropriate for subsequent comparisons. Fig 1 shows representative results for the type I error and power of the

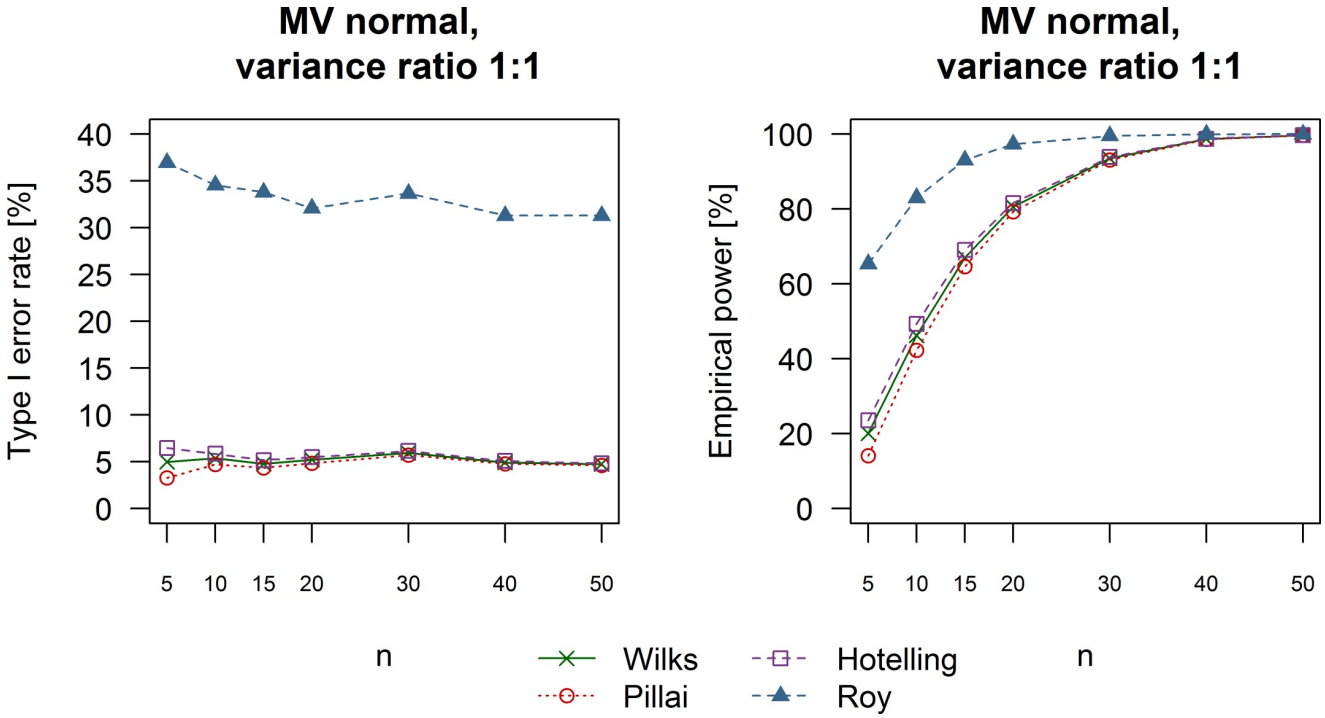

Fig 1. Performance of different multivariate statistics. Example plots show empirical type I error and power of the MANOVA test using four common multivariate test statistics. Type I error rate is shown for the simulation scenario with no treatment effects, equal variance in all groups and data drawn from a multivariate normal distribution. An example of power analysis is shown for a simulation with large treatment effects (Cohen's d equal to 0.8), equal variance in all groups and data sampled from a multivariate normal distribution. Hotelling: Lawley-Hotelling trace; Pillai: Pillai's trace; Roy: Roy's largest characteristic root; Wilks: Wilks' lambda.

https://doi.org/10.1371/journal.pone.0230798.g001

MANOVA test (see S1 Appendix of Figs 1–4 for complete results) using the four different statistical criteria. We observed the same trend under all simulation scenarios with Roy's largest root having a considerably high false positives rate over 30%. In contrast, the remaining statistics exhibited very similar type I error rates. Pillai's trace was the most robust measure followed by Wilks' lambda and Lawley-Hotelling trace. Roy's largest root was not considered with regards to power analysis due to the unacceptably high type I error rate. Pillai's trace consistently demonstrated the lowest power. In contrast, Wilks' lambda was associated with a slightly higher probability of correctly rejecting the null hypothesis in the presence of treatment effects than Pillai's trace but it was outperformed by Lawley-Hotelling trace. However, we chose Wilks' lambda for further analysis because it provided a good compromise between type I error rate and power in comparison to the other multivariate test statistics.

False positive rate

Empirical type I error rates of the methods we evaluated under different simulation scenarios are summarized in Fig 2. Differences between univariate and multivariate methods were negligible under all simulation conditions. Furthermore, all methods managed to remain close to the nominal level of type I error rate around 5% even in the case of extreme variance heterogeneity (variance ratio between control and treatment group equal to 1:5). Interestingly, Welch's ANOVA was associated with a slightly higher false positive rate compared to other methods when data were sampled from a multivariate lognormal distribution combined with extreme variance heterogeneity. Furthermore, linear mixed effects models had a slightly higher type I error rate in the case of 5 subjects per group.

Empirical power

The results we obtained for empirical power under different simulation conditions are depicted in Figs 3–5. Linear mixed effects models outperformed the remaining methods in the case of variance equality or moderate variance heterogeneity (variance ratio 1:2) with smaller sample sizes of 5 to 20 subjects per group regardless of the effect size we simulated. Welch's ANOVA was as powerful as regular ANOVA when the variance between the control and treatment groups was equal. Furthermore, Welch's ANOVA outperformed all other methods when we simulated moderate or small effect sizes combined with extreme variance heterogeneity (ratio of 1:5 between the control and treatment groups) and data coming from multivariate lognormal or gamma distributions. MANOVA tests were slightly more powerful than the two types of ANOVA in the cases of equal variance but still failed to outperform linear mixed effects models under these simulation scenarios. The multivariate strategy of ANOVA tests on PCA scores was universally associated with the lowest rate of rejecting H_0. It is also worth mentioning that adequate levels of power of around 80% were achieved in the case of at least 20 measurements per group and large treatment effects (Cohen's d equal to 0.8, Fig 3). Simulating moderate treatment effects (Cohen's d equal to 0.5, Fig 4) required a sample size of at least 40 replicates per group in order to achieve levels of power of around 80% Finally, the rate of rejecting H_0 varied between 5% and 25% when we simulated small treatment effects (Cohen's d equal to 0.2, Fig 5).

Comparison of ordination techniques for pattern analysis of treatment effects

We investigated if the dimensionality reduction techniques LDA, PCA, RDA, and PLS-DA could be useful for investigating patterns of treatment effects without formal hypothesis testing. In 1000 simulated data sets without treatment effects and 5 measurements per group, we counted how often the control group was separated from treatment groups along the first and

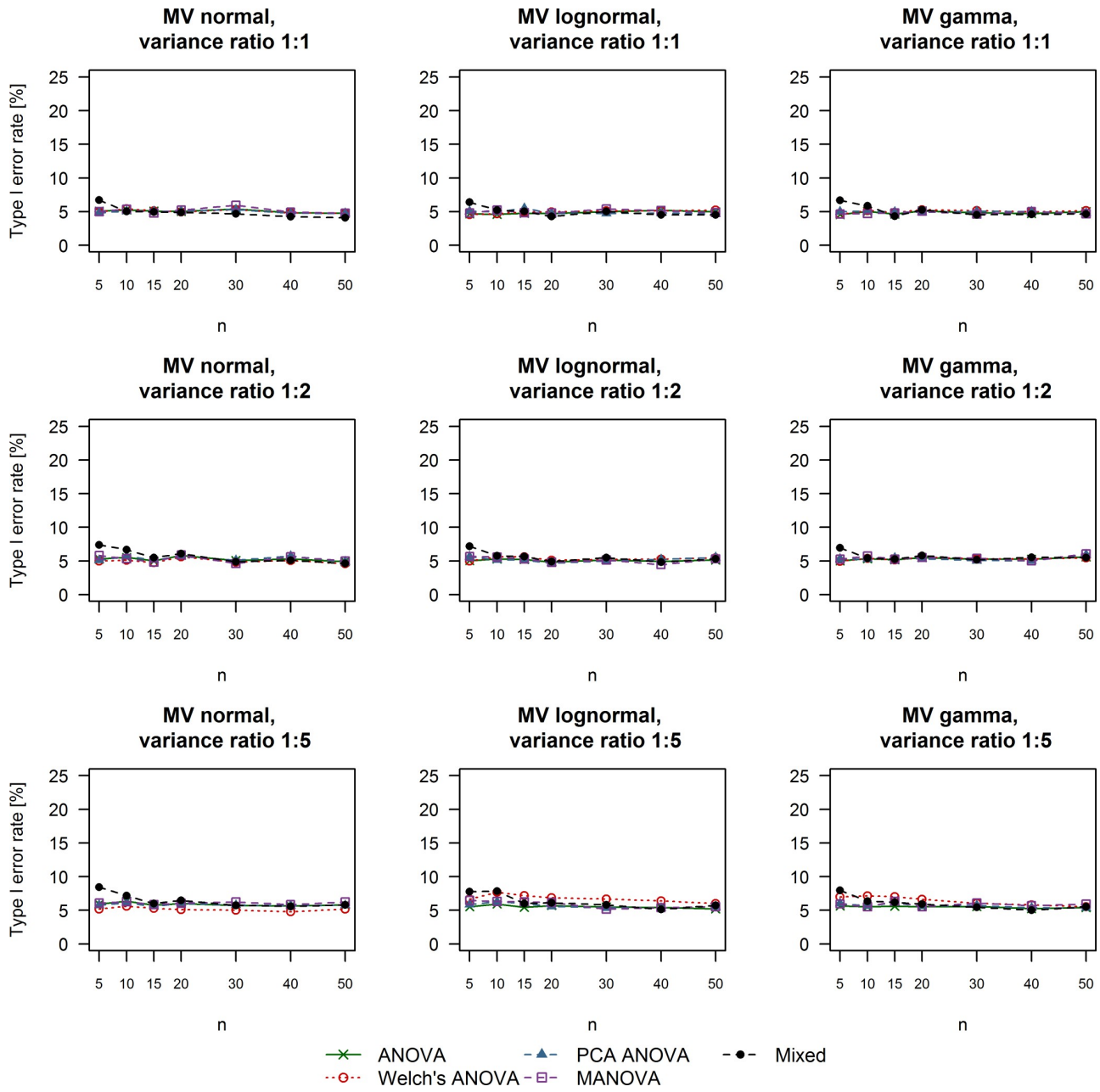

Fig 2. Type I error rate of univariate and multivariate techniques under different simulation conditions. The title of each plot reports the multivariate distribution from which the data were sampled as well as the variance ratio between the simulated control and treatment groups. ANOVA: Analysis of variance; MANOVA: Multivariate analysis of variance; Mixed: Linear mixed effects model; MV: Multivariate; PCA: Principal component analysis.

https://doi.org/10.1371/journal.pone.0230798.g002

second multivariate dimensions (indicated by non-overlapping 95% confidence ellipses). LDA captured a false treatment effect pattern in 387 cases corresponding to a false positive rate of 38.7%. In contrast, the control group was not separated from treatment groups in any of the simulated sets when using PCA, PLS-DA, or RDA for dimensionality reduction. Example plots are shown in Fig 6 (the whole set of plots is available in S2 Appendix). Due to the unacceptably high false positive rate, we did not further consider LDA. Next, we simulated 1000

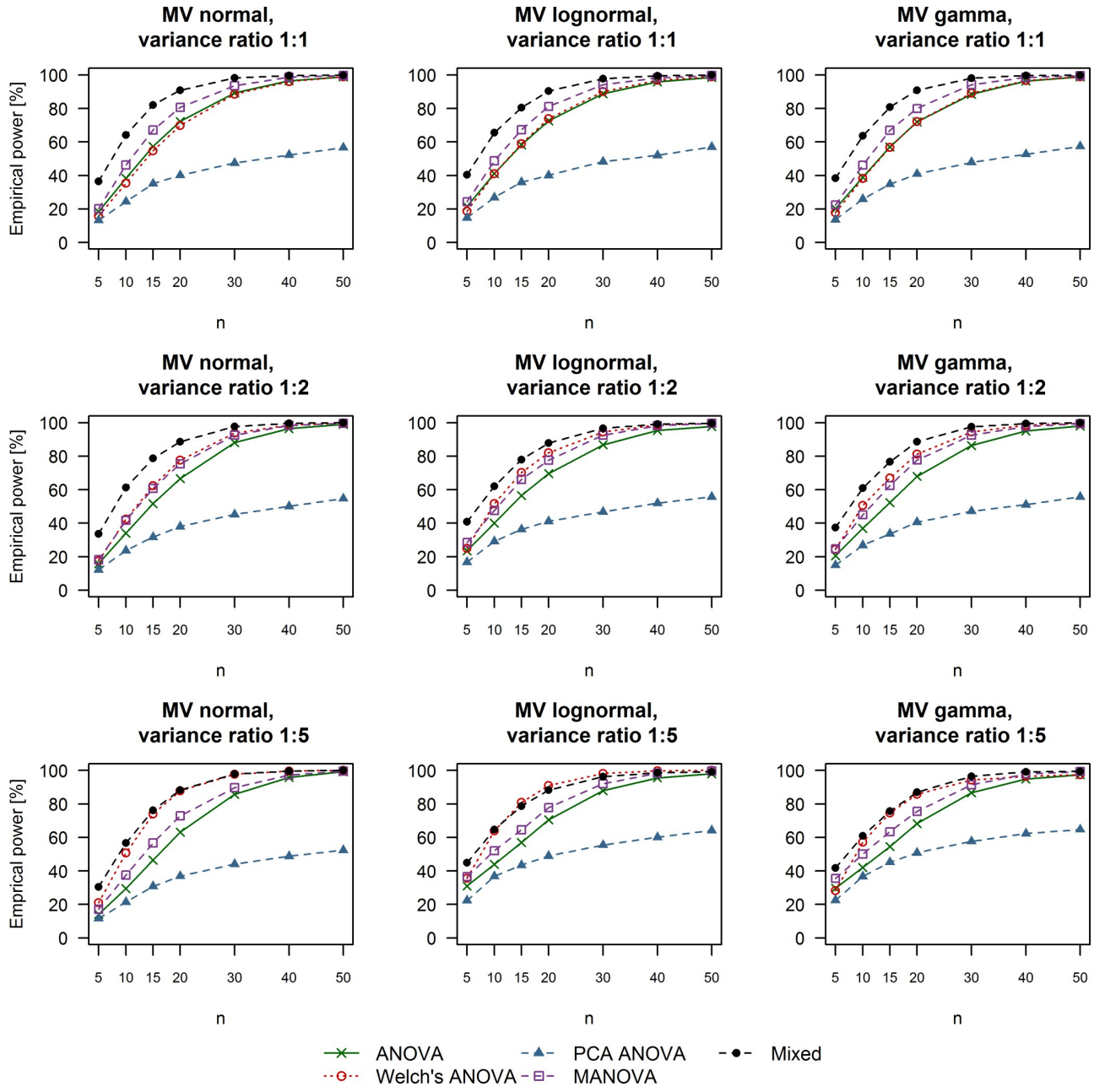

Fig 3. Empirical power of univariate and multivariate techniques in case of large treatment effects (Cohen's d equal to 0.8). The multivariate distribution from which the data were drawn as well as the variance ratio between simulated control and treatment groups are summarized in the title of each respective plot. ANOVA: Analysis of variance; MANOVA: Multivariate analysis of variance; Mixed: Linear mixed effects model; MV: Multivariate; PCA: Principal component analysis.

https://doi.org/10.1371/journal.pone.0230798.g003

data sets with huge treatment effects (Cohen's d equal to 2.0) with 5 measurements per group and investigated how often the control group was separated from treatment groups in reduced multivariate space. PLS-DA managed to capture the true treatment pattern in 13.8% of the cases whereas PCA only separated the control from treatment groups in 7.7% of the simulations. RDA only marginally outperformed PCA and reported a true treatment effect pattern in 9.6% of the cases (the complete simulated set of plots is available in S3 Appendix).

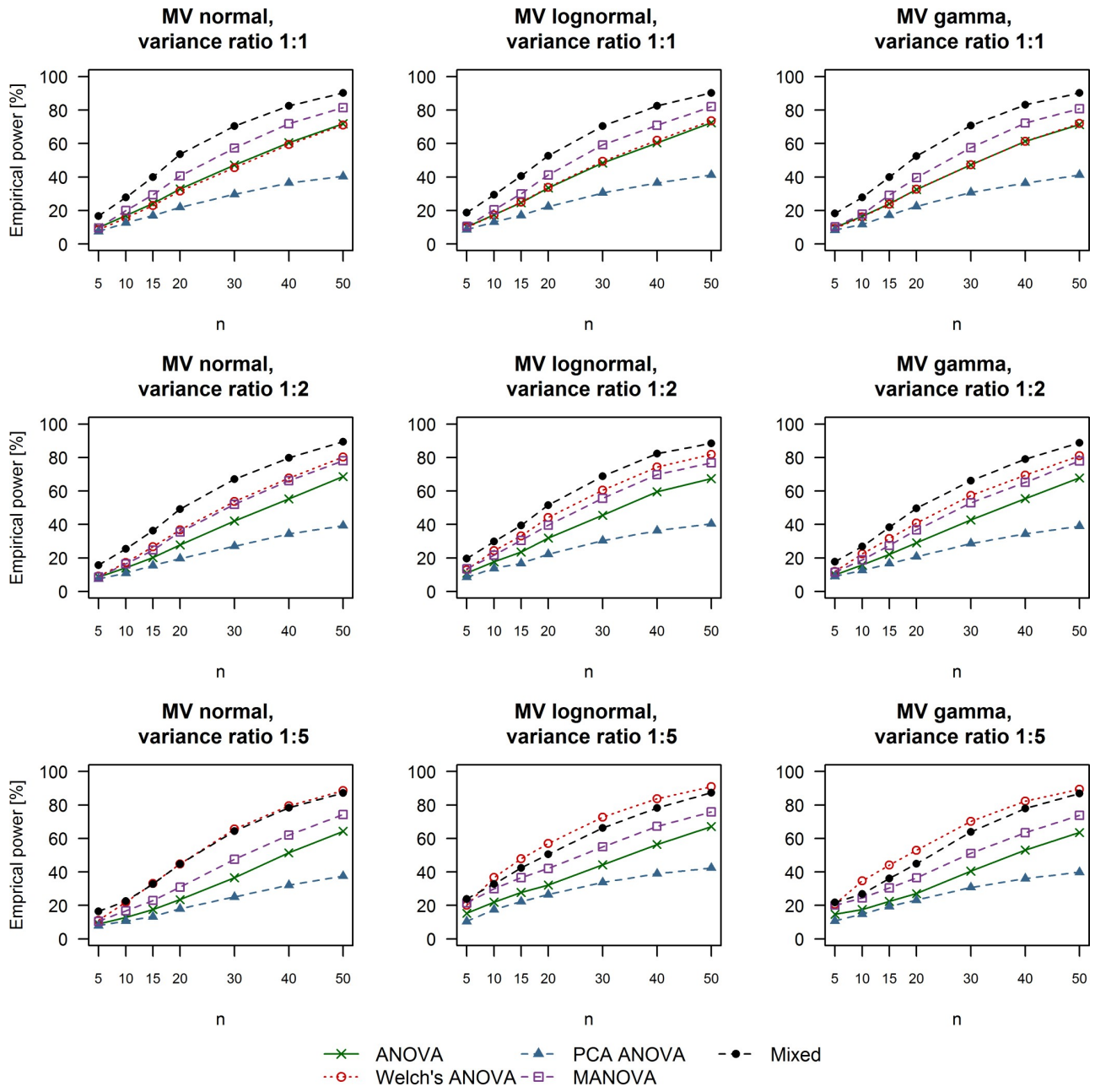

Fig 4. Empirical power of univariate and multivariate techniques in case of moderate treatment effects (Cohen's d equal to 0.5). The multivariate distribution from which the data were drawn as well as the variance ratio between simulated control and treatment groups are summarized in the title of each respective plot. ANOVA: Analysis of variance; MANOVA: Multivariate analysis of variance; Mixed: Linear mixed effects model; MV: Multivariate; PCA: Principal component analysis.

https://doi.org/10.1371/journal.pone.0230798.g004

A practical example of applying ordination techniques and statistical testing methods

In order to give an example of how ordination techniques can be combined with statistical testing methods in practice, we simulated a data set with 5 variables per group and huge treatment effects for 9 out of the total 18 variables which we randomly selected. The endpoints with

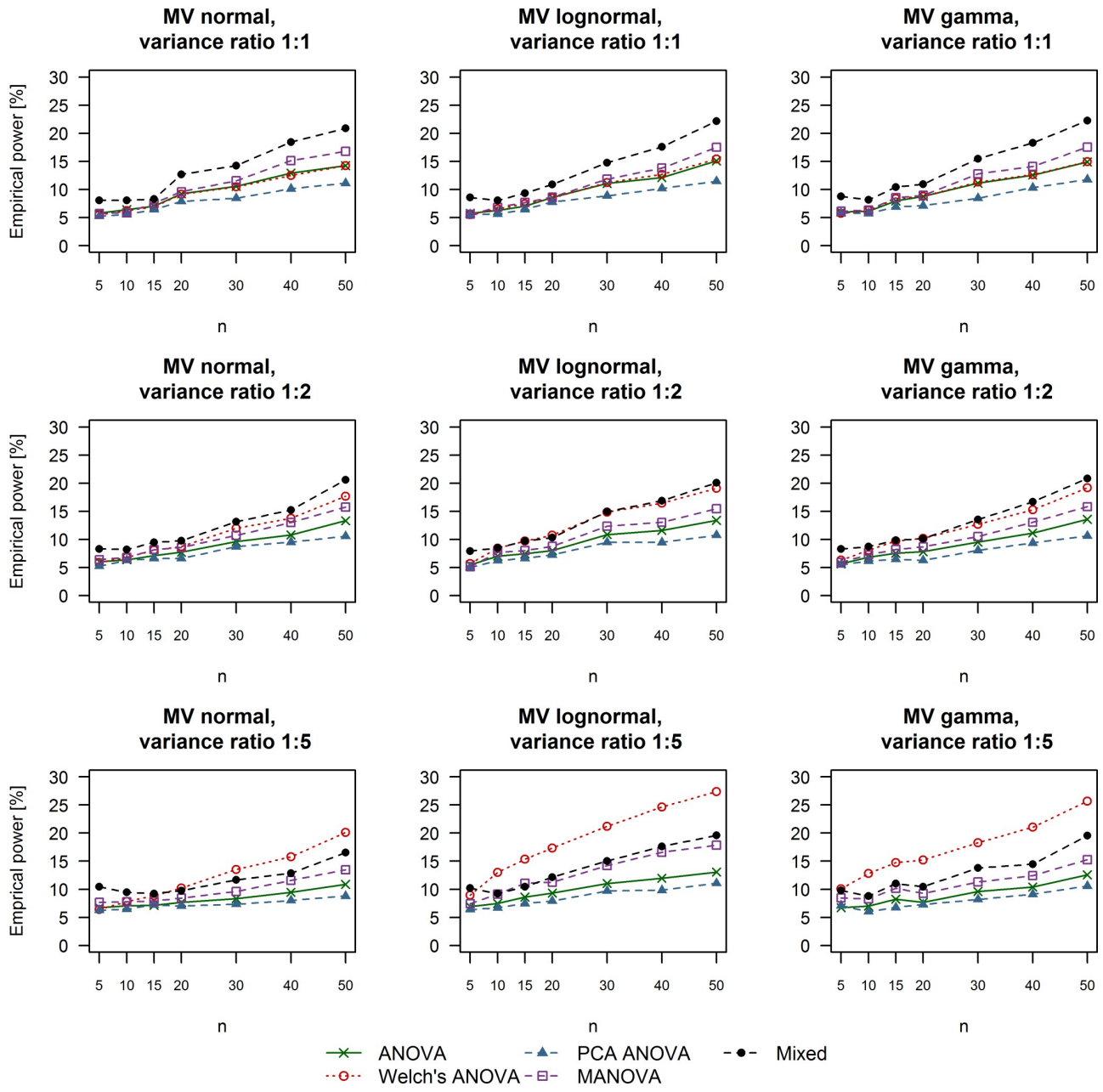

Fig 5. Empirical power of univariate and multivariate techniques in case of small treatment effects (Cohen's d equal to 0.2). The multivariate distribution from which the data were drawn as well as the variance ratio between simulated control and treatment groups are summarized in the title of each respective plot. ANOVA: Analysis of variance; MANOVA: Multivariate analysis of variance; Mixed: Linear mixed effects model; MV: Multivariate; PCA: Principal component analysis.

https://doi.org/10.1371/journal.pone.0230798.g005

simulated treatment effects were 20-point neuroscore on day 1 and day 7, limb placing score on day 1 and day 7, lesion volume on day 1 and day 7, edema volume on day 1 and day 14 and T2 lesion in the contralateral cortex on day 1. The remaining 9 variables were drawn from the same distributions in the control and the 3 treatment groups without simulated treatment effects.

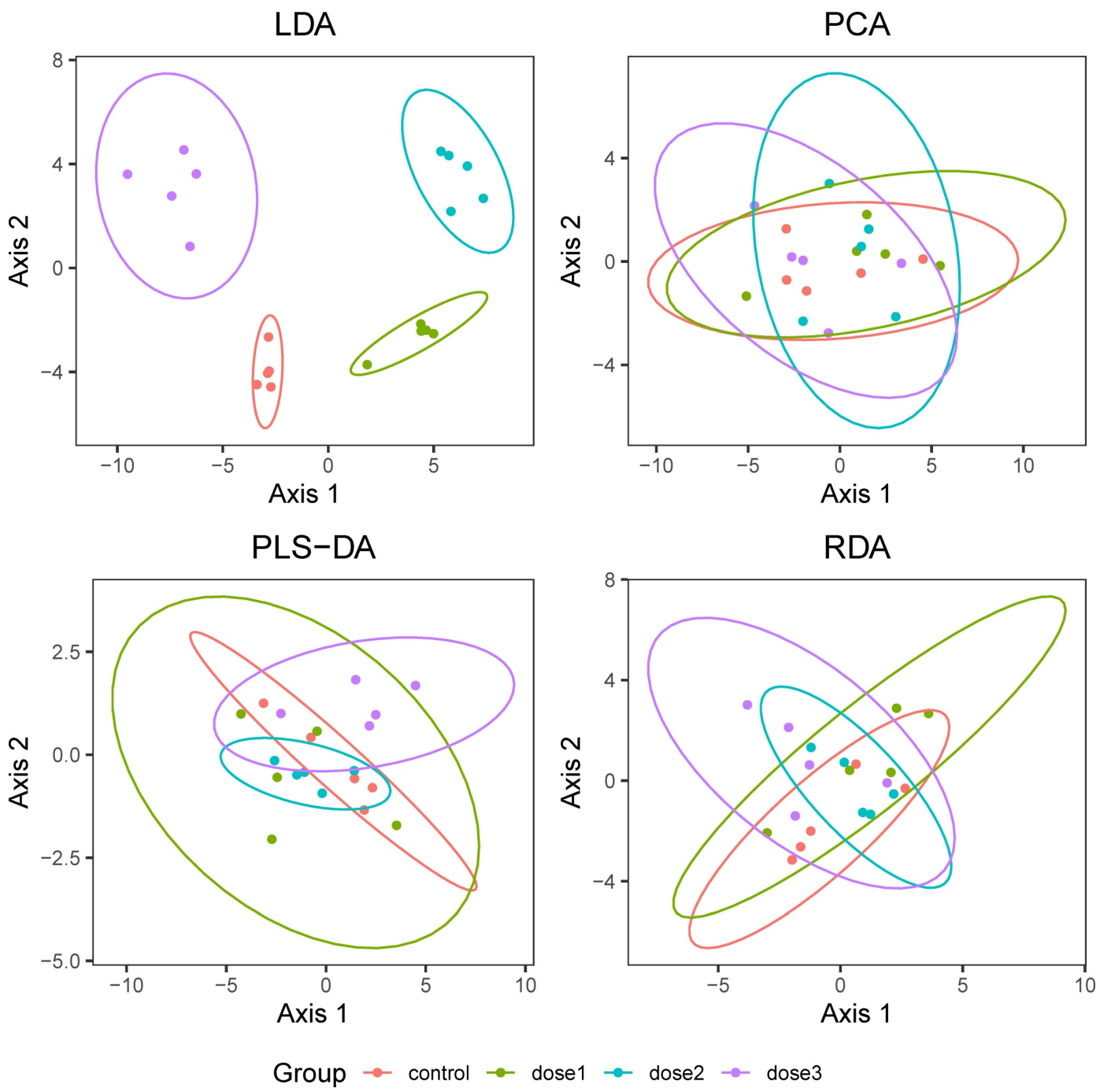

Fig 6. Comparison of ordination techniques for pattern analysis in the case when no treatment effects were simulated. Plots show results for one out of 1000 simulations with 5 measurements per group drawn from a multivariate normal distribution with equal variance between control and treatment groups. The ordination technique was considered to falsely capture a treatment effect pattern in the data in case of non-overlapping 95% confidence ellipse of the control group with the confidence ellipses for the treatment groups (dose1 to dose3). LDA: Linear discriminant analysis; PCA: Principal component analysis; PLS-DA: Partial least squares discriminant analysis; RDA; Redundancy analysis.

https://doi.org/10.1371/journal.pone.0230798.g006

In the first step of the analysis, we applied PLS-DA which was the most sensitive technique in our simulations to investigate if the control group differed from the treatment groups in

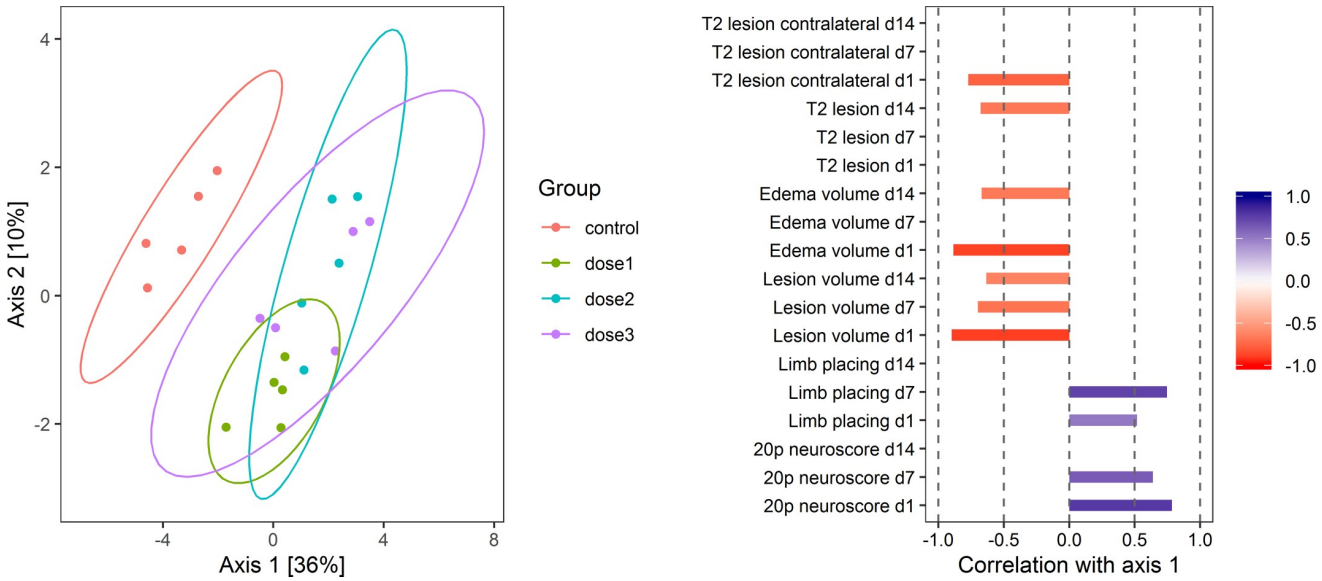

Fig 7. Partial least squares discriminant analysis (PLS-DA) to identify treatment effect patterns. We simulated a data set with 5 measurements per group and huge treatment effects for 9 randomly selected endpoints out of the 18 variables in the data set. The control group was separated from the treatment groups along the first multivariate dimension in the PLS-DA analysis We calculated the correlation of the original variables with this dimension to identify which original endpoints explained the multivariate pattern. Correlations with an absolute value below 0.5 were set to 0 in order to filter out unimportant variables. All 9 variables with simulated treatment effects were significantly correlated with the first multivariate axis. Two additional variables without simulated treatment effects (lesion volume at day 14 and T2 lesion at day 14) were also significantly correlated with the first multivariate axis.

https://doi.org/10.1371/journal.pone.0230798.g007

reduced multivariate space. We observed that the control group was separated from the treatment groups along the first multivariate axis which accounted for 36% of the variance (Fig 7). In order to investigate which of the original variables are responsible for group separation, we calculated the correlations of the original variables with the first PLS-DA multivariate dimension (axis 1) along which the control and treatment groups were separated. Correlations with an absolute value below 0.5 were set to 0 in order to filter out unimportant variables. The correlation pattern indicated that all variables with simulated treatment effects along with two additional variables (lesion volume at day 14 and T2 lesion at day 14) contributed to the separation of the control from the treatment groups. Therefore, PLS-DA managed to capture the treatment effect pattern by identifying all original variables with simulated treatment effects as important for group separation in reduced space.

Next, we followed up on the multivariate pattern analysis by performing statistical testing with linear mixed effects models for each variable with repeated measures. The interaction term between treatment and time was highly significant for all six endpoints thereby rejecting H_0 of no treatment effects even for T2 lesion, which was the only variable without any simulated treatment effects at any time point. Next, we performed post-hoc analysis comparing the treatment groups against the control group for each time point separately. Results are shown in Table 1. The difference for the 20-point neuroscore was significant only between treatment groups 2 and 3 compared to the control group and no statistically significant difference was detected for 20-point neuroscore at day 7. Similarly, post-hoc analysis did not detect a treatment effect for any of the groups for lesion volume at day 7 and edema volume at day 14. In contrast, all treatment effects were identified for lesion volume at day 1, edema volume at day 1 and T2 lesion in the contralateral cortex at day 1.

The difference between the control and treatment groups 2 and 3 for T2 lesion at day 14 was reported as significant even though we did not simulate treatment effects for this variable.

Table 1. Post-hoc analysis following linear mixed effects models for variables with repeated measures.

Variable	Control vs. dose 1	Control vs. dose 2	Control vs. dose 3
20 point neuroscore day 1	0.51	**0.0001**	**0.0027**
20 point neuroscore day 7	0.293	0.095	0.074
20 point neuroscore day 14	0.688	0.593	0.354
Limb placing score day 1	1.000	0.483	**0.047**
Limb placing score day 7	0.298	**0.033**	**0.047**
Limb placing score day 14	0.297	0.483	0.383
Lesion volume day 1	**<0.0001**	**<0.0001**	**<0.0001**
Lesion volume day 7	0.119	0.117	0.131
Lesion volume day 14	0.778	0.332	0.487
Edema volume day 1	**0.0002**	**<0.0001**	**<0.0001**
Edema volume day 7	0.266	0.494	0.824
Edema volume day 14	0.129	0.122	0.087
T2 lesion day 1	0.309	0.338	0.453
T2 lesion day 7	0.826	0.627	0.827
T2 lesion day 14	0.203	**0.001**	**0.05**
T2 lesion contralateral cortex day 1	**0.004**	**0.0005**	**<0.0001**
T2 lesion contralateral cortex day 7	0.230	0.286	0.316
T2 lesion contralateral cortex day 14	0.828	0.201	0.529

We performed linear mixed effects analysis for each endpoint with repeated measures followed by post-hoc pairwise comparisons between the control and each treatment group for each time point separately. Variables with simulated treatment effects are highlighted with a bold font. The p-values from the post-hoc comparisons are reported in the table. P-values less than 0.05 are highlighted with a bold font.

https://doi.org/10.1371/journal.pone.0230798.t001

Altogether, post-hoc analysis following linear mixed effects models captured most but not all individual differences between the control and treatment groups. In contrast, the multivariate pattern analysis using PLS-DA marked all variables with simulated treatment effects as important for group separation in reduced multivariate space.

Discussion

Using Monte Carlo simulations, we evaluated the performance of a number of univariate and multivariate techniques in an effort to identify the most optimal strategy for detecting treatment effects in preclinical neurotrauma studies.

Importantly, type I error rate was not drastically inflated beyond the 5% nominal rate for all hypothesis testing methods under the simulation scenarios we investigated, even when assumptions of normality and homogeneity of variance were violated. Nevertheless, we only simulated a maximal variance inequality ratio of 1:5 between control and treatment group. Moreover, sample size was always equal. Extreme heterogeneity is more problematic in case of unequal group sizes especially when the smallest group exhibits the largest variance [38]. In such cases, a variance-stabilizing transformation such as log-transformation of the response variables is advisable. Alternatively, in the univariate case, a non-parametric technique might be used (e.g. Friedman or Kruskal-Wallis test). In case that MANOVA is performed, a more robust statistic might be chosen. Our results suggest that Pillai's trace would be the most appropriate under these conditions.

In terms of power, taking the repeated measures nature of the data into account proved to be the optimal strategy as linear mixed effects models outperformed the other methods when variance between groups was equal or when variance heterogeneity was moderate. Linear

mixed effects are a flexible class of statistical methods which allow building models of increasing complexity with different combinations of random intercepts and slopes. In practice, however, it might be challenging to assess the significance of fixed effects in the model based on F-tests as the degrees of freedom might not be correctly estimated. In our current study, we used the Kenward-Roger approximation for determining the degrees of freedom [39]. Alternatively, likelihood ratio tests might be used in order to test if including the factor of interest significantly improves the model fit compared to a model without the specific factor. Importantly, this requires refitting the linear mixed effects model using maximum likelihood to estimate parameters as usually these models are calculated using restricted maximum likelihood.

When the assumptions of normality and homogeneity of variance were violated, univariate Welch's ANOVA tests outperformed the remaining methods especially with small effect sizes. Furthermore, the rate of rejecting H_0 was equivalent to that of standard ANOVA when data were sampled from a multivariate normal distribution with equal variance between groups. These results suggest that Welch's ANOVA might be more appropriate for statistical testing of treatment effects than the much more popular standard ANOVA F-test. Additionally, univariate methods offer the advantage of directly investigating differences on endpoints of interest whereas multivariate tests are applied on a linear combination of the original variables. Nevertheless, ignoring the correlation structure of the response variables may result in misleading conclusions. Correlated variables reflect overlapping variance and therefore univariate tests provide little information about the unique contribution of each dependent variable [30].

The issue of correlated outcome measures is addressed by employing multivariate methods. When differences are evaluated between groups which are known a priori, MANOVA is the technique of choice. In our study, MANOVA offered a marginally higher power than univariate ANOVAs when the assumption of variance homogeneity was met. However, a practical issue of this method is that standard software reports four different statistics which do not always provide compatible results. Under all simulation conditions we investigated, Roy's largest root was associated with an unacceptably high type I error rate. This would make interpretation of results with real high-dimensional data sets with few measurements per variable very ambiguous. However, Wilks' lambda, Lawley-Hotelling trace and Pillai's trace were robust to false positives. In agreement with previous reports, Pillai's criterion was the most conservative, which would make it more appropriate when assumptions of MANOVA are violated [40, 41]. Nevertheless, we opted to use Wilks' lambda for subsequent comparisons between different techniques because it offered similar robustness but slightly increased power. Another trade-off of MANOVA and multivariate techniques in general is the complexity of interpretation. If the omnibus test is significant, a researcher will often want to more precisely identify the variables which are responsible for group separation. Ideally, follow-up tests should retain the multivariate nature of the analysis. Such strategies include descriptive discriminant analysis [30, 42] or Roy-Bargmann stepdown analysis [30, 43].

A crucial factor we did not consider in our study is missing data which cannot be handled by multivariate statistical methods. If the degree of missingness is within a reasonable range (e.g. not more than 10%) and the assumption of missing at random is satisfied, then a multiple imputation technique might be employed to estimate the missing data from the existing measurements. Otherwise, a more flexible data analysis method must be employed such as for instance linear mixed effects models, which are able to handle missing data.

Since MANOVA only very marginally outperformed univariate ANOVAs and failed to provide an increase of power compared to linear mixed effects models, we believe that this does not offset the increased complexity and inability to handle missing data. Therefore, our results would suggest that MANOVA tests are not a practical option for formal hypothesis testing in preclinical studies with small sample sizes.

It is important to note that different methods achieved acceptable levels of power of around 80% only when we simulated large treatment effects with 20 measurements per group or moderate effects with at least 40 replicates per group. This finding highlights a serious issue not only in neurotrauma models but in preclinical research altogether, namely that typical sample sizes in animal studies do not ensure adequate power unless the effect size is large. Accordingly, some authors argue that animal studies should more closely adhere to the standards for study conduct and reporting applicable to controlled clinical trials [1, 44]. In a randomized clinical study, sample size is calculated a priori based on a specific effect size, assumptions about the variance in the response variable, and the desired level of power. In theory, the ARRIVE guidelines which were developed in order to improve the quality of study conduct and reporting of animal trials [45] as well as animal welfare authorities [46] require formal justification for sample size selection. Group size should be appropriate to detect a certain effect with adequate power while simultaneously ensuring that no more animals than necessary are used [46]. In practice, power calculations for preclinical trials are challenging for a number of reasons. For instance, information about the variance in the response variable might not be available a priori, however this issue might be tackled by performing a small scale pilot study. Another problem may be that the estimated effect is small while the variance in the selected endpoint is high, which results in such large group sizes that might not be acceptable for animal welfare regulators. One possible way to address this problem is to identify methods which are associated with higher power in small samples or try to reduce the variability in the response variables by possibly including other covariates in the analysis [47]. A recent development in the effort to increase power of animal studies includes performing systematic reviews and meta-analysis of existing studies [48]. This approach is well established in clinical research and it allows scientists to appraise estimated effect sizes more systematically and put them in the context of existing reports. The majority of preclinical meta-analyses which have been performed in the field of neurotrauma so far are related to experimental stroke (e.g. [49–54]). However pre-clinical meta-analyses on e.g. spinal cord injury [55, 56] and subarachnoid hemorrhage [57] have also been published.

However, since a meta-analysis is not always practicable, especially when a novel study is conducted, we investigated if ordination techniques might be useful to detect treatment effect patterns with small sample sizes. Multivariate techniques classically rely on data sets consisting of more observations than variables, which is not always the case in animal studies especially in the omics era. Therefore, we first evaluated if LDA, PCA, PLS-DA, or RDA falsely report non-existing patterns in simulated data sets without treatment effects. With 5 measurements per group and 18 variables, LDA was associated with a false positive rate of 38.7% while PCA, PLS-DA, and RDA did not capture false patterns in the data. The extreme over-fitting we observed for LDA is due to multicollinearity in the data set (see S1 Appendix of Table 2 for the correlation matrix used for simulating multivariate data sets) combined with a small sample size [58]. While this is not necessarily a novel finding, our simulation results highlight the dangers of carelessly applying a dimensionality reducing technique to multivariate data sets with more variables than measurements, which often leads to false inferences. In contrast, PCA is capable of overcoming the "large p, small n" problem by reducing the large number of variables to a few uncorrelated components. The method only imposes the constraint that the first component captures the direction of greatest variance in the data hyper-ellipsoid [32] and does not perform regression or classification of data. Therefore multicollinearity poses no issue. However, group assignment is ignored and so differences between groups do not necessarily become apparent in reduced space. RDA is the supervised version of PCA and it imposes the constrain that the dependent variables in reduced space are linear combinations of the grouping variable. Surprisingly, RDA demonstrated only a slightly increased sensitivity to

detect true treatment effect patterns in our simulations compared to PCA. Conversely, PLS-DA clearly outperformed both PCA and RDA. Although PLS-DA uses the quantitative variables to predict group membership similarly to classical LDA, classification is performed after dimensionality reduction [59]. PLS-DA thereby overcomes the problem of multicollinearity and simultaneously tries to maximize group differences, which was the most effective strategy in our simulations. Nevertheless, differences between methods only became apparent when we simulated huge treatment effects (Cohen's d equal to 2.0). However, in our practical example of combining ordination techniques with statistical testing methods to investigate treatment effects, PLS-DA managed to identify all variables with simulated treatment effects as important for the observed multivariate pattern. Follow-up statistical tests did not capture all differences successfully. PLS-DA might therefore be a useful strategy to preselect important endpoints for targeted statistical testing with the goal of reducing the overall number of tests.

Conclusion

Assessing therapeutic success in preclinical neurotrauma studies remains challenging when small samples are combined with small effect sizes. Our simulation study demonstrated that linear mixed effects models offer a slightly increased power in case of equal variance whereas Welch's ANOVA should be used when homogeneity of variance is not present. Additionally, PLS-DA offers a higher sensitivity to detect treatment effect patterns than PCA and RDA, whereas classical LDA leads to overfitting and false inferences in multivariate data sets with few measurements per group. Although we based our simulation on a real neurotrauma preclinical study, our findings might be more generally applicable to multivariate data sets with a similar correlation structure as we applied standardized measures of effect sizes which are not restricted to a specific endpoint or type of study.

Ultimately, translational success of animal trials in neurotrauma would greatly benefit from appropriate sample size calculation prior to conduct of the study. When this is not feasible, it is advantageous to re-evaluate estimates of treatment effect with combined evidence from existing studies (if available) by performing systematic reviews and meta-analyses.

Supporting information

S1 Appendix. The file contains the mean and variance vector of the simulated control group and the correlation matrix used to sample data from multivariate distributions under different simulation scenarios. Figs 1–4 show comparisons of type I error rate and empirical power of the four different multivariate statistics used to evaluate the significance of MANOVA tests.
(PDF)

S2 Appendix. Comparison of ordination techniques to detect treatment effect patterns when no treatment effects were simulated. The file contains the results from 1000 simulated data sets without treatment effects, 5 measurements per group with data obtained from a multivariate normal distribution with equal variance in all groups. LDA, PCA, RDA, or PLS-DA were considered to falsely capture a non-existing treatment effect pattern if the 95% confidence ellipse around the control group did not overlap with the confidence ellipses of treatment groups (dose1 to dose3).
(PDF)

S3 Appendix. Comparison of ordination techniques to detect treatment effect patterns with huge simulated treatment effects (Cohen's d equal to 2.0). The file contains results from 1000 simulated data sets with 5 measurements per group and data obtained from a

multivariate normal distribution with equal variance in all groups. PCA, RDA, or PLS-DA were considered to correctly capture a treatment effect pattern if the 95% confidence ellipse around the control group did not overlap with the confidence ellipses of the treatment groups (dose 1 to dose3).
(PDF)

Author Contributions

Conceptualization: Susanne Gerber.

Data curation: Hristo Todorov.

Formal analysis: Hristo Todorov.

Investigation: Hristo Todorov.

Methodology: Hristo Todorov.

Supervision: Susanne Gerber.

Validation: Emily Searle-White.

Visualization: Hristo Todorov.

Writing – original draft: Hristo Todorov.

Writing – review & editing: Emily Searle-White, Susanne Gerber.

References

1. Everitt JI. The Future of Preclinical Animal Models in Pharmaceutical Discovery and Development: A Need to Bring In Cerebro to the In Vivo Discussions. Toxicologic Pathology. 2014; 43(1):70–7. https://doi.org/10.1177/0192623314555162 PMID: 25351920
2. Kropf S, Hothorn LA, Läuter J. Multivariate many-to-one procedures with applications to preclinical trials. Drug Information Journal. 1997; 31:433–47.
3. Ferguson AR, Irvine K-A, Gensel JC, Nielson JL, Lin A, Ly J, et al. Derivation of Multivariate Syndromic Outcome Metrics for Consistent Testing across Multiple Models of Cervical Spinal Cord Injury in Rats. PLOS ONE. 2013; 8(3):e59712. https://doi.org/10.1371/journal.pone.0059712 PMID: 23544088
4. Ferguson AR, Stück ED, Nielson JL. Syndromics: A Bioinformatics Approach for Neurotrauma Research. Translational Stroke Research. 2011; 2(4):438–54. https://doi.org/10.1007/s12975-011-0121-1 PMC3236294. PMID: 22207883
5. Nielson JL, Paquette J, Liu AW, Guandique CF, Tovar CA, Inoue T, et al. Topological data analysis for discovery in preclinical spinal cord injury and traumatic brain injury. Nature Communications. 2015; 6:8581. https://doi.org/10.1038/ncomms9581 https://www.nature.com/articles/ncomms9581#supplementary-information. PMID: 26466022
6. Nielson JL, Guandique CF, Liu AW, Burke DA, Lash AT, Moseanko R, et al. Development of a Database for Translational Spinal Cord Injury Research. Journal of Neurotrauma. 2014; 31(21):1789–99. https://doi.org/10.1089/neu.2014.3399 PMC4186058. PMID: 25077610
7. Nielson JL, Haefeli J, Salegio EA, Liu AW, Guandique CF, Stück ED, et al. Leveraging biomedical informatics for assessing plasticity and repair in primate spinal cord injury. Brain research. 2015; 1619:124–38. https://doi.org/10.1016/j.brainres.2014.10.048 PMC4418964. PMID: 25451131
8. Couillard-Despres S, Bieler L, Vogl M. Pathophysiology of Traumatic Spinal Cord Injury. In: Weidner N, Rupp R, Tansey K, editors. Neurological Aspects of Spinal Cord Injury: Springer; 2017.
9. Frizzell JP. Acute Stroke: Pathophysiology, Diagnosis, and Treatment. AACN Advanced Critical Care. 2005; 16(4):421–40.
10. Lee J, Thumbikat P. Pathophysiology, presentation and management of spinal cord injury. Surgery (Oxford). 2015; 33(6):238–47. https://doi.org/10.1016/j.mpsur.2015.04.003.
11. Prins M, Greco T, Alexander D, Giza CC. The pathophysiology of traumatic brain injury at a glance. Disease Models & Mechanisms. 2013; 6(6):1307–15. https://doi.org/10.1242/dmm.011585 PMC3820255. PMID: 24046353

12. Crowe MJ, Bresnahan JC, Shuman SL, Masters JN, Crowe MS. Apoptosis and delayed degeneration after spinal cord injury in rats and monkeys. Nature Medicine. 1997; 3:73. https://doi.org/10.1038/nm0197-73 PMID: 8986744

13. Liu XZ, Xu XM, Hu R, Du C, Zhang SX, McDonald JW, et al. Neuronal and Glial Apoptosis after Traumatic Spinal Cord Injury. The Journal of Neuroscience. 1997; 17(14):5395. https://doi.org/10.1523/JNEUROSCI.17-14-05395.1997 PMID: 9204923

14. Beck KD, Nguyen HX, Galvan MD, Salazar DL, Woodruff TM, Anderson AJ. Quantitative analysis of cellular inflammation after traumatic spinal cord injury: evidence for a multiphasic inflammatory response in the acute to chronic environment. Brain. 2010; 133(2):433–47. https://doi.org/10.1093/brain/awp322 PMC2858013. PMID: 20085927

15. Kigerl KA, McGaughy VM, Popovich PG. A Comparative Analysis of Lesion Development and Intraspinal Inflammation in Four Strains of Mice Following Spinal Contusion Injury. The Journal of comparative neurology. 2006; 494(4):578–94. https://doi.org/10.1002/cne.20827 PMC2655318. PMID: 16374800

16. Lisa S, Sara F, Henry K, SM E., Hugh PV. Acute inflammatory responses to mechanical lesions in the CNS: differences between brain and spinal cord. European Journal of Neuroscience. 1999; 11(10):3648–58. https://doi.org/10.1046/j.1460-9568.1999.00792.x PMID: 10564372

17. HJC E., PJ V., Hugh PV, M-TA T. Docosahexaenoic acid, but not eicosapentaenoic acid, reduces the early inflammatory response following compression spinal cord injury in the rat. Journal of Neurochemistry. 2012; 121(5):738–50. https://doi.org/10.1111/j.1471-4159.2012.07726.x PMID: 22404382

18. Huang WL, King VR, Curran OE, Dyall SC, Ward RE, Lal N, et al. A combination of intravenous and dietary docosahexaenoic acid significantly improves outcome after spinal cord injury. Brain. 2007; 130(11):3004–19. https://doi.org/10.1093/brain/awm223 PMID: 17901087

19. Azbill RD, Mu X, Bruce-Keller AJ, Mattson MP, Springer JE. Impaired mitochondrial function, oxidative stress and altered antioxidant enzyme activities following traumatic spinal cord injury. Brain Research. 1997; 765(2):283–90. https://doi.org/10.1016/s0006-8993(97)00573-8 PMID: 9313901

20. Singh IN, Sullivan PG, Deng Y, Mbye LH, Hall ED. Time Course of Post-Traumatic Mitochondrial Oxidative Damage and Dysfunction in a Mouse Model of Focal Traumatic Brain Injury: Implications for Neuroprotective Therapy. Journal of Cerebral Blood Flow & Metabolism. 2006; 26(11):1407–18. https://doi.org/10.1038/sj.jcbfm.9600297 PMID: 16538231

21. Resnick DK, Schmitt C, Miranpuri GS, Dhodda VK, Isaacson J, Vemuganti R. Molecular evidence of repair and plasticity following spinal cord injury. NeuroReport. 2004; 15(5):837–9. 00001756-200404090-00020. https://doi.org/10.1097/00001756-200404090-00020 PMID: 15073526

22. Rosenzweig ES, Courtine G, Jindrich DL, Brock JH, Ferguson AR, Strand SC, et al. Extensive Spontaneous Plasticity of Corticospinal Projections After Primate Spinal Cord Injury. Nature neuroscience. 2010; 13(12):1505–10. https://doi.org/10.1038/nn.2691 PMC3144760. PMID: 21076427

23. Sutherland BA, Minnerup J, Balami JS, Arba F, Buchan AM, Kleinschnitz C. Neuroprotection for Ischaemic Stroke: Translation from the Bench to the Bedside. International Journal of Stroke. 2012; 7(5):407–18. https://doi.org/10.1111/j.1747-4949.2012.00770.x PMID: 22394615.

24. Kim Y-H, Ha K-Y, Kim S-I. Spinal Cord Injury and Related Clinical Trials. Clinics in Orthopedic Surgery. 2017; 9(1):1–9. https://doi.org/10.4055/cios.2017.9.1.1 PMC5334017. PMID: 28261421

25. Hurlbert RJ, Hadley MN, Walters BC, Aarabi B, Dhall SS, Gelb DE, et al. Pharmacological Therapy for Acute Spinal Cord Injury. Neurosurgery. 2013; 72(suppl_3):93–105. https://doi.org/10.1227/NEU.0b013e31827765c6 PMID: 23417182

26. Maas AIR, Roozenbeek B, Manley GT. Clinical trials in traumatic brain injury: Past experience and current developments. Neurotherapeutics. 2010; 7(1):115–26. https://doi.org/10.1016/j.nurt.2009.10.022 PMC5084118. PMID: 20129503

27. Team RC. R: A Language and Environment for Statistical Computing. Vienna, Austria: R Foundation for Statistical Computing; 2017.

28. Burton A, Altman DG, Royston P, Holder RL. The design of simulation studies in medical statistics. Statistics in Medicine. 2006; 25(24):4279–92. https://doi.org/10.1002/sim.2673 PMID: 16947139

29. Cohen J. Statistical power analysis for the behavioural sciences. 2 ed. USA: Lawrence Erlbaum Associates; 1988.

30. Tabachnick B, Fidell L. Using multivariate statistics. 6 ed. Essex: Pearson Education, Ltd.; 2014.

31. Welch BL. On the Comparison of Several Mean Values: An Alternative Approach. Biometrika. 1951; 38(3/4):330–6. https://doi.org/10.2307/2332579

32. Todorov H, Fournier D, Gerber S. Principal components analysis: theory and application to gene expression data analysis. Genomics and Computational Biology. 2018; 4(2):e100041. https://doi.org/10.18547/gcb.2018.vol4.iss2.e100041

33. Kaiser HF. The Application of Electronic Computers to Factor Analysis. Educational and Psychological Measurement. 1960; 20(1):141–51. https://doi.org/10.1177/001316446002000116

34. Wilks SS. Certain Generalizations in the Analysis of Variance. Biometrika. 1932; 24(3/4):471–94. https://doi.org/10.2307/2331979

35. Hotelling H, editor A Generalized T Test and Measure of Multivariate Dispersion. Proceedings of the Second Berkeley Symposium on Mathematical Statistics and Probability; 1951 1951; Berkeley, Calif.: University of California Press.

36. Pillai KCS. Some New Test Criteria in Multivariate Analysis. The Annals of Mathematical Statistics. 1955; 26(1):117–21.

37. Roy SN. On a Heuristic Method of Test Construction and its use in Multivariate Analysis. Ann Math Statist. 1953; 24(2):220–38. https://doi.org/10.1214/aoms/1177729029

38. Blanca MJ, Alarcón R, Arnau J, Bono R, Bendayan R. Effect of variance ratio on ANOVA robustness: Might 1.5 be the limit? Behavior Research Methods. 2018; 50(3):937–62. https://doi.org/10.3758/s13428-017-0918-2 PMID: 28643157

39. Kenward MG, Roger JH. Small Sample Inference for Fixed Effects from Restricted Maximum Likelihood. Biometrics. 1997; 53(3):983–97. https://doi.org/10.2307/2533558 PMID: 9333350

40. Olson CL. On choosing a test statistic in multivariate analysis of variance. Psychological Bulletin. 1976; 83(4):579–86. https://doi.org/10.1037/0033-2909.83.4.579

41. Olson CL. Practical considerations in choosing a MANOVA test statistic: A rejoinder to Stevens. Psychological Bulletin. 1979; 86(6):1350–2. https://doi.org/10.1037/0033-2909.86.6.1350

42. Warne R. A Primer on Multivariate Analysis of Variance (MANOVA) for Behavioral Scientists. Practical Assessment, Research & Evaluation. 2014; 19(17).

43. Finch H. Performance of the Roy-Bargmann Stepdown Procedure as a Follow Up to a Significant MANOVA. Multiple Linear Regression Viewpoints. 2007; 33(1):12–22.

44. Muhlhausler BS, Bloomfield FH, Gillman MW. Whole Animal Experiments Should Be More Like Human Randomized Controlled Trials. PLOS Biology. 2013; 11(2):e1001481. https://doi.org/10.1371/journal.pbio.1001481 PMID: 23424284

45. Kilkenny C, Browne WJ, Cuthill IC, Emerson M, Altman DG. Improving Bioscience Research Reporting: The ARRIVE Guidelines for Reporting Animal Research. PLOS Biology. 2010; 8(6):e1000412. https://doi.org/10.1371/journal.pbio.1000412 PMID: 20613859

46. Fitts DA. Ethics and Animal Numbers: Informal Analyses, Uncertain Sample Sizes, Inefficient Replications, and Type I Errors. Journal of the American Association for Laboratory Animal Science: JAALAS. 2011; 50(4):445–53. PMC3148647. PMID: 21838970

47. Laajala TD, Jumppanen M, Huhtaniemi R, Fey V, Kaur A, Knuuttila M, et al. Optimized design and analysis of preclinical intervention studies in vivo. Scientific Reports. 2016; 6:30723. https://doi.org/10.1038/srep30723 https://www.nature.com/articles/srep30723#supplementary-information. PMID: 27480578

48. van Luijk J, Bakker B, Rovers MM, Ritskes-Hoitinga M, de Vries RBM, Leenaars M. Systematic Reviews of Animal Studies; Missing Link in Translational Research? PLOS ONE. 2014; 9(3):e89981. https://doi.org/10.1371/journal.pone.0089981 PMID: 24670965

49. Bath PMW, Gray LJ, Bath AJG, Buchan A, Miyata T, Green AR, et al. Effects of NXY-059 in experimental stroke: an individual animal meta-analysis. British journal of pharmacology. 2009; 157(7):1157–71. Epub 2009/04/27. https://doi.org/10.1111/j.1476-5381.2009.00196.x PMID: 19422398.

50. Maysami S, Wong R, Pradillo JM, Denes A, Dhungana H, Malm T, et al. A cross-laboratory preclinical study on the effectiveness of interleukin-1 receptor antagonist in stroke. Journal of cerebral blood flow and metabolism: official journal of the International Society of Cerebral Blood Flow and Metabolism. 2016; 36(3):596–605. Epub 2015/09/30. https://doi.org/10.1177/0271678X15606714 PMID: 26661169.

51. McCann Sarah K, Irvine C, Mead Gillian E, Sena Emily S, Currie Gillian L, Egan Kieren E, et al. Efficacy of Antidepressants in Animal Models of Ischemic Stroke. Stroke. 2014; 45(10):3055–63. https://doi.org/10.1161/STROKEAHA.114.006304 PMID: 25184357

52. McCann SK, Cramond F, Macleod MR, Sena ES. Systematic Review and Meta-Analysis of the Efficacy of Interleukin-1 Receptor Antagonist in Animal Models of Stroke: an Update. Translational stroke research. 2016; 7(5):395–406. Epub 2016/08/15. https://doi.org/10.1007/s12975-016-0489-z PMID: 27526101.

53. Milidonis X, Marshall I, Macleod Malcolm R, Sena Emily S. Magnetic Resonance Imaging in Experimental Stroke and Comparison With Histology. Stroke. 2015; 46(3):843–51. https://doi.org/10.1161/STROKEAHA.114.007560 PMID: 25657177

54. Pedder H, Vesterinen Hanna M, Macleod Malcolm R, Wardlaw Joanna M. Systematic Review and Meta-Analysis of Interventions Tested in Animal Models of Lacunar Stroke. Stroke. 2014; 45(2):563–70. https://doi.org/10.1161/STROKEAHA.113.003128 PMID: 24385271

55. Batchelor PE, Wills TE, Skeers P, Battistuzzo CR, Macleod MR, Howells DW, et al. Meta-analysis of pre-clinical studies of early decompression in acute spinal cord injury: a battle of time and pressure. PloS one. 2013; 8(8):e72659–e. https://doi.org/10.1371/journal.pone.0072659 PMID: 24009695.

56. Watzlawick R, Sena ES, Dirnagl U, Brommer B, Kopp MA, Macleod MR, et al. Effect and Reporting Bias of RhoA/ROCK-Blockade Intervention on Locomotor Recovery After Spinal Cord Injury: A Systematic Review and Meta-analysisLocomotor Recovery After Spinal Cord InjuryLocomotor Recovery After Spinal Cord Injury. JAMA Neurology. 2014; 71(1):91–9. https://doi.org/10.1001/jamaneurol.2013.4684 PMID: 24297045

57. Laban KG, Vergouwen MDI, Dijkhuizen RM, Sena ES, Macleod MR, Rinkel GJE, et al. Effect of endothelin receptor antagonists on clinically relevant outcomes after experimental subarachnoid hemorrhage: a systematic review and meta-analysis. Journal of cerebral blood flow and metabolism: official journal of the International Society of Cerebral Blood Flow and Metabolism. 2015; 35(7):1085–9. Epub 2015/05/06. https://doi.org/10.1038/jcbfm.2015.89 PMID: 25944590.

58. Næs T, Mevik B-H. Understanding the collinearity problem in regression and discriminant analysis. Journal of Chemometrics. 2001; 15(4):413–26. https://doi.org/10.1002/cem.676

59. Barker M, Rayens W. Partial least squares for discrimination. Journal of Chemometrics. 2003; 17 (3):166–73. https://doi.org/10.1002/cem.785

2.2.1 Supplementary material to publication 2

Table S1: An overview of outcome measures from a traumatic brain injury rat model included in the simulation study. The mean and covariance vectors were obtained by averaging values from a non-parametric bootstrap with 10,000 samples drawn from the original animal study using the control group.

Nr.	Variable	Mean	Variance
1	20 point neuroscore day 1	15.862	2.612
2	20 point neuroscore day 7	18.446	1.304
3	20 point neuroscore day 14	19.196	1.337
4	Limb placing score day 1	8.78	4.62
5	Limb placing score day 7	11.057	2.945
6	Limb placing score day 14	12.504	1.917
7	Lesion volume day 1 [mm^3]	89.554	1169.808
8	Lesion volume day 7 [mm^3]	43.541	72.754
9	Lesion volume day 14 [mm^3]	24.852	147.991
10	Edema volume day 1 [mm^3]	46.448	696.146
11	Edema volume day 7 [mm^3]	16.926	136.323
12	Edema volume day 14 [mm^3]	14.295	103.103
13	T2 lesion day 1 [ms]	59.447	8.83
14	T2 lesion day 7 [ms]	54.58	5.888
15	T2 lesion day 14 [ms]	61.292	129.32
16	T2 lesion contralateral cortex day 1 [ms]	53.544	1.191
17	T2 lesion contralateral cortex day 7 [ms]	52.859	0.838
18	T2 lesion contralateral cortex day 14 [ms]	54.21	0.422

Table S2 Correlation matrix used for drawing samples from multivariate distributions. The matrix was calculated from the covariance matrix obtained from the non-parametric bootstrap procedure Positive correlations are colored red and negative correlations are colored blue. The numbering of columns and rows corresponds to the variables in Table S1.

	1	2	3	4	5	6	7	8	9	10	11	12	13	14	15	16	17	18
1	1	0.509	0.32	0.658	0.566	0.407	-0.318	-0.257	-0.194	-0.341	-0.208	0.106	-0.057	-0.44	-0.372	0.159	-0.202	-0.29
2	0.509	1	0.829	0.596	0.74	0.513	-0.42	-0.111	-0.511	-0.562	-0.142	0.481	-0.107	0.066	0.059	0.345	0.022	0.123
3	0.32	0.829	1	0.375	0.681	0.669	-0.709	-0.26	-0.558	-0.77	0.071	0.511	-0.3	0.032	-0.099	0.449	0.102	0.226
4	0.658	0.596	0.375	1	0.712	0.449	-0.262	-0.273	-0.17	-0.242	-0.191	0.105	0.034	-0.108	-0.065	0.034	0.086	-0.033
5	0.566	0.74	0.681	0.712	1	0.785	-0.644	-0.261	-0.538	-0.619	-0.02	0.39	-0.102	-0.03	-0.104	0.211	-0.011	-0.102
6	0.407	0.513	0.669	0.449	0.785	1	-0.649	-0.336	-0.326	-0.557	0.116	0.307	-0.055	0.052	-0.084	0.235	-0.009	0.067
7	-0.318	-0.42	-0.709	-0.262	-0.644	-0.649	1	0.354	0.656	0.907	-0.144	-0.45	0.566	0.27	0.415	0.044	0.144	0.04
8	-0.257	-0.111	-0.26	-0.273	-0.261	-0.336	0.354	1	0.378	0.239	0.11	-0.074	0.069	0.312	0.476	-0.002	0.038	-0.06
9	-0.194	-0.511	-0.558	-0.17	-0.538	-0.326	0.656	0.378	1	0.678	0.013	-0.297	0.248	0.357	0.519	0.063	0.244	-0.014
10	-0.341	-0.562	-0.77	-0.242	-0.619	-0.557	0.907	0.239	0.678	1	0.095	-0.418	0.63	0.319	0.412	-0.056	0.134	0.071
11	-0.208	-0.142	0.071	-0.191	-0.02	0.116	-0.144	0.11	0.013	0.095	1	0.321	0.13	0.537	0.177	0.017	0.227	0.002
12	0.106	0.481	0.511	0.105	0.39	0.307	-0.45	-0.074	-0.297	-0.418	0.321	1	-0.344	0.28	0.236	0.142	0.114	-0.134
13	-0.057	-0.107	-0.3	0.034	-0.102	-0.055	0.566	0.069	0.248	0.63	0.13	-0.344	1	0.282	0.315	0.153	-0.091	0.178
14	-0.44	0.066	0.032	-0.108	-0.03	0.052	0.27	0.312	0.357	0.319	0.537	0.28	0.282	1	0.81	0.066	0.476	0.097
15	-0.372	0.059	-0.099	-0.065	-0.104	-0.084	0.415	0.476	0.519	0.412	0.177	0.236	0.315	0.81	1	0.125	0.127	0.25
16	0.159	0.345	0.449	0.034	0.211	0.235	0.044	-0.002	0.063	-0.056	0.017	0.142	0.153	0.066	0.125	1	0.138	0.296
17	-0.202	0.022	0.102	0.086	-0.011	-0.009	0.144	0.038	0.244	0.134	0.227	0.114	-0.091	0.476	0.127	0.138	1	-0.245
18	-0.29	0.123	0.226	-0.033	-0.102	0.067	0.04	-0.06	-0.014	0.071	0.002	-0.134	0.178	0.097	0.25	0.296	-0.245	1

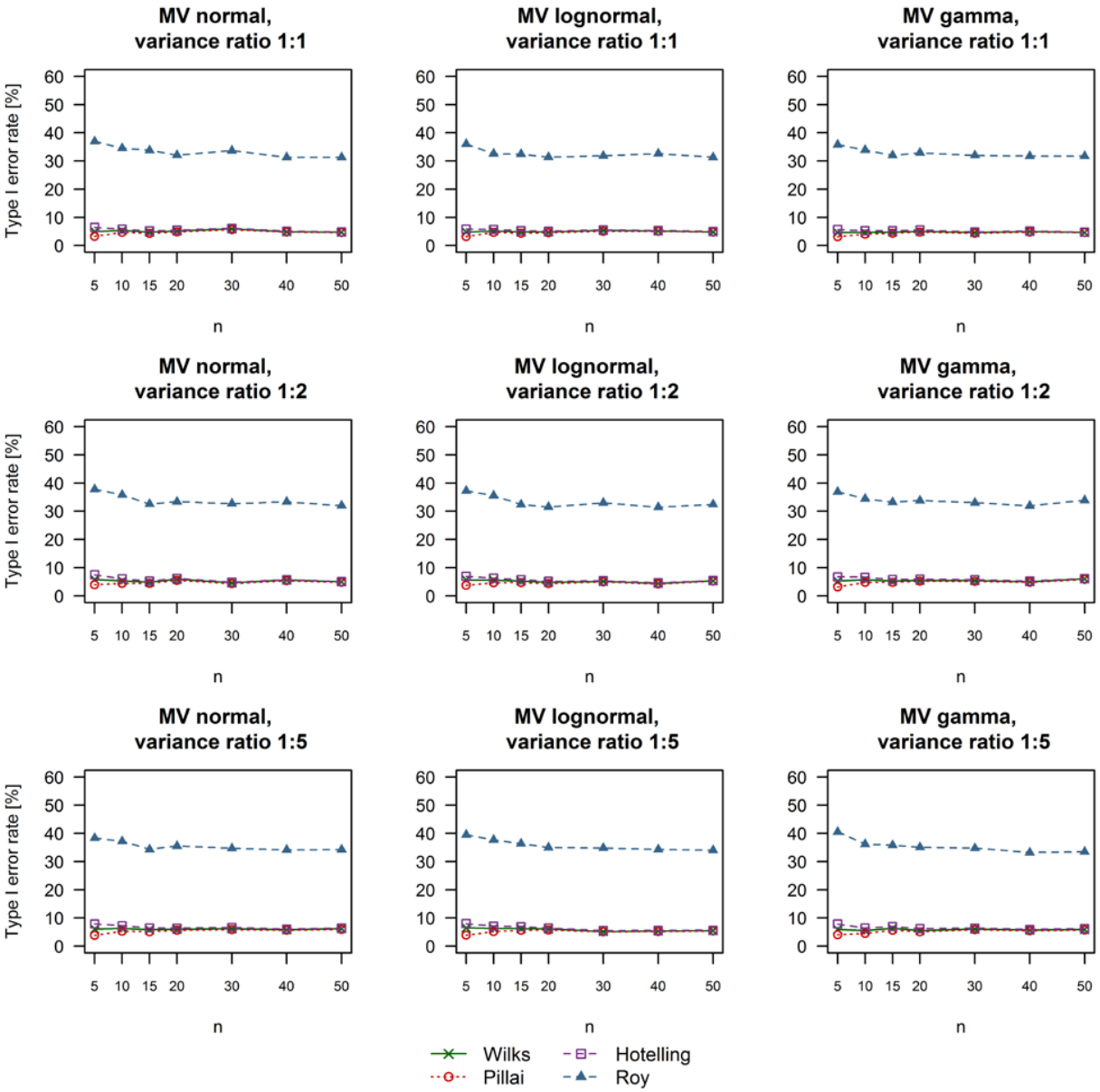

Fig S. Type I error rate of different multivariate statistics used to evaluate the significance of MANOVA tests. The multivariate distribution from which variables were sampled and the variance ratio between control and treatment groups are shown in the title of each plot.
MANOVA: Multivariate analysis of variance; Wilks: Wilks' lambda; Pillai: Pillai's trace; Hotelling: Lawley-Hotelling trace; Roy: Roy's largest root; MV: Multivariate.

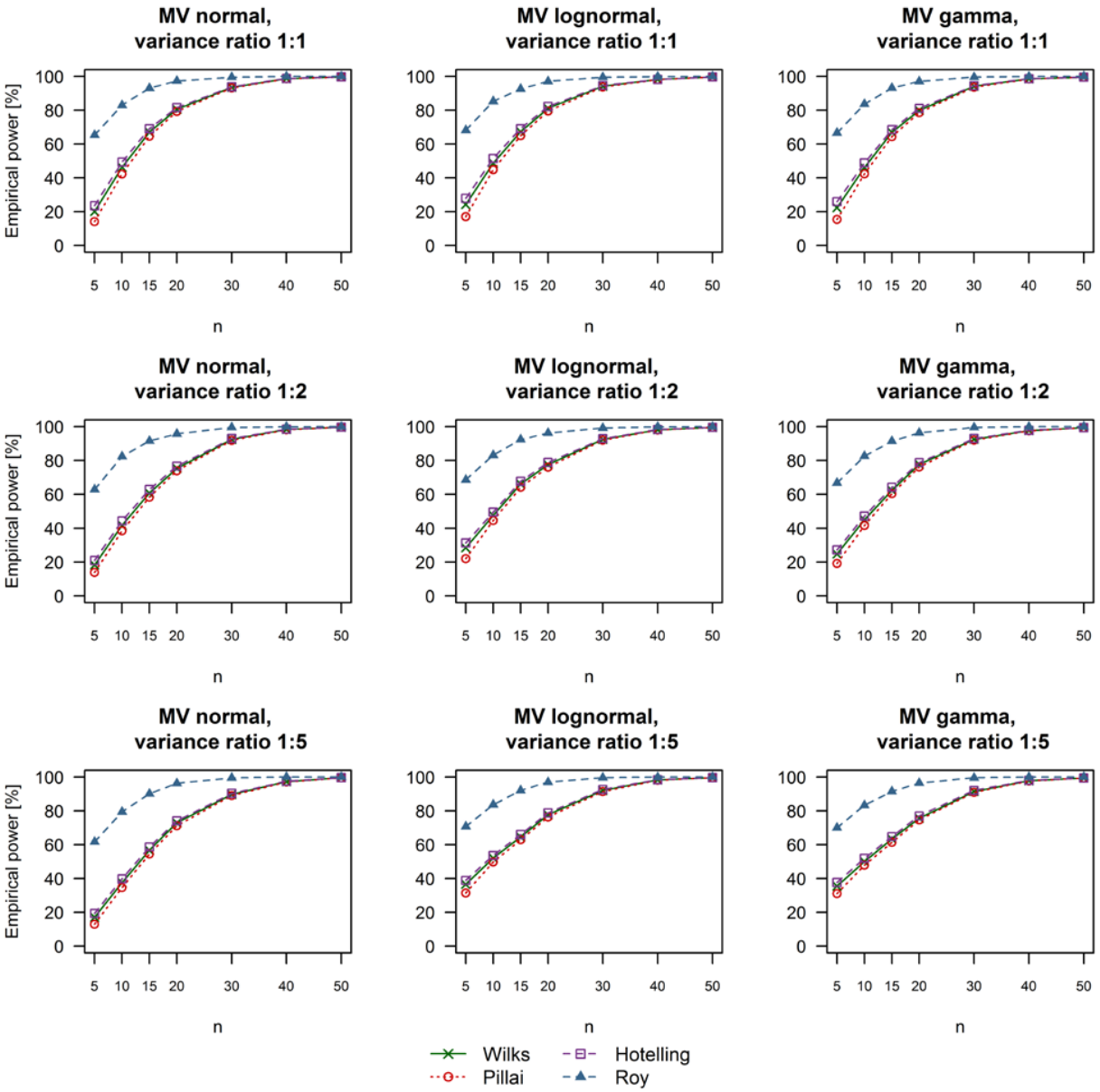

Fig S2. Empirical power of different multivariate statistics used to evaluate the significance of MANOVA with simulated large treatment effects (Cohen's d equal to 0.8). The multivariate distribution from which variables were sampled and the variance ratio between control and treatment groups are shown in the title of each plot.

MANOVA: Multivariate analysis of variance; Wilks: Wilks' lambda; Pillai: Pillai's trace; Hotelling: Lawley-Hotelling trace; Roy: Roy's largest root; MV: Multivariate.

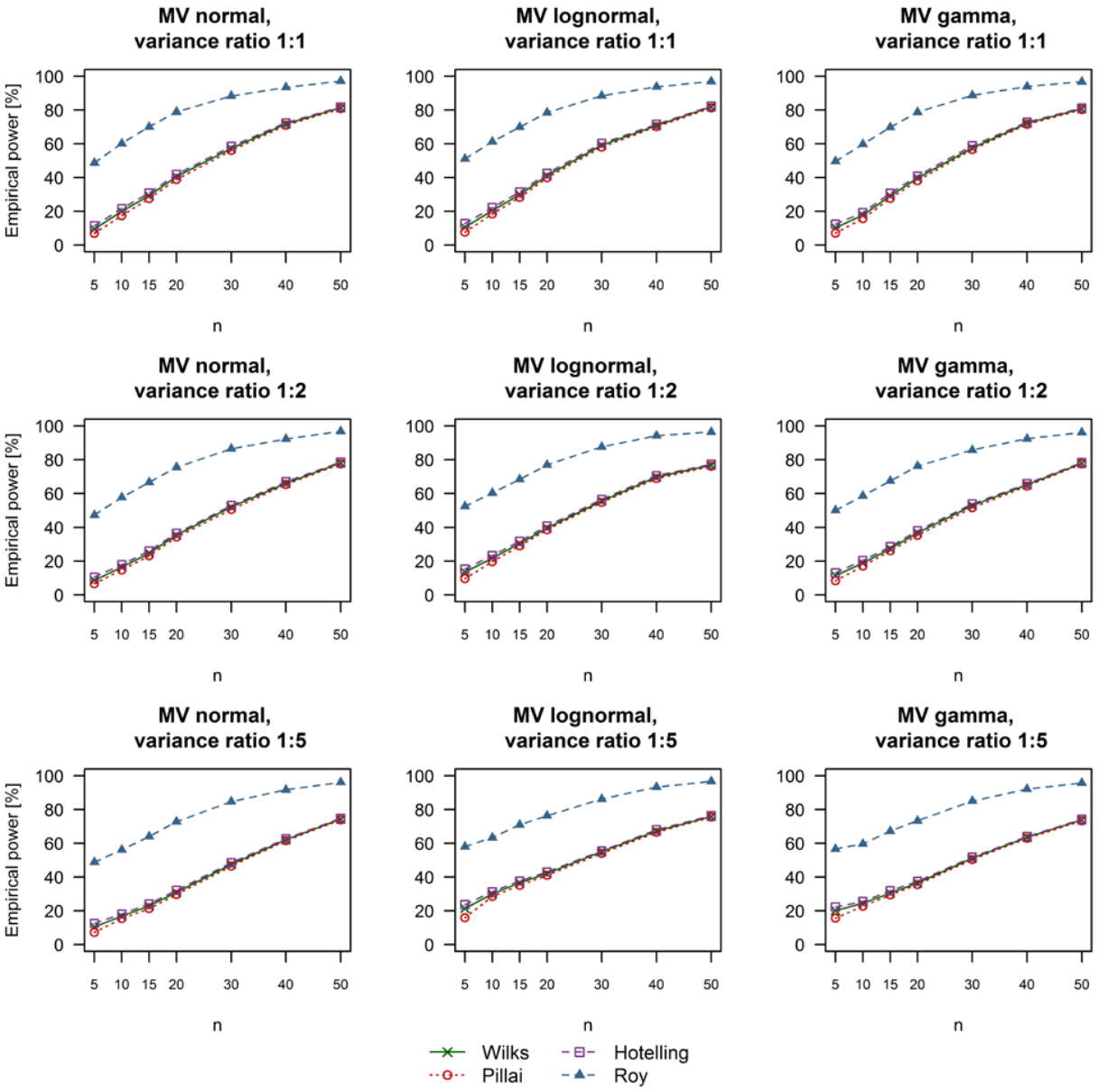

Fig S3. Empirical power of different multivariate statistics used to evaluate the significance of MANOVA with simulated moderate treatment effects (Cohen's d equal to 0.5). The multivariate distribution from which variables were sampled and the variance ratio between control and treatment groups are shown in the title of each plot.
MANOVA: Multivariate analysis of variance; Wilks: Wilks' lambda; Pillai: Pillai's trace; Hotelling: Lawley-Hotelling trace; Roy: Roy's largest root; MV: Multivariate.

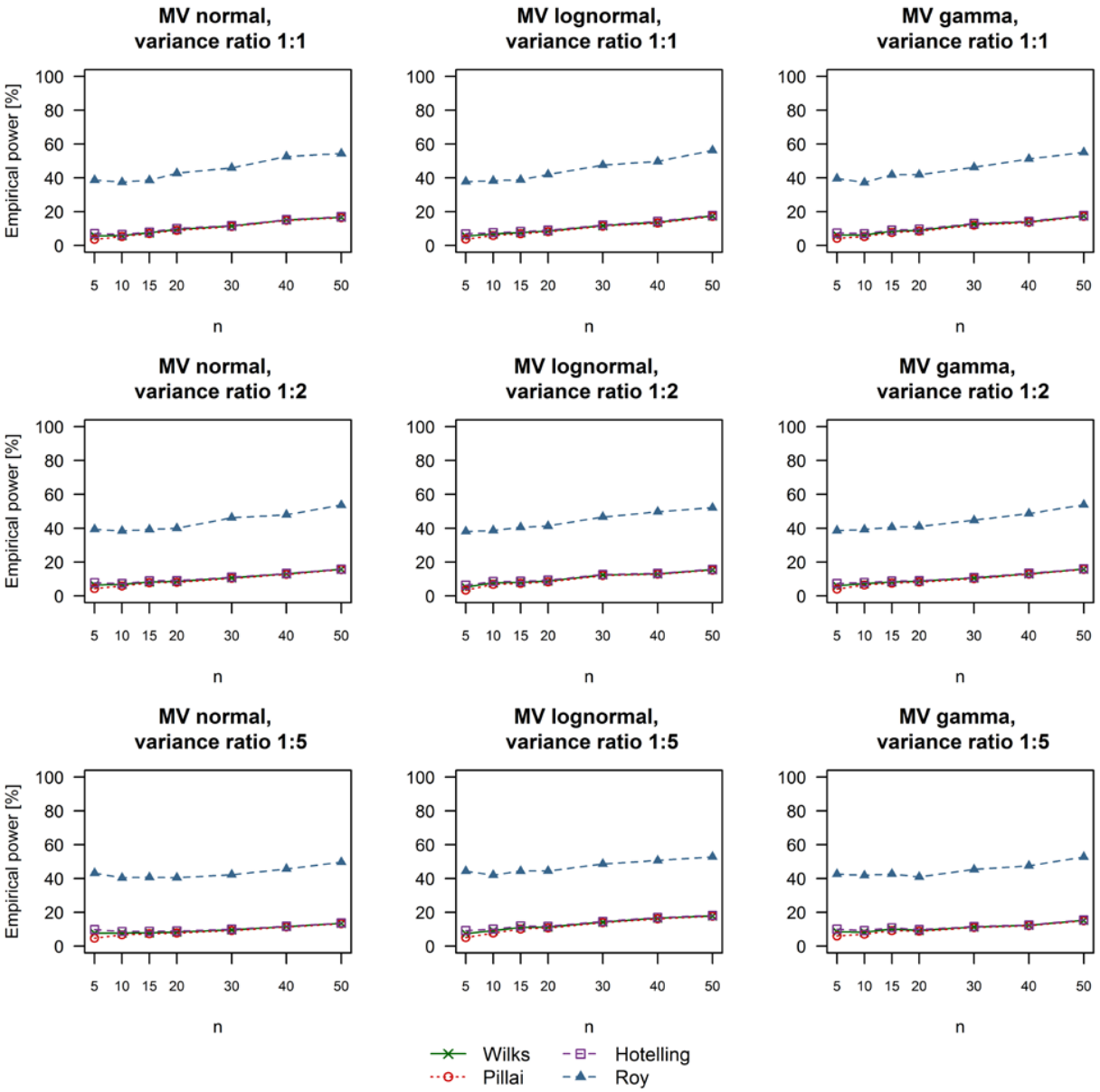

Fig S4. Empirical power of different multivariate statistics used to evaluate the significance of MANOVA with simulated small treatment effects (Cohen's d equal to 0.2). The multivariate distribution from which variables were sampled and the variance ratio between control and treatment groups are shown in the title of each plot.

MANOVA: Multivariate analysis of variance; Wilks: Wilks' lambda; Pillai: Pillai's trace; Hotelling: Lawley-Hotelling trace; Roy: Roy's largest root; MV: Multivariate.

2.3 α-Linolenic acid-rich diet influences microbiota composition and villus morphology of the mouse small intestine

Authors: **Hristo Todorov**[#]; Bettina Kollar[#]; Franziska Bayer; Ines Brandao; Amrit Mann; Julia Mohr; Giulia Pontarollo; Henning Formes; Roland Stauber; Jens M. Kittner; Kristina Endres; Bernhard Watzer; Wolfgang Andreas Nockher; Felix Sommer; Susanne Gerber; Christoph Reinhardt

This article is published in *Nutrients*, 2020, 12(3), 732.
doi: https://doi.org/10.3390/nu12030732

# Authors contributed equally

My contributions to this article are listed in section 4.2 Contributions to individual publications.

nutrients

MDPI

Article

α-Linolenic Acid-Rich Diet Influences Microbiota Composition and Villus Morphology of the Mouse Small Intestine

Hristo Todorov [1,2,†], Bettina Kollar [3,†], Franziska Bayer [3], Inês Brandão [3,4], Amrit Mann [3], Julia Mohr [3], Giulia Pontarollo [3], Henning Formes [3], Roland Stauber [5], Jens M. Kittner [6], Kristina Endres [7], Bernhard Watzer [8], Wolfgang Andreas Nockher [9], Felix Sommer [10], Susanne Gerber [1] and Christoph Reinhardt [3,11,*]

1 Institute for Developmental Biology and Neurobiology, Faculty of Biology and Center for Computational Sciences in Mainz, Johannes Gutenberg-University Mainz, Staudingerweg 9, 55128 Mainz, Germany; hristo_td@yahoo.com (H.T.); gerber.sj@gmail.com (S.G.)
2 Fresenius Kabi Deutschland GmbH, Borkenberg 14, 61440 Oberursel, Germany
3 Center for Thrombosis and Hemostasis (CTH), University Medical Center Mainz, Johannes Gutenberg-University Mainz, Langenbeckstrasse 1, 55131 Mainz, Germany; kollar.lb@gmail.com (B.K.); franziska.bayer@uni-mainz.de (F.B.); inesm.brandao@gmail.com (I.B.); amrit.mann@unimedizin-mainz.de (A.M.); jumohr@students.uni-mainz.de (J.M.); giulia.pontarollo@unimedizin-mainz.de (G.P.); henning.formes@uni-mainz.de (H.F.)
4 Centro de Apoio Tecnológico Agro Alimentar (CATAA), Zona Industrial de Castelo Branco, Rua A, 6000-459 Castelo Branco, Portugal
5 Nanobiomedicine, University Medical Center Mainz, Johannes Gutenberg-University Mainz, Langenbeckstrasse 1, 55131 Mainz, Germany; rstauber@uni-mainz.de
6 Medical Department 2 (Gastroenterology, Hepatology, Pneumology, Endocrinology) Klinikum Darmstadt GmbH, Grafenstr. 9, 64283 Darmstadt, Germany; jens.kittner@mail.klinikum-darmstadt.de
7 Department of Psychiatry and Psychotherapy, University Medical Center of the Johannes Gutenberg-University Mainz, 55131 Mainz, Germany; kristina.endres@unimedizin-mainz.de
8 Metabolomics Core Facility, Philipps-University, 35043 Marburg, Germany; watzer@staff.uni-marburg.de
9 Institute of Laboratory Medicine and Pathobiochemistry, Philipps-University, 35043 Marburg, Germany; andreas.nockher@uk-gm.de
10 Institute of Clinical Molecular Biology, Christian-Albrechts-University Kiel, 24105 Kiel, Germany; f.sommer@ikmb.uni-kiel.de
11 German Center for Cardiovascular Research (DZHK), Partner Site RheinMain, 55131 Mainz, Germany
* Correspondence: Christoph.Reinhardt@unimedizin-mainz.de; Tel.: +49-6131-17-8280
† These authors contributed equally.

Received: 9 October 2019; Accepted: 6 March 2020; Published: 11 March 2020

Abstract: α-Linolenic acid (ALA) is well-known for its anti-inflammatory activity. In contrast, the influence of an ALA-rich diet on intestinal microbiota composition and its impact on small intestine morphology are not fully understood. In the current study, we kept adult C57BL/6J mice for 4 weeks on an ALA-rich or control diet. Characterization of the microbial composition of the small intestine revealed that the ALA diet was associated with an enrichment in *Prevotella* and *Parabacteroides*. In contrast, taxa belonging to the Firmicutes phylum, including *Lactobacillus*, *Clostridium* cluster XIVa, Lachnospiraceae and *Streptococcus*, had significantly lower abundance compared to control diet. Metagenome prediction indicated an enrichment in functional pathways such as bacterial secretion system in the ALA group, whereas the two-component system and ALA metabolism pathways were downregulated. We also observed increased levels of ALA and its metabolites eicosapentanoic and docosahexanoic acid, but reduced levels of arachidonic acid in the intestinal tissue of ALA-fed mice. Furthermore, intestinal morphology in the ALA group was characterized by elongated villus structures with increased counts of epithelial cells and reduced epithelial proliferation rate. Interestingly, the ALA diet reduced relative goblet and Paneth cell counts. Of note, high-fat

Western-type diet feeding resulted in a comparable adaptation of the small intestine. Collectively, our study demonstrates the impact of ALA on the gut microbiome and reveals the nutritional regulation of gut morphology.

Keywords: α-linolenic acid; microbiota; epithelial renewal; goblet cells; paneth cells; villus morphology

1. Introduction

The ω-3 polyunsaturated fatty acid (PUFA) α-linolenic acid (ALA, 18:3 n-3) is an essential plant-derived fatty acid that is abundant in oil produced from perilla, linseed, rapeseed and soy. This macronutrient exerts anti-inflammatory properties through the generation of oxylipins [1]. ALA interferes with the arachidonic acid (AA) metabolism and inhibits the prostaglandin biosynthesis pathway, thereby reducing the concentration of pro-inflammatory oxylipins [2]. In addition to its effects on the formation of anti-inflammatory mediators [3,4] and its anti-hypertensive action [5–7], there is increasing evidence that ALA plays a role in ameliorating intestinal inflammatory disease phenotypes [8–11]. Furthermore, ALA-rich diets were reported to protect from the development of colon carcinomas [12].

In contrast to the recognized role of ALA in inflammatory bowel disease, information on the influence of this essential PUFA in normal gut homeostasis and its interplay with the commensal gut microbiota remains sparse. Nutritional studies on rats fed with perilla oil, a source rich in ALA, indicated a decrease in the Firmicutes to Bacteroidetes ratio and an increase in the abundance of Spirochaetes in the perilla oil group relative to normal lab chow [13]. A study in mice showed that flaxseed/fish oil feeding rich in ω-3 PUFA promoted the growth of *Bifidobacterium* and improved metabolic outcome, indicated by reduced liver weight and hepatic triglyceride concentration compared to palm oil diet [14]. One of the possible mechanisms by which PUFA might beneficially impact host metabolism is through the production of conjugated fatty acids by intestinal bacteria. Research so far has mainly focused on conjugated linoleic acid which is an intermediate metabolite in the saturation pathway of the ω-6 PUFA linoleic acid [15]. However, conjugated isomers of ALA have also gained attention due to their reported anti-inflammatory, anti-carcinogenic and anti-obesogenic properties [16–18]. In vitro studies have shown that certain strains of Bifidobacteria [19,20], Propionibacteria [20] and lactic acid bacteria [21,22] are able to metabolize ALA to conjugated ALA isomers. Furthermore, Druart et al. demonstrated that the commensal gut microbiota contributes to the production of PUFA-derived metabolites in vivo by reporting increased colonic contents of conjugated linoleic acid isomers and non-conjugated metabolites in conventionalized compared to germ-free mice [23]. Ohue-Kitano and colleagues reported that short-term feeding of C57BL/6 mice with ALA and the ALA-derived metabolites of intestinal lactic acid bacteria affect intestinal immune homeostasis [24]. The authors showed that ALA and its metabolite 13-hydroxy-9(*Z*),15(*Z*)-octadecadienoic acid promote the accumulation of anti-inflammatory M2 macrophages in the small intestinal lamina propria. Additionally, PUFA-rich diets may impact the differentiation of the intestinal epithelial lineage as gastric gavage in rat pups with rapeseed oil and sunflower oil, which are both rich in PUFA, decreased mucus secreting goblet cell numbers in the colon [25]. Intestinal epithelial cells originate from stem cells located at the base of the Lieberkühn crypt and differentiate along the crypt-villus axis. To date, it is not completely clear how ALA shifts intestinal microbiota composition. Additionally, investigations on the influence of PUFAs on small intestinal morphology and renewal of the gut epithelial lineage under steady-state conditions are sparse [26].

In the current study, we hypothesized that an ALA-rich diet leads to compositional changes in the commensal microbiota of the mouse small intestine. Furthermore, we investigated the potential impact of increased dietary amounts of ALA on gut morphology in the mid small intestine.

2. Materials and Methods

2.1. Animals

Male C57BL/6J mice that were 10–14 weeks old were obtained from the Jackson Laboratory. Animals were held at the Translational Animal Research Center (TARC) of the University Medical Center Mainz under specific pathogen-free (SPF) conditions in EU Type II individually ventilated cages under constant room temperature and air humidity with a 12 h light-dark cycle. Mice had ad libitum access to water and autoclaved chow. The animals were assigned to a control standard diet group (Altromin Spezialfutter GmbH & Co. KG, Lage, Germany) and to an α-linolenic acid rich diet group (standard Altromin diet + 20% perilla oil). The composition and fatty acid profile of both diets is shown in Table 1. To test the specificity of ALA dietary effects on the gut morphology, we fed an additional group of 7 mice with a pro-inflammatory, cholesterol-rich high-fat Western-type diet (TD.88137, Envigo, Venray, Netherlands). The composition and fatty acid profile of this diet are shown in Table 2. After a 4 week treatment period, mice were sacrificed via cervical dislocation. The small intestine was collected and cut into eight equivalent pieces. Segment 5 was used for all subsequent experiments. We refer to this segment as the mid small intestine or jejunum.

All animal experiments were approved by the Institutional Animal Care and Use Committee of Rhineland-Palatinate (23177-07/G13-1-072; 23177-07/G16-1-013). The authors confirm that all experiments were performed in accordance with relevant guidelines and regulations.

2.2. Histological Analysis of the Small Intestine

2.2.1. Proliferation Assay

The fifth segment of eight equally sized segments of the small intestine was flushed with cold PBS and fixed in Roti®-Histofix (#P087, Roth) at 4 °C overnight. Tissue was processed for paraffin embedding at the Core Facility Histology at University Medical Center Mainz. Tissue sections were cut at 3 µm thickness, dewaxed and heat-induced epitope-retrieval was done using citrate buffer (10 mM sodium citrate, pH 6.6). Unspecific binding was blocked using normal goat serum (#S-1000, Vector Laboratories, 5% *v*/*v* in PBS) and sections were incubated for 1 h at room temperature with rabbit anti mouse-Ki-67 antibody (1:500 in blocking solution, #IHC-00375, Bethyl Laboratories Inc.). After washing, sections were incubated with the biotinylated anti-rabbit antibody (#BA-1000, Vector Laboratories) and signal detection was done using Vectastain® Elite® ABC HRP (#PK-7100, Vector Laboratories) and 3,3′-diaminobenzidine (DAB) as substrate according to the manufacturer's protocol. Sections were dehydrated and mounted using Eukitt® mounting medium (#SIAM03989, VWR). Ki67-positive cells as well as total number of cells per villus/crypt were counted, averaged and represented as percent.

2.2.2. Periodic Acid-Schiff (PAS) Staining

Paraffin slides were stained for analysis of intestinal tissue morphology using PAS staining. Briefly, the hydrated slides were oxidized with periodic acid for 5 min, washed with distilled water 4–5 times and subsequently incubated with Schiff reagent for 15 min at room temperature. The stained slides were then washed for 5 min under tap water and counterstained in hemalaun. Next, slides were held under flowing water until the counterstain was blue. Finally, slides were dehydrated by incubation in ethanol in increasing concentrations (3 min in 30% ethanol, 50% ethanol, 70% ethanol, 90% ethanol, then 2x 5 min in xylol) followed by mounting in Eukitt mounting medium (#SIAM03989, VWR).

Villus morphology of the small intestine was evaluated by inspecting at least 10 villus structures per cross section from 6–7 animals per group. We determined the average number of epithelial cells per villus, mucosal thickness, crypt depth, villus length and villus spacing for each animal. Villus spacing was calculated by measuring the distance from the center of one villus at the villus base to the center of the next villus. We calculated this measure for at least 10 pairs of villi and took the average value as the final estimate. Furthermore, we determined the percentage of Paneth cells and goblet cells

relative to all epithelial cells. Figure 1 shows a schematic representation of how different morphological parameters were measured.

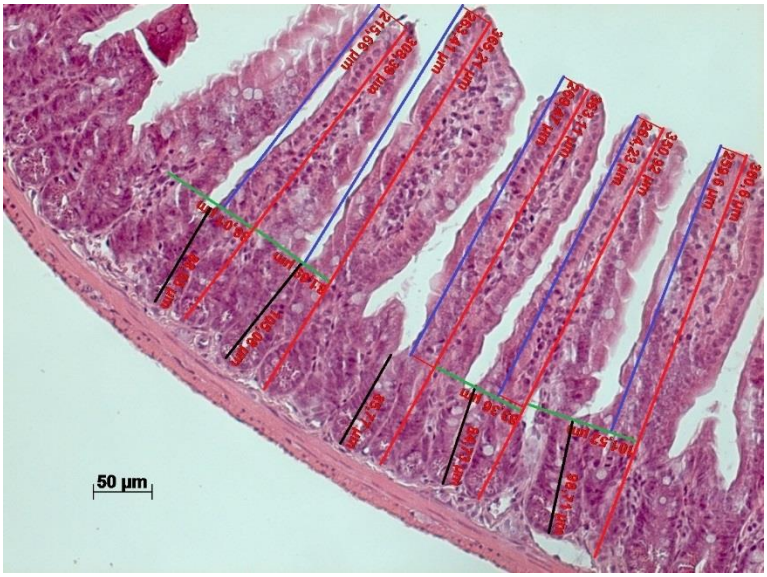

Figure 1. Schematic representation of measurements of intestinal morphology parameters. The vertical red lines correspond to mucosal thickness, blue lines indicate villus length, black lines indicate crypt depth and horizontal green lines demonstrate how villus spacing was determined.

2.3. GC-MS/MS Quantification of Fatty Acids in Intestinal Tissue and Diet

Fatty acid (FA) extraction, derivatization and analysis of the intestine samples was performed with slight modifications as previously described [27]. For FA determination, samples of 25–125 mg lyophilized intestinal tissue were used (n = 10 in the ALA group and n = 9 in the control diet group). The samples were dissolved in 5 mL of a mixture of hexane/isopropanol 3:2 (v/v; VWR International GmbH, Darmstadt, Germany; LC-MS grade) spiked with 1 µg of heptadecenoic acid (cis-10; Larodan, Malmö, Sweden) as internal standard. Then, 3 mL of a 6.7% Na_2SO_4 solution (Merck KGaA, Darmstadt, Germany) was added. From the centrifuged mixture, the supernatant hexane phase was removed and evaporated to dryness under a gentle stream of nitrogen. A solution of 14% boron trifluoride (BF3) in methanol (Sigma-Aldrich, Hamburg, Germany) was added and incubated at 100 °C for 10 min for complete esterification. The formed FA-methyl esters were extracted after addition of 1 mL water and 3 mL hexane then evaporated under nitrogen and resolved in 500 µL of hexane. To determine the FAs, a 1 µL aliquot of the hexane solution was injected into a Triple Quad GC-MS/MS (Agilent 7000) system. A multiple reaction monitoring (MRM) method was used for analyte detection. Individual FA concentrations were calculated as relative percentage with an evaluated FA reference standard set (GLC-744, Nu-Chek Prep, Inc. Elysian, MN, USA) at 100% or as absolute values. Mass Hunter Quant 5.0 and Mass Hunter Qual 5.0 software were used for data analysis.

The fatty acid profile of the control and ALA-rich diets was determined using the methods described above. The amount of each fatty acid relative to all fatty acids was determined in technical triplicates for each diet and the average value was reported. The amount of each fatty acid as percentage from the diet (as reported in Table 1) was obtained by multiplying the experimentally measured amount with the total relative amount of fat in the control and ALA-rich diet, respectively.

2.4. Microbial Composition of the Small Intestine

Upon sacrifice, the contents of the small intestine from 4 mice in the control group and 3 mice from the ALA-rich diet group were collected. Genomic DNA was purified from these digesta samples with the NucleoSpin Soil kit (Macherey-Nagel GmbH & Co.KG, Düren, Germany). Targeted sequencing

of the 16S rRNA marker gene was employed in order to investigate the microbiome composition of the small intestine under the different dietary conditions. The V4-V5 hypervariable region of the bacterial 16S gene was amplified using specific PCR primers 515F-Y and 909R [28–30]. Paired-end sequencing was performed on the MiSeq Illumina platform by StarSEQ GmbH (Mainz, Germany). Subsequently, 16S data were processed with mothur v1.40.5 [31] following the MiSeq standard operating procedure [32]. Paired end-reads were merged into contigs, sequences with any ambiguous bases were removed and maximum homopolymer length was set to 8. Chimeric sequences were identified and removed with the VSEARCH algorithm within mothur [33]. Sequences were aligned to the SILVA database [34] and clustered to operational taxonomic units (OTUs) at 97% similarity. Taxonomic assignment was facilitated with the Ribosomal Database Project v9 [35] and OTUs with non-bacterial or unknown taxonomy were removed. Data were further analyzed and graphically represented with the help of the phyloseq R package v1.26.1 [36]. α-diversity was evaluated using the observed richness and Shannon index. For this analysis, each sample was normalized to the smallest library size by drawing a random subset of sequences with replacement. This step was repeated 100 times and the average values over all runs were reported as the final estimates for α-diversity. β-diversity was analyzed by computing the Bray-Curtis dissimilarity and the Jaccard binary distance. Canonical analysis of principal coordinates (CAP) [37], a constrained ordination procedure belonging to the same class of ordination methods as the unconstrained principal component analysis (PCA) [38] was employed to visualize results and investigate the multivariate hypothesis if an ALA diet significantly influences the microbial composition of the small intestine. Univariate differential abundance analysis was performed using the DESeq2 R package v1.22.2 [39]. For this purpose, OTUs were binned into phylotypes on the genus level. Taxa were considered to be differentially abundant if the adjusted p-value of the corresponding log2 fold change (FC) was $p < 0.1$. This more liberal threshold was selected because of the small sample size in an effort to increase power. P-values were adjusted for multiple comparisons with the Benjamini–Hochberg method.

2.5. Metagenome Prediction and Characterization

In order to gain insight into the potential functional profile of the small intestinal microbiome of mice under the different dietary conditions, we analyzed the 16S data using PICRUSt [40]. First, OTUs were re-assigned to a taxonomy using the Greengenes data base v13.5 [41]. Metagenome prediction was then performed up to Kyoto Encyclopedia of Genes and Genomes (KEGG) Orthology (https://www.genome.jp/kegg/ko.html) tier 3 using the PICRUSt online tool (http://huttenhower.sph.harvard.edu/galaxy/). Finally, results were visualized in STAMP v2.1.3 [42].

2.6. Statistical Analysis of Fatty Acid Profile and Small Intestinal Morphology

Data were graphically represented as mean values + standard error of the mean (SEM) and as individual values. Differences between two groups were statistically evaluated using unpaired t-test in case of normally distributed data or Mann–Whitney test when assumptions of normality were violated (according to the Kolmogorov Smirnov test). More than two groups were statistically compared with an ANOVA followed by Dunnett's post-hoc test. P values were two-tailed and differences were considered statistically significant in case of $p < 0.05$. Statistical analysis was performed with GraphPad Prism version 6.07 (GraphPad Software Inc, San Diego, CA).

3. Results

3.1. Fatty Acid Profile of Different Diets

Perilla oil was chosen due to its very high content of ALA varying between 51%–64% [43–46]. In order to obtain an ALA-rich diet containing approximately 10% ALA, we mixed the control Altromin diet with perilla oil at a ratio of 8:2. The nutrient and energy content of the control diet were directly obtained from the feed producer (Table 1). The nutrient content of the ALA-rich diet was calculated

based on the Altromin control chow by taking into account the addition of 20% fat. Furthermore, we experimentally confirmed the amount of ALA in the diet using GC-MS/MS. The fatty acid profile of the control and ALA-rich diet is shown in Table 1. ALA represented approx. 9.27% of the total ALA-rich diet and only 0.03% of the control chow. The addition of fat to the ALA-rich diet resulted in a calorie increase of approximately 30% relative to the control diet. In order to test the specificity of the effect of ALA-rich diet on gut morphology, we included a pro-inflammatory Western-type high-fat diet (HFD) (TD.88137, Envigo, Venray, Netherlands) with a comparable energy content. The composition and fatty acid profile of this HFD as obtained from the feed producer are summarized in Table 2.

Table 1. Composition and fatty acid profile of the standard Altromin 1814 laboratory chow and ALA-rich diet.

Ingredient	Relative amount in control chow (% of diet)	Relative amount in ALA-Rich diet (% of diet)
Proteins	17.61%	~14.1%
Fat	5.1%	~24%
Fiber	4.05%	~3.24%
Disaccharides	11.1%	~8.88%
Polysaccharides	47.2%	~37.76%
Fatty acid	**Relative amount (% of diet)**	**Relative amount (% of diet)**
Palmitic acid C-16:0	0.36%	4.1%
Stearic acid C-18:0	0.35%	5.55%
Oleic acid C-18:1 cis	0.93%	1.61%
Linoleic acid C-18:2 cis	3.3%%	2.96%
α-Linolenic acid C-18:3 n3	0.03%	9.27%
γ-Linolenic acid C18:3 n6	0.0002%	0.05%
Arachidic acid C-20:0	0.04%	0.21%
Eicosanoic acid C-20:1	0.01%	0.04%
Behenic acid C-22:0	0.04%	0.04%
Erucic acid C-22:1	0.02%	0.14%
Lignoceric acid C-24:0	0.01%	0.02%
Metabolizable energy	3518 kcal/kg	~4582 kcal/kg

Table 2. Composition and fatty acid profile of the pro-inflammatory TD.88137 high-fat Western diet.

Ingredient	Relative amount (% of diet)
Proteins	17.3%
Carbohydrates	48.5%
Fat	21.2%
Fatty acid	**Relative amount (% of diet)**
Saturated fat	13.1%
C-16:1	0.323%
Oleic acid C-18:1 cis	4.43%
C-18:1 isomers	0.85%
Linoleic acid C-18:2 cis	0.49%
C-18:2 isomers	0.28%
α-Linolenic acid C18:3 n3	0.15%
Metabolizable energy	4500 kcal/kg

3.2. ALA-Rich Diet Alters the Composition of the Microbiota in the Mid Small Intestine of Adult Mice

Microbial characterization of the commensal microbiota in the mid small intestine (jejunum) of mice resulted in identifying as many as 6747 unique OTUs. The majority of these OTUs were associated with the most dominant phyla Firmicutes and Bacteroidetes (Figure 2a). The average Firmicutes/Bacteroidetes ratio was considerably lower in animals fed with ALA-rich diet compared to

the control diet (CTR) group (Figure 2b). The impact of ALA-rich diet feeding on microbiome diversity was in contrast to 16 weeks Western-type HFD feeding, which yielded an elevated Firmicutes/Bacteroides ratio [47]. Nevertheless, the difference was not statistically significant (unpaired *t*-test, $p = 0.143$) due to high intragroup variability. The remaining bacterial phyla represented in the ALA and CTR groups included Actinobacteria, Proteobacteria and Verrucomicrobia. The relative abundance of these phyla was comparably low under both feeding conditions. Microbiota composition of individual samples at the genus level is shown in Supplementary Figure S1.

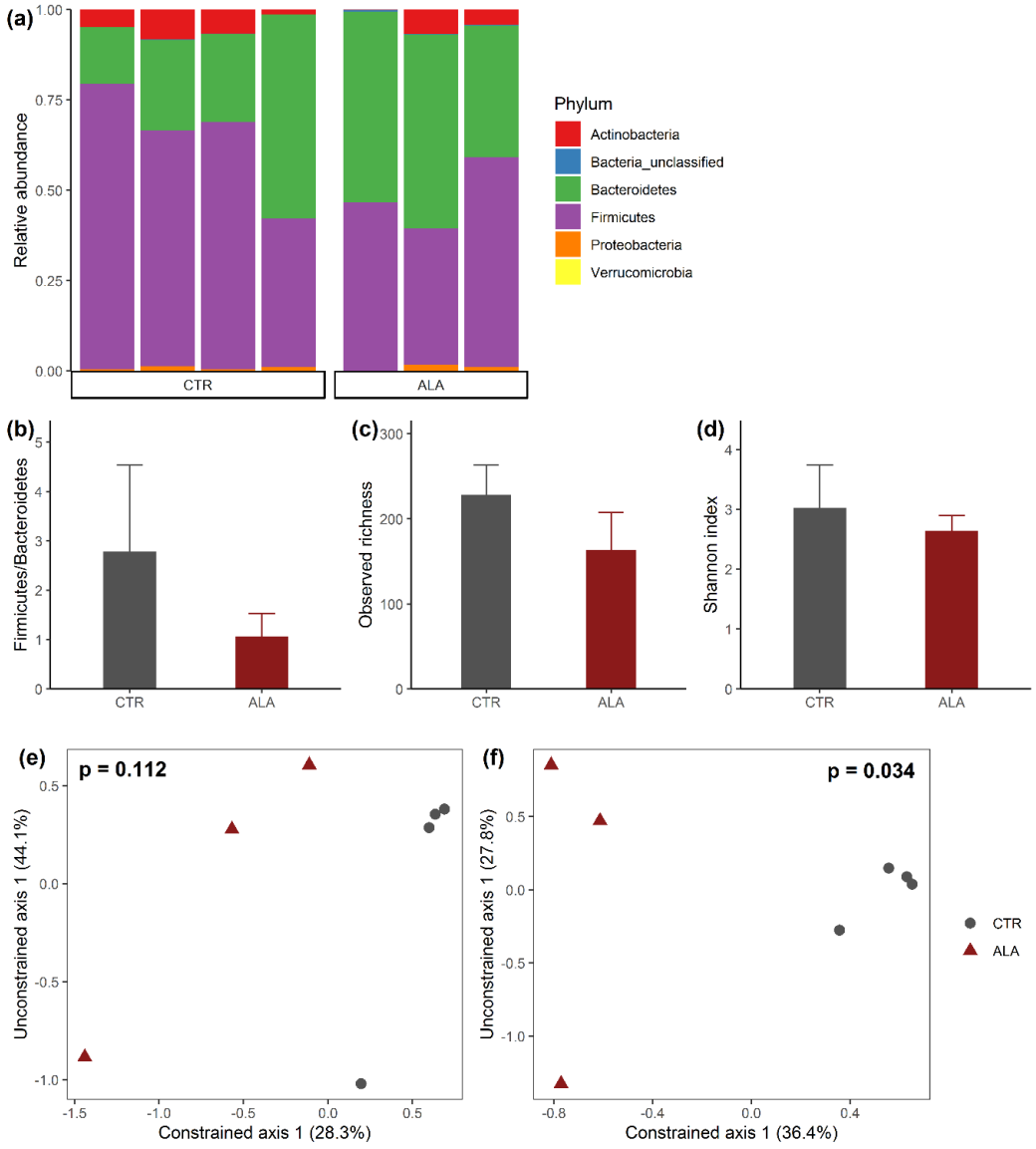

Figure 2. Microbial composition of the small intestine. (**a**) Bar plots show the relative abundance of bacterial phyla of individual animals in the control chow (CTR) or α-linolenic acid-rich diet group (ALA). (**b**) Firmicutes/Bacteroidetes ratio of CTR compared to ALA animals. α-diversity was investigated by estimating (**c**) the observed richness or (**d**) the Shannon index. Bar plots show mean + standard deviation for each measure per group. β-diversity was visualized using Canonical analysis of principle coordinates (CAP) based on (**e**) the Bray–Curtis dissimilarity or (**f**) binary Jaccard distance. P-values for the constrained axis from CAP were obtained using permutational analysis of variance (PERMANOVA) with 999 permutations. Since the treatment variable has only two levels (CTR or ALA), CAP produced only one constrained multivariate dimension. The percentage of the total inertia captured by each multivariate dimension is shown in brackets on the plots.

ALA-rich diet was not associated with statistically significant changes in the estimates of α-diversity (Figure 2c,d). However, it is worth mentioning that the average observed richness was lower in the ALA group compared to CTR animals (mean difference = −141.14, 95% confidence interval (CI) = −141.5 to 10.7, $p = 0.078$). Analysis of β-diversity revealed that ALA mice were separated from the CTR group along the constrained multivariate dimension following CAP analysis based on the Bray–Curtis dissimilarity (Figure 2e) as well as the Jaccard distance (Figure 2f). Permutational analysis of variance (PERMANOVA) on the constrained axis confirmed that the dietary effect of ALA on microbial composition of the jejunum was statistically significant based on the Jaccard distance ($p = 0.034$).

After observing a shift in the multivariate profile of the commensal microbiota between both feeding conditions, we wanted to identify OTUs responsible for group differences at the genus level. For this purpose, we estimated the log2 fold changes (FC) of bacterial abundance in the small intestine of animals fed with an ALA-rich diet compared to control chow. This analysis was based on OTUs binned into phylotypes on the genus level, which resulted in 89 bins. Out of these, 11 phylotypes were differentially abundant (Figure 3). Interestingly, most of these OTUs were associated with a significantly lower abundance in the ALA group. All but one of the OTUs with significantly reduced abundance following ALA-rich diet were related to the Firmicutes phylum. The effect was most pronounced for OTUs associated with the genus *Anaerotruncus* (log2 FC = −7.26, 95% CI = −10.99 to −3.53, adj. $p = 0.0046$) and *Clostridium* cluster XIVa (log2 FC = −6.51, 95% CI = -9.57 to −3.15, adj. $p = 0.0046$). Both of these belong to the Clostridiales order and two other representatives of this order, namely *Anaerovorax* and Lachnospiraceae demonstrated significantly lower abundance in the ALA group as well. Two representatives of the lactic acid bacteria, namely *Lactobacillus* and *Streptococcus*, also decreased in abundance. An OTU related to the genus *Olsenella* (phylum Actinobacteria) was the only taxon, which did not belong to the Firmicutes phylum and had significantly reduced abundance in animals fed with an ALA-rich diet. In contrast, only three OTUs were enriched in the ALA group compared to CTR animals. All of these were related to the Bacteroidetes phylum. One OTU could not be classified beyond the phylum level. The remaining enriched OTUs were associated with the genera *Parabacteroides* (log2 FC = 6.23, 95% CI = 1.34 to 11.12, adj. $p = 0.0125$) and *Prevotella* (log2 FC = 5.19, 95% CI = 0.94 to 9.44, $p = 0.0992$).

3.3. ALA-Rich Diet Might Impact the Metagenome Profile of Commensal Microbiota in the Small Intestine

We employed the PICRUSt algorithm in order to predict the metagenome profile of the microbiome in the small intestine beyond its taxonomic composition. This analysis identified 21 KEGG orthology (KO) pathways, which might significantly differ between CTR and ALA dietary conditions (Figure 4). Out of these, 13 pathways were enriched following the ALA diet, though effect sizes (differences in mean proportions) were universally small. The most significantly enriched pathways in the ALA group included homologous recombination, ribosome, prenyltransferases, amino acid related enzymes and notably, the bacterial secretion system pathway. In contrast, eight pathways were predicted to be significantly downregulated in the ALA group. It is worth mentioning that the number of gene sequences predicted to be associated with the ALA metabolism pathway was significantly lower in the ALA group compared to controls (Figure 4).

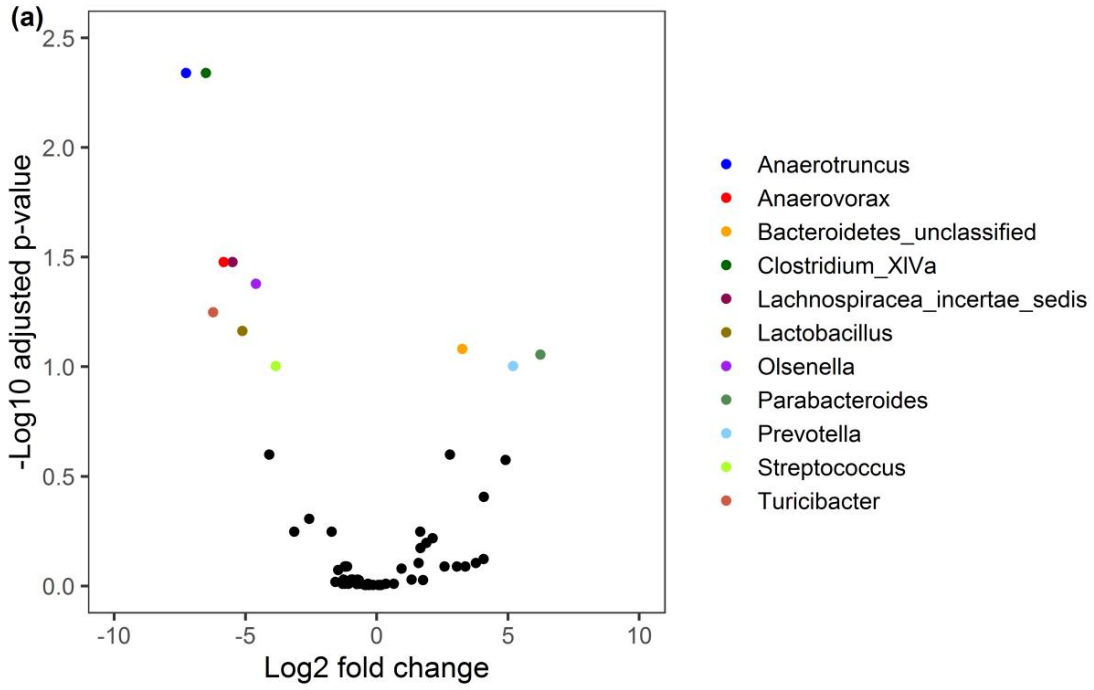

(b)

Genus	Log2 fold change (95% CI)	p-Value	Adj. p-Value
Anaerotruncus	-7.26 (-10.99 to -3.53)	0.0001	0.0046
Clostridium XlVa	-6.51 (-9.87 to -3.15)	0.0001	0.0046
Turicibacter	-6.24 (-10.63 to -1.85)	0.0054	0.0563
Anaerovorax	-5.83 (-9.55 to -2.11)	0.0021	0.0333
Lachnospiracea incertae sedis	-5.5 (-8.97 to -2.03)	0.0019	0.0333
Lactobacillus	-5.12 (-8.88 to -1.36)	0.0076	0.0686
Olsenella	-4.61 (-7.68 to -1.53)	0.0033	0.0418
Streptococcus	-3.85 (-7.02 to -0.68)	0.0173	0.0992
Bacteroidetes unclassified	3.26 (0.76 to 5.76)	0.0105	0.0829
Prevotella	5.19 (0.94 to 9.44)	0.0166	0.0992
Parabacteroides	6.23 (1.34 to 11.12)	0.0125	0.0878

Figure 3. Univariate analysis of differentially abundant genera in the mid small intestine. (**a**) The plot shows the estimated log2 fold change (FC) of operational taxonomic unit (OTU) abundance in animals receiving an α-linolenic acid rich diet (ALA) relative to animals in the control chow group (CTR). The adjusted p-value for each FC is given as the negative decadic logarithm. More significant results appear as higher values on the y axis. Black dots indicate OTUs with non-significant FC whereas differentially abundant OTUs appear as colored dots. Negative FCs correspond to OTUs with a significantly reduced abundance in the ALA group compared to CTR animals. Positive FCs indicate OTUs with significantly increased abundance following ALA diet. Specific values for the log2 FC together with the corresponding 95% confidence interval (CI) and the raw and adjusted *p*-value are shown in (**b**).

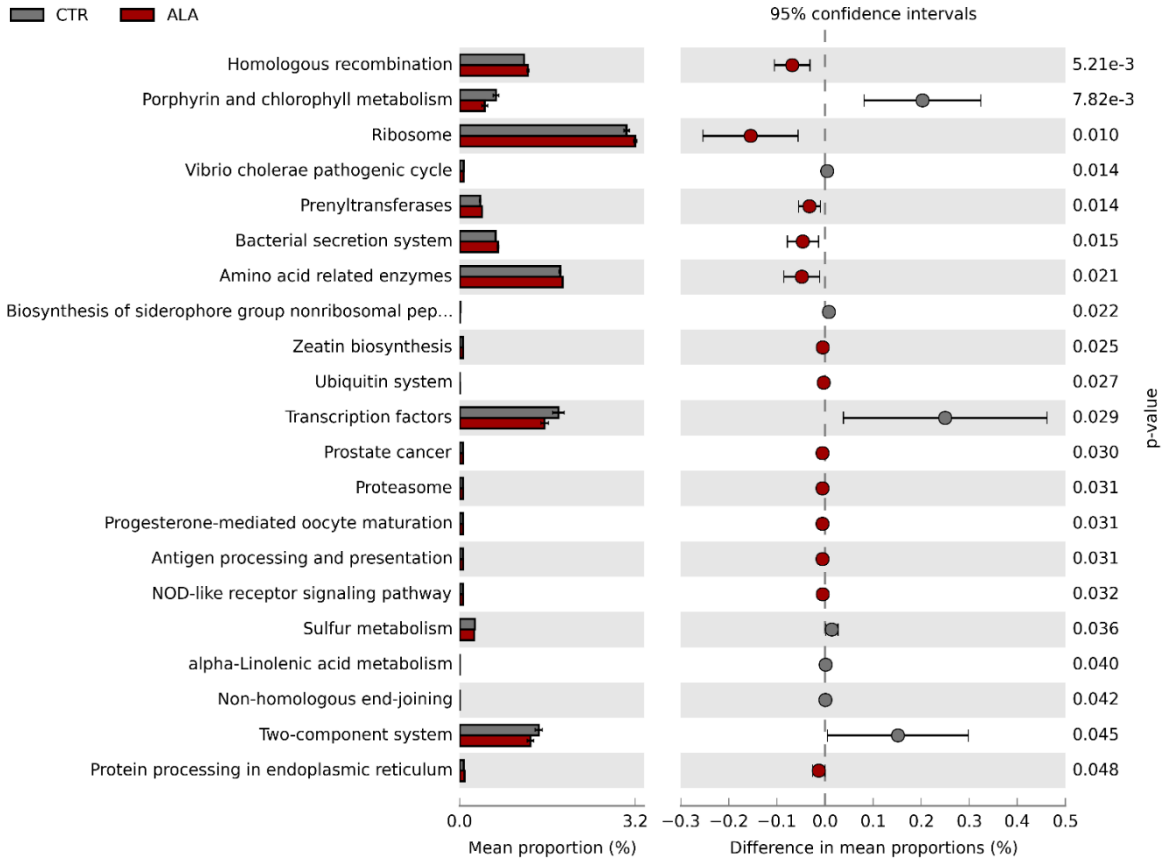

Figure 4. PICRUSt prediction of Kyoto Encyclopedia of Genes and Genomes (KEGG) orthology pathways predicted to be significantly different between the control group and animals receiving ALA-rich diet. Bar plots show the average proportion of sequences, which were predicted to be associated with the respective pathway. Circles correspond to the difference in mean proportions together with the 95% confidence interval. Red circles show pathways, which were enriched in the ALA group. Groups were compared statistically with an unpaired *t*-test. ALA: α-linolenic acid; CTR: control.

3.4. ALA-Rich Diet Induces Changes in the Fatty Acid Composition of the Jejunum

Next, we investigated if increased dietary amounts of ALA are associated with changes in the fatty acid profile of the small intestine (Figure 5). The basal level of ALA in intestinal tissue as percentage of total fatty acids was around 0.1% in animals in the CTR group (Figure 5a). The ALA-rich diet led to a significant increase in the intestinal content of this fatty acid to approximately 13.6% (median difference = 13.91%, $p < 0.0001$). Similarly, levels of eicosapentanoic acid (EPA) were very low in the CTR group and significantly increased to approximately 2.7% following the ALA enriched-diet ($p < 0.0001$, Figure 5b). In contrast, the basal amount of docosahexanoic acid (DHA) was close to 0.9% (Figure 5c). The ALA diet was associated with a two-fold increase in DHA amount (mean difference = 0.92%, $p = 0.027$). The amount of arachidonic acid (AA) was significantly decreased in the ALA group compared to CTR animals (mean difference = −2.9%, 95% CI = −4.36% to −1.45%. $p = 0.0006$, Figure 5d). We did not observe a significant change in the amount of the ω-6 PUFA linoleic acid (Figure 5e). Furthermore, the ALA-rich diet led to a significant increase in the relative amount of γ-linolenic acid (Figure 5f).

We performed a more extensive profiling of fatty acid composition of the small intestinal tissue in a subset of animals ($n = 5$/group). ALA-rich diet significantly impacted the amount of 5 saturated fatty acids, lauric acid, myristic acid, pentadecanoic acid, palmitic acid and arachidic acid (Supplementary Table S1). The relative amount of all these saturated fatty acids was significantly lower in the ALA group compared to the CTR diet group. The levels of the monounsaturated fatty acids myristoleic

acid, palmitoleic acid, oleic acid and 11-eicosanoic acid were also significantly reduced following ALA-rich diet. Furthermore, the relative amount of the ω-9 PUFA mead acid and the ω-6 PUFAs adrenic acid and osbond acid was significantly lower in the ALA group. In contrast, ALA-rich diet was associated with a significant increase in the levels of the ω-3 PUFAs stearidonic acid, eicosatrienoic acid, eicosatetranoic acid, docosatrienoic acid and docosapentanoic acid (Supplementary Table S1).

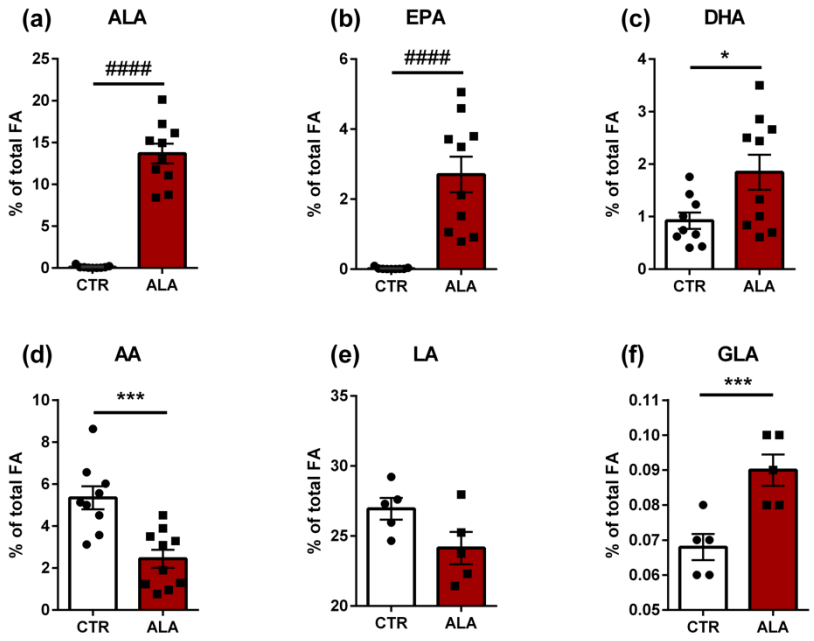

Figure 5. Impact of the ALA-rich diet on fatty acid composition of the mouse small intestine. Bar plots show mean values + standard error of the mean (SEM). n = 9 in control group, n =10 in ALA group for (**a**) ALA, (**b**) EPA, (**c**) DHA and (**d**) AA. n = 5 per group for (**e**) LA and (**f**) GLA. #### $p < 0.0001$, Mann-Whitney test; *** $p < 0.001$, * $p < 0.05$, unpaired t-test. ALA: α-linolenic acid; AA: arachidonic acid; CTR: control diet; DHA: docosahexanoic acid; EPA: eicosapentanoic acid; GLA: γ-linolenic acid; LA: linoleic acid.

3.5. ALA-Rich Diet Shapes Small Intestinal Morphology

Since the PUFA-rich diet was suggested to affect the differentiation of the epithelial lineage [25], we investigated the impact of the ALA-rich diet on the morphology of the small intestine. In order to test the specificity of the ALA-rich diet effects, we also included a group of seven animals fed with a Western-type cholesterol-rich HFD. Both the ALA-rich and HFD were associated with significant increases in mucosal thickness and villus length compared to the CTR group and the effect was more pronounced in the HFD group (Figure 6a,b). Neither crypt depth nor villus spacing were significantly affected by the dietary intervention (Figure 6c,d). However, the ALA group showed a trend towards reduced villus spacing relative to the CTR group. The increased villus length was also reflected by the significantly higher number of epithelial cells in both the ALA and HFD groups relative to CTR animals (Figure 6e). However, the proportion of goblet and Paneth cells per villus was significantly reduced in the ALA-rich and HFD diet groups compared to control chow (Figure 6f,g). Representative images from PAS staining of goblet cells and Paneth cells are shown in Figure 7a,b, respectively. Finally, both the ALA-rich and Western-type HFD were accompanied by a significantly reduced proliferation rate, measured by the percentage of Ki67-positive cells per villus (Figure 6h).

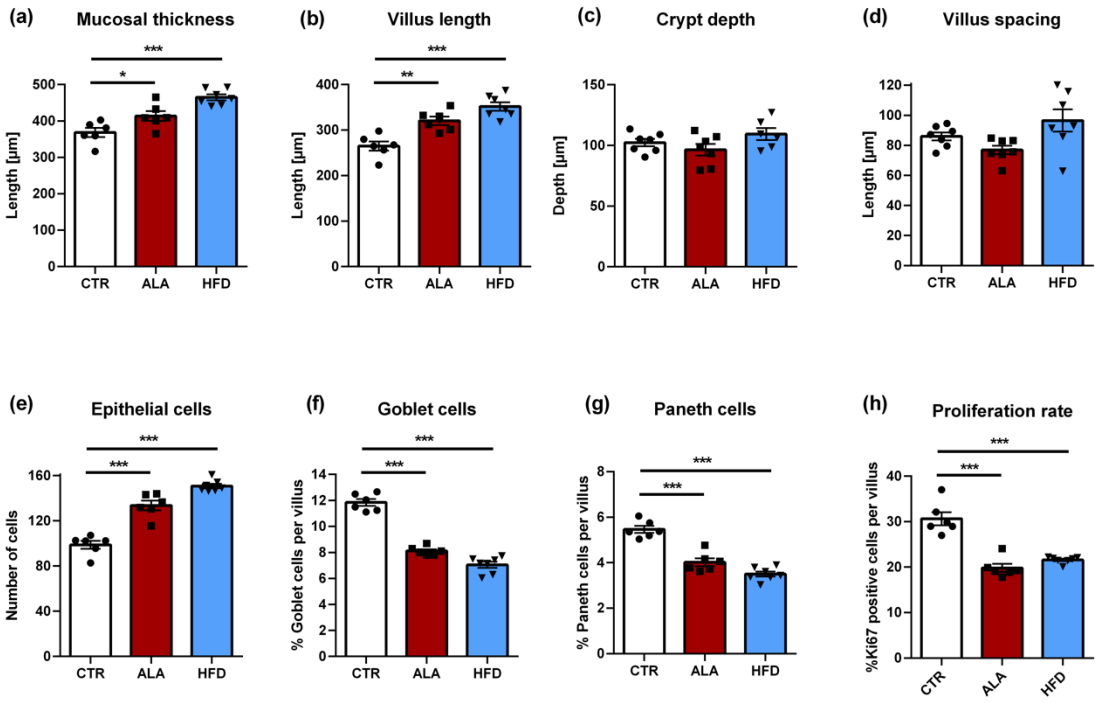

Figure 6. Impact of ALA-rich diet and Western-type high-fat diet (HFD) on villus morphology of the mid small intestine. Morphometric analysis of (**a**) mucosal thickness, (**b**) villus length, (**c**) crypt depth, and (**d**) villus spacing. Counts of (**e**) epithelial cells, (**f**) goblet cells, (**g**) Paneth cells. Based on Ki67 stained cells the proliferation rate was calculated (**h**). Bar plots show mean values + standard error of the mean (SEM). $n = 6$ in the CTR group, $n = 6$–7 in the ALA group and $n = 7$ in the HFD group. *** $p < 0.001$, ** $p < 0.01$, * $p < 0.05$, ANOVA followed by Dunnett's post-hoc test. ALA: α-linolenic acid; CTR: control diet; HFD: Western-type high-fat diet.

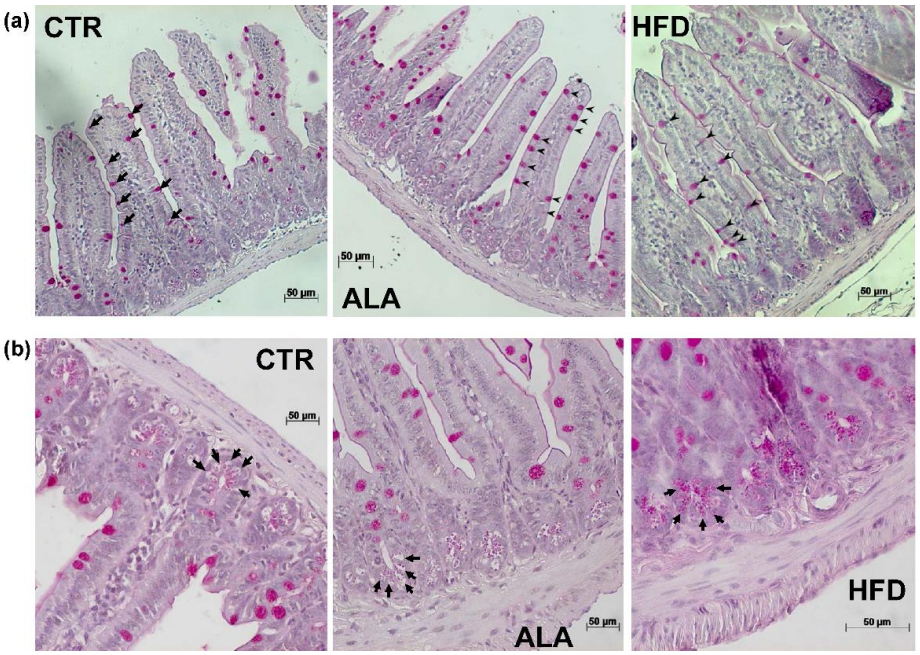

Figure 7. Representative images of Periodic acid-Schiff (PAS) staining of goblet and Paneth cells under different dietary conditions. Panel (**a**) shows PAS-stained goblet cells indicated by black arrows/arrow heads. PAS-stained Paneth cells in intestinal crypts are indicated with black arrows in panel (**b**). ALA: α-linolenic acid-rich diet; CTR: control diet; HFD: Western-type high-fat diet.

4. Discussion

Our study demonstrates that ALA-rich high-fat diet leads to an altered composition of the commensal microbiota in the mid small intestine in healthy adult mice. This shift was more qualitative in nature as indicated by the statistically significant effect of diet in the CAP analysis based on the binary Jaccard index. In contrast, ordination analysis, based on the Bray–Curtis dissimilarity, which accounts for differences in bacterial abundance between groups, was not associated with a significant effect of diet. The small intestine of the ALA diet-fed mice showed increased total ALA content along with changed villus morphology. Specifically, villus length was increased both in ALA-rich and HFD-fed mice, accompanied with an increased mucosal thickness and number of epithelial cells. The epithelial proliferation rate as well as the proportion of goblet and Paneth cells was significantly reduced in the ALA-rich diet and HFD groups.

With regards to the gut microbiome composition, we observed an increase in Bacteroidetes and a corresponding reduction in the relative abundance of Firmicutes following ALA-rich diet. The difference in the Firmicutes/Bacteroidetes ratio between groups was not statistically significant, but this is most likely due to small the sample size. Additionally, differential abundance analysis at the genus level confirmed these trends as most of the OTUs with reduced abundance in the ALA group were associated with the Firmicutes phylum. Remarkably, all enriched OTUs belonged to the Bacteroidetes group. Previous studies reported the opposite effect of an increase in Firmicutes abundance and a corresponding decrease in Bacteroidetes attributed to the Western-type high-fat diet [48,49]. Such a shift of the phylum composition has been linked to obesity in both mice and humans [49–52]. Mujico and colleagues observed that increased abundance of Firmicutes as well as *Clostridium* cluster XIVa and *Lactobacillus* was positively correlated with body weight in mice with diet induced obesity, whereas Bacteroidetes abundance was negatively correlated [49]. In our study, both *Lactobacillus* and *Clostridium* cluster XIVa associated OTUs showed decreased abundance in the ALA-rich diet group. Our results could therefore imply that an ALA-rich diet might have the potential to shift the microbiota composition to the lean phenotype. In agreement with this assumption, the Firmicutes/Bacteroidetes ratio was significantly decreased in type II diabetic patients following 6 months of EPA and DHA-rich diet compared to baseline [53]. Additionally, *Bacteroides-Prevotella* abundance was increased, which is similar to our finding of enhanced *Prevotella* growth in the ALA group. This suggests that ω-3 PUFA might exert similar effects on the gut microbiome.

It is important to mention that previous studies investigated microbial composition of the colon or cecum whereas we focused on the mid small intestine, which might also contribute to differences in results. In this line of thought, we did not observe a change in the abundance of the *Bifidobacterium* genus, although *Bifidobacterium* strains were previously shown to produce ALA-derived metabolites [19]. This outcome might simply be due to the fact that these predominantly obligate anaerobic bacteria [54] are not abundant in the small intestine due to remaining small amounts of oxygen. Supporting this claim, we detected *Bifidobacteria*-associated OTUs only in one animal of the ALA group at a relative abundance of 0.02%. However, the abundance of OTUs associated with the *Lactobacillus* genus was also reduced following ALA-rich diet. It is important to mention that the ALA metabolism to conjugated fatty acids and growth inhibition was reported to be strain specific [19], whereas our analysis lacks the biological resolution to differentiate between individual bacterial strains. Additionally, Druart et al. detected the highest amounts of PUFA derived metabolites in the cecum and colon compared to jejunum and ileum, even though the small intestine is where the majority of fatty acid absorption takes place [55].

In our current study, we did not investigate the effects of the Western-type HFD on intestinal commensals as the influence of the HFD was addressed in previous work [48,49,51]. Furthermore, we tested the same HFD diet in a previous study, where we described a reduced Bacteroidetes and an increased Firmicutes abundance compared to control diet [47]. This finding is in agreement with previous reports. In contrast, we observed the opposite trend after feeding mice an ALA-rich diet. An ALA-rich diet was associated with a reduced abundance of *Anaerotruncus* and *Streptococcus*, whereas in

our previous study the growth of these genera was stimulated by the Western-type HFD feeding [47]. Since both the ALA-rich diet and Western-type HFD had comparable caloric and fat content, these results suggest that the fatty acid pattern itself is an important factor shaping the composition of the intestinal microbiota. In support of this, we included a summary of further studies, which reported similar effects on microbiota composition following ALA or PUFA-rich diets in Supplementary Table S2.

Our predictive functional metagenome analysis implied that the ALA-rich diet might significantly impact a number of pathways, although effect sizes were generally small. Contrary to our expectations, we found the ALA metabolism pathway to be downregulated in the ALA group compared to control animals. This is probably due to the reduced abundance of OTUs associated with *Lactobacillus* and Lachnospiraceae as specific strains of these bacteria are reportedly able to metabolize ALA [21–23]. Furthermore, increased dietary amounts of ALA might interfere with the adaptive capabilities of gut bacteria since we observed a downregulation of the two-component system in the ALA-rich diet group. In line, we predicted significantly more sequences associated with the bacterial secretion system pathway compared to control animals, which might be an adaptive response of the commensal microbiota. Unsaturated fatty acids were previously reported to activate components of the bacterial secretion system of *Staphylococcus aureus* as part of its stress response [56,57]. Interestingly, the prostate cancer pathway was enriched in the ALA-group and a few reports have linked ALA levels with an increased risk for prostate cancer [58–60]. Nevertheless, other studies did not identify such association, so results remain controversial [16]. However, our findings regarding the functional metagenome are only based on in silico predictions and would have to be validated by whole metagenome shotgun sequencing.

Apart from the pronounced changes in gut microbiota composition, ALA-enriched diet resulted in an expected increase in ALA levels in the small intestinal tissue of mice. In line, the relative amount of EPA and DHA, oxylipins linked to reduced synthesis of inflammatory cytokines [61], was elevated in these tissues. The higher increase of EPA levels compared to DHA supports the conventional assumption that ALA is a better precursor for EPA than DHA in vivo [62]. In contrast to a previous study on the absorption of essential fatty acids in the rat jejunum [63], we noted a significant reduction in small intestinal AA levels in the ALA diet-fed group. Of note, the ALA diet-dependent up-regulation of fatty acid-binding protein 1 (FABP1; L-FABP) was reported in the small intestine of the C57BL/KsJ-db/dg obesity mouse model [64], demonstrating a direct influence of this essential fatty acid on the regulation of host metabolism. Overall, the ALA-rich diet was linked to a very consistent effect on the fatty acid profile of the small intestine as different classes of fatty acids were all regulated in the same direction. Namely, all significantly altered saturated fatty acids (SFA), monounsaturated fatty acids (MUFA), ω-6 PUFA and ω-9 PUFA demonstrated reduced levels in the ALA group whereas all significantly altered ω-3 PUFA showed an increased concentration. This indicates that an ALA-rich diet drives the fatty acid composition of the intestinal tissue towards an anti-inflammatory phenotype. For instance, decreasing the dietary ω-6/ ω-3 PUFA ratio was associated with significantly lower circulating levels of the pro-inflammatory marker interleukin-6 as well as non-high-density lipoprotein (non-HDL) cholesterol in low-density lipoprotein (LDL) receptor-deficient mice, which in turn led to attenuated aortic lesion formation [65]

In addition to influences on host metabolism, trophic effects on the mid small intestine were reported for bolus doses of essential fatty acids (i.e., ALA) [66]. In our study, the enrichment of ALA-derived metabolites in the small intestinal tissue was accompanied by the morphometric adaptation of the small intestine, as shown by increased mucosal thickness, increased villus length and an elevated number of epithelial cells per crypt-villus axis. These ALA-rich diet-induced elongated villus structures were associated with a vastly decreased epithelial cell proliferation rate. Considering that 4 weeks of Western-type HFD feeding yielded a similar gut mucosal morphology, the observed adaptation in gut morphology likely is a general feature of fat-rich diets. Noteworthy, the ALA-rich diet group showed a tendency of reduced villus spacing relative to the CTR group. Remarkably, our findings on dietary ALA, evoking reduced epithelial cell proliferation in the small intestine, are in

support of the identified proliferation inhibitory effect of conjugated isomers of ALA (C18:3 c9, t11, c15 conjugated ALA), generated by *Bifidobacterium breve* National Collection of Industrial Food and Marine Bacteria (NCIMB) 702258 on the SW480 colon cancer cell line. Thus, we here provide direct evidence for the functional role of an ALA-enriched diet in influencing the small intestinal architecture. The functional involvement of HFD-induced dysbiosis in pathways driving morphometric adaptation of the small intestinal architecture is subject to further investigation. This aspect is in particular interesting since elongated villus structures and a decreased epithelial proliferation rate is a prominent trait of the germ-free mouse model [67]. The impact of a fat-rich diet on the morphogenetic adaptation of the small intestine may consequently have broad implications for nutrient uptake.

The nutritional impact on ALA-rich diet may also influence the differentiation of the secretory lineage. Specifically, we observed a marked decrease in the percentage of goblet and Paneth cells in the ALA group. This strongly suggests that additional gut developmental pathways are likewise influenced by fat-rich diet. In line with this, Benoit and colleagues demonstrated that ALA led to a significant decrease in the secretion of mucin 2 (MUC2) in a HT29-MTX cell line in vitro. Furthermore, the expression of the human atonal homolog 1 transcription factor (ATOH1), which is involved in goblet cell differentiation [68], was downregulated by ALA [25]. Interestingly, in the same study, oral administration of rapeseed oil to rat pups, which is rich in ω-3 PUFAs, was associated with reduced goblet cell numbers. An alternative mechanism through which a high-fat diet might influence intestinal morphology is via modifications in the composition of the commensal microbiota. Further studies such as feeding experiments in germ-free and conventionally raised mice would be necessary to investigate these hypotheses. As recent studies showed that modern nano-sized food additives are able to interact with both gut microbiota and biomolecules, it will be interesting to study the combined effects of nanoparticulates and macronutrients, such as ALA, in future studies [69–73].

Limitation of the Analysis

The main limitation of our study is the small sample size for the analysis of the commensal microbiota composition in the small intestine. Due to the resulting low statistical power, our analysis was theoretically only able to detect large effect sizes. Therefore, an ALA-rich diet might result in additional changes in microbiome composition, which remained undetected. This limitation is partially offset by the statistical technique we employed. DESeq was previously shown to have increased sensitivity for differential abundance analysis in small samples compared to other methods [74]. Hence, our results on the effects of an ALA-rich diet on microbiota composition in the mouse small intestine should be verified in a larger cohort.

5. Conclusions

Our study on adult C57BL/6J mice revealed that an ALA-rich diet influences the microbiota composition and the predicted metagenome of the small intestine. Interestingly, the two-component system was downregulated, and the bacterial secretion system was upregulated in the ALA group, suggesting that an ALA-rich diet might affect bacterial adaptive responses. Moreover, we demonstrated the adaptation of gut morphology to an ALA-enriched diet, a trait that was also observed by feeding a Western-type HFD. Strikingly, the percentage of goblet and Paneth cells per crypt-villus axis was dramatically reduced under ALA-rich diet and Western-type HFD feeding conditions.

Supplementary Materials: The following are available online at http://www.mdpi.com/2072-6643/12/3/732/s1, Table S1. Fatty acid profile of intestinal tissue of mice receiving α-linolenic acid-rich diet or control diet; Table S2. Studies reporting similar effects of ALA- or PUFA-rich diet on microbiome composition; Figure S1. Composition of the small intestine microbiota at the genus level.

Author Contributions: Conceptualization, C.R.; methodology, H.T., B.K., F.B., I.B., J.M.K., B.W., A.M., J.M., K.E., G.P., H.F., R.S., W.A.N., F.S., S.G. and C.R.; software, H.T. and S.G.; validation, H.T., B.K., F.B. and C.R.; formal analysis, H.T., B.K., F.B. and C.R.; investigation, H.T., B.K., F.B., I.B., J.M.K., B.W., A.M., J.M., G.P., H.F., R.S., W.A.N., F.S., S.G. and C.R.; resources, K.E., S.G. and C.R.; data curation, H.T., B.K., F.B., and C.R.; writing—original draft preparation, H.T. and C.R.; writing—review and editing, H.T., B.K., F.B., I.B., J.M.K., B.W., A.M., J.M., G.P.,

K.E., R.S., W.A.N., F.S., S.G. and C.R.; visualization, H.T.; supervision, S.G. and C.R.; project administration, C.R.; funding acquisition, C.R. All authors have read and agreed to the published version of the manuscript.

Funding: The study was supported by grants from the German Ministry for Education and Research (BMBF, 01EO1003 and 01EO1503), a Deutsche Forschungsgemeinschaft (DFG) individual grant (RE 3450/5-2), the consortium grant "novel and neglected cardiovascular risk factors: molecular mechanisms and therapeutic implications" from the Boehringer Ingelheim Stiftung to C.R., a grant from the Naturwissenschaftlich-Medizinische Forschungszentrum (NMFZ) to C.R., as well as a grant from the Inneruniversitäre Forschungsförderung (Stufe 1) of the Johannes Gutenberg University-Mainz to J.M.K. and C.R. F.S. is thankful for support from DFG collaborative research center (CRC) 1182 (project C2), cluster of excellence EXC 306 and DFG EXS2167.

Acknowledgments: We are grateful to Klaus-Peter Derreth for expert technical assistance.

Conflicts of Interest: The authors declare no conflict of interest.

References

1. Caligiuri, S.P.B.; Parikh, M.; Stamenkovic, A.; Pierce, G.N.; Aukema, H.M. Dietary modulation of oxylipins in cardiovascular disease and aging. *Am. J. Physiol. Heart Circ. Physiol.* **2017**, *313*, H903–H918. [CrossRef] [PubMed]
2. Carroll, A.E.; Hwang, D.H. Decreased formation of porstaglandins derived from arachidonic acid by dietary linolenate in rats. *Am. J. Clin. Nutr.* **1980**, *33*, 590–597. [CrossRef]
3. Horii, T.; Satouchi, K.; Kobayashi, Y.; Saito, K.; Watanabe, S.; Yoshida, Y.; Okuyama, H. Effect of dietary alpha-linolenate on platelet-activating factor production in rat peritoneal polymorphonuclear leukocytes. *J. Immunol.* **1991**, *147*, 1607.
4. Thies, F.; Miles, E.A.; Nebe-von-Caron, G.; Powell, J.R.; Hurst, T.L.; Newsholme, E.A.; Calder, P.C. Influence of dietary supplementation with long-chain n−3 or n−6 polyunsaturated fatty acids on blood inflammatory cell populations and functions and on plasma soluble adhesion molecules in healthy adults. *Lipids* **2001**, *36*, 1183–1193. [CrossRef] [PubMed]
5. Caligiuri, S.P.B.; Aukema, H.M.; Ravandi, A.; Guzman, R.; Dibrov, E.; Pierce, G.N. Flaxseed consumption reduces blood pressure in patients with hypertension by altering circulating oxylipins via an α-linolenic acid-induced inhibition of soluble epoxide hydrolase. *Hypertension* **2014**, *64*, 53–59. [CrossRef]
6. Caligiuri, S.P.B.; Rodriguez-Leyva, D.; Aukema, H.M.; Ravandi, A.; Weighell, W.; Guzman, R.; Pierce, G.N. Dietary flaxseed reduces central aortic blood pressure without cardiac involvement but through changes in plasma oxylipins. *Hypertension* **2016**, *68*, 1031–1038. [CrossRef]
7. Kulkarni, P.S.; Eakins, K.E. The enzymatic conversion of prostaglandin endoperoxides to thromboxane-A2-like activity by human iris microsomes. *Prostaglandins* **1977**, *14*, 601–605. [CrossRef]
8. Ibrahim, A.; Aziz, M.; Hassan, A.; Mbodji, K.; Collasse, E.; Coëffier, M.; Bounoure, F.; Savoye, G.; Déchelotte, P.; Marion-Letellier, R. Dietary α-linolenic acid–rich formula reduces adhesion molecules in rats with experimental colitis. *Nutrition* **2012**, *28*, 799–802. [CrossRef]
9. Reifen, R.; Karlinsky, A.; Stark, A.H.; Berkovich, Z.; Nyska, A. α-Linolenic acid (ALA) is an anti-inflammatory agent in inflammatory bowel disease. *J. Nutr. Biochem.* **2015**, *26*, 1632–1640. [CrossRef]
10. Trebble, T.M.; Pearl, D.S.; Eiden, M.; Masoodi, M.; Brümmer, B.J.; Gullick, D.; Mills, G.; Brown, J.F.; Shute, J.K.; Mckeever, T.M.; et al. Altered colonic mucosal availability of n-3 and n-6 polyunsaturated fatty acids in ulcerative colitis and the relationship to disease activity. *J. Crohns Colitis* **2014**, *8*, 70–79. [CrossRef]
11. Tyagi, A.; Kumar, U.; Reddy, S.; Santosh, V.S.; Mohammed, S.B.; Ehtesham, N.Z.; Ibrahim, A. Attenuation of colonic inflammation by partial replacement of dietary linoleic acid with α-linolenic acid in a rat model of inflammatory bowel disease. *Br. J. Nutr.* **2012**, *108*, 1612–1622. [CrossRef] [PubMed]
12. Narisawa, T.; Takahashi, M.; Kotanagi, H.; Kusaka, H.; Yamazaki, Y.; Koyama, H.; Fukaura, Y.; Nishizawa, Y.; Kotsugai, M.; Isoda, Y. Inhibitory effect of dietary perilla oil rich in the n-3 polyunsaturated fatty acid alpha-linolenic acid on colon carcinogenesis in rats. *Jpn. J. Cancer Res. Gann* **1991**, *82*, 1089–1096. [CrossRef] [PubMed]
13. Tian, Y.; Wang, H.; Yuan, F.; Li, N.; Huang, Q.; He, L.; Wang, L.; Liu, Z. Perilla oil has similar protective effects of fish oil on high-fat diet-induced nonalcoholic fatty liver disease and gut dysbiosis. *BioMed Res. Int.* **2016**, *2016*, 11. [CrossRef] [PubMed]

14. Patterson, E.; O'Doherty, R.M.; Murphy, E.F.; Wall, R.; O'Sullivan, O.; Nilaweera, K.; Fitzgerald, G.F.; Cotter, P.D.; Ross, R.P.; Stanton, C. Impact of dietary fatty acids on metabolic activity and host intestinal microbiota composition in C57BL/6J mice. *Br. J. Nutr.* **2014**, *111*, 1905–1917. [CrossRef]
15. Salsinha, A.S.; Pimentel, L.L.; Fontes, A.L.; Gomes, A.M.; Rodríguez-Alcalá, L.M. Microbial production of conjugated linoleic acid and conjugated linolenic acid relies on a multienzymatic system. *Microbiol. Mol. Biol. Rev.* **2018**, *82*. [CrossRef]
16. Hennessy, A.A.; Ross, R.P.; Devery, R.; Stanton, C. The health promoting properties of the conjugated isomers of α-linolenic acid. *Lipids* **2011**, *46*, 105–119. [CrossRef]
17. Yuan, G.-F.; Chen, X.-E.; Li, D. Conjugated linolenic acids and their bioactivities: A review. *Food Funct.* **2014**, *5*, 1360–1368. [CrossRef]
18. Fontes, A.L.; Pimentel, L.L.; Simões, C.D.; Gomes, A.M.P.; Rodríguez-Alcalá, L.M. Evidences and perspectives in the utilization of CLNA isomers as bioactive compounds in foods. *Crit. Rev. Food Sci. Nutr.* **2017**, *57*, 2611–2622. [CrossRef]
19. Gorissen, L.; Raes, K.; Weckx, S.; Dannenberger, D.; Leroy, F.; De Vuyst, L.; De Smet, S. Production of conjugated linoleic acid and conjugated linolenic acid isomers by Bifidobacterium species. *Appl. Microbiol. Biotechnol.* **2010**, *87*, 2257–2266. [CrossRef]
20. Hennessy, A.A.; Barrett, E.; Paul Ross, R.; Fitzgerald, G.F.; Devery, R.; Stanton, C. The production of conjugated α-linolenic, γ-linolenic and stearidonic acids by strains of Bifidobacteria and Propionibacteria. *Lipids* **2012**, *47*, 313–327. [CrossRef]
21. Kishino, S.; Ogawa, J.; Ando, A.; Shimizu, S. Conjugated α-linolenic acid production from α-linolenic acid by Lactobacillus plantarum AKU 1009a. *Eur. J. Lipid Sci. Technol.* **2003**, *105*, 572–577. [CrossRef]
22. Ogawa, J.; Kishino, S.; Ando, A.; Sugimoto, S.; Mihara, K.; Shimizu, S. Production of conjugated fatty acids by lactic acid bacteria. *J. Biosci. Bioeng.* **2005**, *100*, 355–364. [CrossRef] [PubMed]
23. Druart, C.; Bindels, L.B.; Schmaltz, R.; Neyrinck, A.M.; Cani, P.D.; Walter, J.; Ramer-Tait, A.E.; Delzenne, N.M. Ability of the gut microbiota to produce PUFA-derived bacterial metabolites: Proof of concept in germ-free versus conventionalized mice. *Mol. Nutr. Food Res.* **2015**, *59*, 1603–1613. [CrossRef] [PubMed]
24. Ohue-Kitano, R.; Yasuoka, Y.; Goto, T.; Kitamura, N.; Park, S.-B.; Kishino, S.; Kimura, I.; Kasubuchi, M.; Takahashi, H.; Li, Y.; et al. α-Linolenic acid–derived metabolites from gut lactic acid bacteria induce differentiation of anti-inflammatory M2 macrophages through G protein-coupled receptor 40. *FASEB J.* **2017**, *32*, 304–318. [CrossRef]
25. Benoit, B.; Kayal, F.; Bruno, J.; Estienne, M.; Plaisancié, P.; Debard, C.; Ducroc, R. Saturated and unsaturated fatty acids differently modulate colonic goblet cells in vitro and in rat pups. *J. Nutr.* **2015**, *145*, 1754–1762. [CrossRef] [PubMed]
26. Konieczka, P.; Barszcz, M.; Choct, M.; Smulikowska, S. The interactive effect of dietary n-6: n-3 fatty acid ratio and vitamin E level on tissue lipid peroxidation, DNA damage in intestinal epithelial cells, and gut morphology in chickens of different ages. *Poult. Sci.* **2018**, *97*, 149–158. [CrossRef] [PubMed]
27. Schober, Y.; Wahl, H.G.; Renz, H.; Nockher, W.A. Determination of red blood cell fatty acid profiles: Rapid and high-confident analysis by chemical ionization-gas chromatography-tandem mass spectrometry. *J. Chromatogr. B* **2017**, *1040*, 1–7. [CrossRef]
28. Walters, W.; Hyde, E.R.; Berg-Lyons, D.; Ackermann, G.; Humphrey, G.; Parada, A.; Gilbert, J.A.; Jansson, J.K.; Caporaso, J.G.; Fuhrman, J.A.; et al. Improved bacterial 16S rRNA gene (V4 and V4-5) and fungal internal transcribed spacer marker gene primers for microbial community surveys. *MSystems* **2015**, *1*, e00009–e00015. [CrossRef]
29. Parada, A.E.; Needham, D.M.; Fuhrman, J.A. Every base matters: Assessing small subunit rRNA primers for marine microbiomes with mock communities, time series and global field samples. *Environ. Microbiol.* **2016**, *18*, 1403–1414. [CrossRef]
30. Apprill, A.; McNally, S.; Parsons, R.; Weber, L. Minor revision to V4 region SSU rRNA 806R gene primer greatly increases detection of SAR11 bacterioplankton. *Aquat. Microb. Ecol.* **2015**, *75*, 129–137. [CrossRef]
31. Schloss, P.D.; Westcott, S.L.; Ryabin, T.; Hall, J.R.; Hartmann, M.; Hollister, E.B.; Lesniewski, R.A.; Oakley, B.B.; Parks, D.H.; Robinson, C.J.; et al. Introducing mothur: Open-source, platform-independent, community-supported software for describing and comparing microbial communities. *Appl. Environ. Microbiol.* **2009**, *75*, 7537–7541. [CrossRef] [PubMed]

32. Kozich, J.J.; Westcott, S.L.; Baxter, N.T.; Highlander, S.K.; Schloss, P.D. Development of a dual-index sequencing strategy and curation pipeline for analyzing amplicon sequence data on the MiSeq Illumina sequencing platform. *Appl. Environ. Microbiol.* **2013**, *79*, 5112–5120. [CrossRef] [PubMed]
33. Rognes, T.; Flouri, T.; Nichols, B.; Quince, C.; Mahé, F. VSEARCH: A versatile open source tool for metagenomics. *PeerJ* **2016**, *4*, e2584. [CrossRef] [PubMed]
34. Fuchs, B.M.; Quast, C.; Pruesse, E.; Peplies, J.; Knittel, K.; Ludwig, W.; Glöckner, F.O. SILVA: A comprehensive online resource for quality checked and aligned ribosomal RNA sequence data compatible with ARB. *Nucleic Acids Res.* **2007**, *35*, 7188–7196. [CrossRef]
35. Kulam-Syed-Mohideen, A.S.; Chai, B.; McGarrell, D.M.; Cardenas, E.; Garrity, G.M.; Fish, J.; Tiedje, J.M.; Wang, Q.; Farris, R.J.; Marsh, T.; et al. The Ribosomal Database Project: Improved alignments and new tools for rRNA analysis. *Nucleic Acids Res.* **2008**, *37*, D141–D145. [CrossRef]
36. McMurdie, P.J.; Holmes, S. phyloseq: An R package for reproducible interactive analysis and graphics of microbiome census data. *PLoS ONE* **2013**, *8*, e61217. [CrossRef] [PubMed]
37. Anderson, M.J.; Willis, T.J. Canonical analysis of principal coordinates: A useful method of constrained ordination for ecology. *Ecology* **2003**, *84*, 511–525. [CrossRef]
38. Todorov, H.; Fournier, D.; Gerber, S. Principal components analysis: Theory and application to gene expression data analysis. *Genom. Comput. Biol.* **2018**, *4*, e100041. [CrossRef]
39. Love, M.I.; Huber, W.; Anders, S. Moderated estimation of fold change and dispersion for RNA-seq data with DESeq2. *Genome Biol.* **2014**, *15*, 550. [CrossRef]
40. Langille, M.G.I.; Zaneveld, J.; Caporaso, J.G.; McDonald, D.; Knights, D.; Reyes, J.A.; Clemente, J.C.; Burkepile, D.E.; Vega Thurber, R.L.; Knight, R.; et al. Predictive functional profiling of microbial communities using 16S rRNA marker gene sequences. *Nat. Biotechnol.* **2013**, *31*, 814. [CrossRef]
41. McDonald, D.; Price, M.N.; Goodrich, J.; Nawrocki, E.P.; DeSantis, T.Z.; Probst, A.; Andersen, G.L.; Knight, R.; Hugenholtz, P. An improved Greengenes taxonomy with explicit ranks for ecological and evolutionary analyses of bacteria and archaea. *ISME J.* **2012**, *6*, 610–618. [CrossRef] [PubMed]
42. Parks, D.H.; Tyson, G.W.; Hugenholtz, P.; Beiko, R.G. STAMP: Statistical analysis of taxonomic and functional profiles. *Bioinformatics* **2014**, *30*, 3123–3124. [CrossRef]
43. Shin, H.-S.; Kim, S.-W. Lipid composition of perilla seed. *J. Am. Oil Chem. Soc.* **1994**, *71*, 619–622. [CrossRef]
44. Ding, Y.; Mokgolodi, N.C.; Hu, Y.; Shi, L.; Ma, C.; Liu, Y.-J. Characterization of fatty acid composition from five perilla seed oils in China and its relationship to annual growth temperature. *J. Med. Plants Res.* **2012**, *6*, 1645–1651.
45. Peirett, P. Fatty acid content and chemical composition of vegetative parts of Perilla (Perilla frutescens) after different growth lengths. *J. Med. Plants Res.* **2011**, *5*, 72–78. [CrossRef]
46. Gwari, G.; Lohani, H.; Haider, S.Z.; Bhandari, U.; Chauhan, N.; Rawat, D.S. Fatty acid and nutrient composition of Perilla (Perilla frutescens L.) accessions collected from Uttarakhand. *Int. J. Phytopharm.* **2014**, *5*, 379–382.
47. Kiouptsi, K.; Jäckel, S.; Pontarollo, G.; Grill, A.; Kuijpers, M.J.E.; Wilms, E.; Weber, C.; Sommer, F.; Nagy, M.; Neideck, C.; et al. The Microbiota Promotes Arterial Thrombosis in Low-Density Lipoprotein Receptor-Deficient Mice. *MBio* **2019**, *10*, e02298-19. [CrossRef]
48. Hildebrandt, M.A.; Hoffmann, C.; Sherrill-Mix, S.A.; Keilbaugh, S.A.; Hamady, M.; Chen, Y.-Y.; Knight, R.; Ahima, R.S.; Bushman, F.; Wu, G.D. High-fat diet determines the composition of the murine gut microbiome independently of obesity. *Gastroenterology* **2009**, *137*, 1716–1724. [CrossRef]
49. Mujico, J.R.; Baccan, G.C.; Gheorghe, A.; Díaz, L.E.; Marcos, A. Changes in gut microbiota due to supplemented fatty acids in diet-induced obese mice. *Br. J. Nutr.* **2013**, *110*, 711–720. [CrossRef]
50. Ley, R.E.; Bäckhed, F.; Turnbaugh, P.; Lozupone, C.A.; Knight, R.D.; Gordon, J.I. Obesity alters gut microbial ecology. *Proc. Natl. Acad. Sci. USA* **2005**, *102*, 11070–11075. [CrossRef]
51. Ley, R.E.; Turnbaugh, P.J.; Klein, S.; Gordon, J.I. Human gut microbes associated with obesity. *Nature* **2006**, *444*, 1022. [CrossRef] [PubMed]
52. Turnbaugh, P.J.; Ley, R.E.; Mahowald, M.A.; Magrini, V.; Mardis, E.R.; Gordon, J.I. An obesity-associated gut microbiome with increased capacity for energy harvest. *Nature* **2006**, *444*, 1027. [CrossRef] [PubMed]

53. Balfegó, M.; Canivell, S.; Hanzu, F.A.; Sala-Vila, A.; Martínez-Medina, M.; Murillo, S.; Mur, T.; Ruano, E.G.; Linares, F.; Porras, N.; et al. Effects of sardine-enriched diet on metabolic control, inflammation and gut microbiota in drug-naïve patients with type 2 diabetes: A pilot randomized trial. *Lipids Health Dis.* **2016**, *15*, 78. [CrossRef] [PubMed]
54. Biavati, B.; Vescovo, M.; Torriani, S.; Bottazzi, V. Bifidobacteria: History, ecology, physiology and applications. *Ann. Microbiol.* **2000**, *50*, 117–131.
55. Druart, C.; Neyrinck, A.M.; Vlaeminck, B.; Fievez, V.; Cani, P.D.; Delzenne, N.M. Role of the lower and upper intestine in the production and absorption of gut microbiota-derived PUFA metabolites. *PLoS ONE* **2014**, *9*, e87560. [CrossRef] [PubMed]
56. Lopez, M.S.; Tan, I.S.; Yan, D.; Kang, J.; McCreary, M.; Modrusan, Z.; Austin, C.D.; Xu, M.; Brown, E.J. Host-derived fatty acids activate type VII secretion in Staphylococcus aureus. *Proc. Natl. Acad. Sci. USA* **2017**, *114*, 11223–11228. [CrossRef]
57. Kenny, J.G.; Ward, D.; Josefsson, E.; Jonsson, I.-M.; Hinds, J.; Rees, H.H.; Lindsay, J.A.; Tarkowski, A.; Horsburgh, M.J. The Staphylococcus aureus response to unsaturated long chain free fatty acids: Survival mechanisms and virulence implications. *PLoS ONE* **2009**, *4*, e4344. [CrossRef]
58. Katan, M.B.; Zock, P.L.; Brouwer, I.A. Dietary α-linolenic acid is associated with reduced risk of fatal coronary heart disease, but increased prostate cancer risk: A meta-analysis. *J. Nutr.* **2004**, *134*, 919–922. [CrossRef]
59. Ramon, J.M.; Bou, R.; Romea, S.; Alkiza, M.E.; Jacas, M.; Ribes, J.; Oromi, J. Dietary fat intake and prostate cancer risk: A case–control study in Spain. *Cancer Causes Control* **2000**, *11*, 679–685. [CrossRef]
60. De Stéfani, E.; Deneo-Pellegrini, H.; Boffetta, P.; Ronco, A.; Mendilaharsu, M. α-linolenic acid and risk of prostate cancer: A case-control study in Uruguay. *Cancer Epidemiol. Prev. Biomark.* **2000**, *9*, 335–338.
61. Dessì, M.; Noce, A.; Bertucci, P.; Manca di Villahermosa, S.; Zenobi, R.; Castagnola, V.; Addessi, E.; Di Daniele, N. Atherosclerosis, dyslipidemia, and inflammation: The significant role of polyunsaturated fatty acids. *ISRN Inflamm.* **2013**, *2013*, 191823. [CrossRef] [PubMed]
62. Burdge, G.C. Metabolism of α-linolenic acid in humans. *Prostaglandins Leukot. Essent. Fat. Acids* **2006**, *75*, 161–168. [CrossRef] [PubMed]
63. Punchard, N.A.; Green, A.T.; Mullins, J.G.; Thompson, R.P.H. Analysis of the intestinal absorption of essential fatty acids in vivo in the rat. *Prostaglandins Leukot. Essent. Fat. Acids* **2000**, *62*, 27–33. [CrossRef]
64. Nagasawa, A.; Suzuki, J.; Hase, T.; Murase, T.; Wakisaka, T.; Tokimitsu, I. Dietary α-linolenic acid–rich diacylglycerols reduce body weight gain accompanying the stimulation of intestinal β-oxidation and related gene expressions in C57BL/KsJ-db/db mice. *J. Nutr.* **2002**, *132*, 3018–3022. [CrossRef]
65. Wang, S.; Wu, D.; Matthan, N.R.; Lamon-Fava, S.; Lecker, J.L.; Lichtenstein, A.H. Reduction in dietary omega-6 polyunsaturated fatty acids: Eicosapentaenoic acid plus docosahexaenoic acid ratio minimizes atherosclerotic lesion formation and inflammatory response in the LDL receptor null mouse. *Atherosclerosis* **2009**, *204*, 147–155. [CrossRef]
66. Jenkins, A.P.; Thompson, R.P. Does the fatty acid profile of dietary fat influence its trophic effect on the small intestinal mucosa? *Gut* **1993**, *34*, 358–364. [CrossRef]
67. Abrams, G.D.; Baurer, H.; Sprinz, H. Influence of the normal flora on mucosal morphology and cellular renewal in the ileum. A comparison of germ-free and conventional mice. *Lab. Investig.* **1963**, *12*, 355–364.
68. Zheng, X.; Tsuchiya, K.; Okamoto, R.; Iwasaki, M.; Kano, Y.; Sakamoto, N.; Nakamura, T.; Watanabe, M. Suppression of hath1 gene expression directly regulated by hes1 via notch signaling is associated with goblet cell depletion in ulcerative colitis. *Inflamm. Bowel Dis.* **2011**, *17*, 2251–2260. [CrossRef]
69. Docter, D.; Westmeier, D.; Markiewicz, M.; Stolte, S.; Knauer, S.K.; Stauber, R.H. The nanoparticle biomolecule corona: Lessons learned—Challenge accepted. *Chem. Soc. Rev.* **2015**, *44*, 6094–6121. [CrossRef]
70. Westmeier, D.; Hahlbrock, A.; Reinhardt, C.; Frohlich-Nowoisky, J.; Wessler, S.; Vallet, C.; Poschl, U.; Knauer, S.K.; Stauber, R.H. Nanomaterial-microbe cross-talk: Physicochemical principles and (patho)biological consequences. *Chem. Soc. Rev.* **2018**, *47*, 5312–5337. [CrossRef]
71. Siemer, S.; Hahlbrock, A.; Vallet, C.; McClements, D.J.; Balszuweit, J.; Voskuhl, J.; Docter, D.; Wessler, S.; Knauer, S.K.; Westmeier, D.; et al. Nanosized food additives impact beneficial and pathogenic bacteria in the human gut: A simulated gastrointestinal study. *NPJ Sci. Food* **2018**, *2*, 22. [CrossRef] [PubMed]
72. Stauber, R.H.; Siemer, S.; Becker, S.; Ding, G.B.; Strieth, S.; Knauer, S.K. Small Meets Smaller: Effects of Nanomaterials on Microbial Biology, Pathology, and Ecology. *ACS Nano* **2018**, *12*, 6351–6359. [CrossRef] [PubMed]

73. Siemer, S.; Westmeier, D.; Vallet, C.; Steinmann, J.; Buer, J.; Stauber, R.H.; Knauer, S.K. Breaking resistance to nanoantibiotics by overriding corona-dependent inhibition using a pH-switch. *Mater. Today* **2018**, *26*, 19–29. [CrossRef]
74. Weiss, S.; Xu, Z.Z.; Peddada, S.; Amir, A.; Bittinger, K.; Gonzalez, A.; Lozupone, C.; Zaneveld, J.R.; Vázquez-Baeza, Y.; Birmingham, A.; et al. Normalization and microbial differential abundance strategies depend upon data characteristics. *Microbiome* **2017**, *5*, 27. [CrossRef] [PubMed]

2.3.1 Supplementary material to publication 3

Table S1. Fatty acid profile of intestinal tissue of mice receiving α-linolenic acid-rich diet or control diet.

Fatty acid	Control diet (mean ± SEM)	ALA diet (mean ± SEM)	p-value
C8:0 Caprylic acid	0.00 ± 0.00	0.00 ± 0.00	n.s.
C10:0 Capric acid	0.00 ± 0.00	0.00 ± 0.00	n.s.
C11:0 Undecylic acid	0.00 ± 0.00	0.00 ± 0.00	n.s.
C12:0 Lauric acid	0.026 ± 0.007	0.006 ± 0.002	0.032$^{\#}$
C13:0 Tridecylic acid	0.00 ± 0.00	0.00 ± 0.00	n.s.
C14:0 Myristic acid	1.84 ± 0.24	0.45 ± 0.06	0.003**
C14:1 Myristoleic acid	0.038 ± 0.010	0.002 ± 0.002	0.008$^{\#\#}$
C15:0 Pentadecanoic acid	0.086 ± 0.002	0.07 ± 0.003	0.024$^{\#}$
C15:1 Pentadecenoic acid	0.00 ± 0.00	0.00 ± 0.00	n.s.
C16:0 Palmitic acid	31.43 ± 1.01	14.82 ± 0.54	<0.0001***
C16:1 Palmitoleic acid	4.50 ± 0.96	0.41 ± 0.09	0.013*
C17:0 Margaric acid	0.17 ± 0.02	0.20 ± 0.02	n.s.
C18:0 Stearic acid	9.51 ± 1.05	12.54 ± 1.10	n.s.
C18:1 trans Elaidic acid	0.048 ± 0.024	0.042 ± 0.004	n.s.
C18:1 cis Oleic acid	15.16 ± 0.68	7.20 ± 0.88	<0.0001***
C18:2 trans Linolelaidic acid	0.016 ± 0.016	0.002 ± 0.002	n.s.
C20:0 Arachidic acid	0.32 ± 0.03	0.25 ± 0.01	0.048*
C20:1 11-Eicosanoic acid	0.44 ± 0.03	0.24 ± 0.02	0.016$^{\#}$
C21:0 Heneicosylic acid	0.01 ± 0.0	0.008 ± 0.002	n.s.
C18:4 n3 Stearidonic acid	0.37 ± 0.14	10.64 ± 0.63	0.008$^{\#\#}$
C20:2 Eicosadienoic acid	0.12 ± 0.011	0.13 ± 0.013	n.s.
C22:0 Behenic acid	0.08 ± 0.014	0.056 ± 0.006	n.s.
C20:3 n9 Mead acid	1.13 ± 0.07	0.61 ± 0.09	0.002**
C20:3 n3 Eicosatrienoic acid	0.00 ± 0.00	0.16 ± 0.02	<0.0001***
C23:0 Tricosylic acid	1.34 ± 0.38	1.15 ± 0.55	n.s.
C22:2 Docosadienoic acid	0.00 ± 0.00	0.002 ± 0.002	n.s.

C24:0 Lignoceric acid	0.048 ± 0.007	0.046 ± 0.006	n.s.
C20:4 n3 Eicosatetranoic acid	0.042 ± 0.042	2.64± 0.53	0.008$^{\#\#}$
C22:3 Docosatrienoic acid	0.00 ± 0.00	5.49 ± 0.36	0.008$^{\#\#}$
C24:1 Nervonic acid	0.036 ± 0.005	0.04 ± 0.004	n.s.
C22:4 n6 Adrenic acid	0.64 ± 0.08	0.094 ± 0.011	0.002**
C22:5 n6 Osbond acid	0.45 ± 0.05	0.012 ± 0.002	0.008$^{\#\#}$
C22:5 n3 Docosapentanoic acid	0.056 ± 0.019	1.29 ± 0.19	0.008$^{\#\#}$

n.s. not significant *** p<0.001, ** p<0.01, *p<0.05 unpaired t-test; ### p<0.001, ## p<0.01, #p<0.05 Mann-Whitney U test.

Table S2. Studies reporting similar effects of ALA- or PUFA-rich diet on microbiome composition

Study	Study population	Diet	ALA/PUFA effects on microbiome comparable to our study
Tial et al. 2016[1]	Male Sprague-Dawley rats, 8-9 weeks old at study start	1. Normal chow diet with 10kcal% fat for 16 weeks 2. Western style lard-rich diet with 45 kcal% fat 3. Fish oil rich diet with 10% fish oil 4. Perilla-oil rich diet with 5.5 % perilla oil	Reduced Firmicutes/Bacteroidetes ratio; enhanced *Prevotella* and *Parabacteroides* growth; reduced *Lactobacillus* growth
Wang et al. 2018[2]	8-week old spontaneously diabetic male KKay mice (DM) or age-matched C57L/6 mice (NC)	1. NC + normal chow 2. DM + control chow 3. DM + low dose perilla oil (0.67 g/kg/bw/d) 4. DM + middle dose perilla oil (1.33 g/kg/bw/d) 5. DM + high dose perilla oil (2 g/kg/bw/d)	Enhanced *Parabacteroides* growth; reduced abundance of Lachnospiraceae in low dose perilla oil group compared to DM control.
Power et al 2016[3]	4-week old male C57Bl/6 mice	1. Basal diet for 3 weeks 2. Basal diet supplemented with 10% whole ground flaxseed oil	Enhanced abundance of *Prevotella*
Patterson et al. 2014[4]	8-week old male C57Bl/6 mice	1. Low fat- high maize starch diet for 16 weeks 2. Low fat-high sucrose diet 3. High fat-palm oil	Reduced *Anaerotruncus* growth in flaxseed/fish oil group compared to low fat-high sucrose group

		4. High fat-olive oil 5. High fat-safflower oil 6. High fat-flaxseed/fish oil	
Pusceddu et al. 2015[5]	17-week old female Sprague-Dawley rats (maternally separated and non-separated animals)	1. Saline water 2 Low dose EPA/DHA (0.4 g/kg/day mixture with 80% EPA and 20%DHA) 3. High dose EPA/DHA (1 g/kg/day mixture with 80% EPA and 20%DHA)	Enhanced *Prevotella* growth in low dose and high dose EPA/DHA group compared to control group (non-separated animals)
Beilharz et al. 2016[6]	Male Sragues-Dawley rats	1. Control diet (12 or 13 days) 2. Saturated fat diet (with lard as source) 3. PUFA rich diet (with sunflower oil as source) 4. Sugar diet	Reduced *Lactobacillus* growth in PUFA group compared to control diet

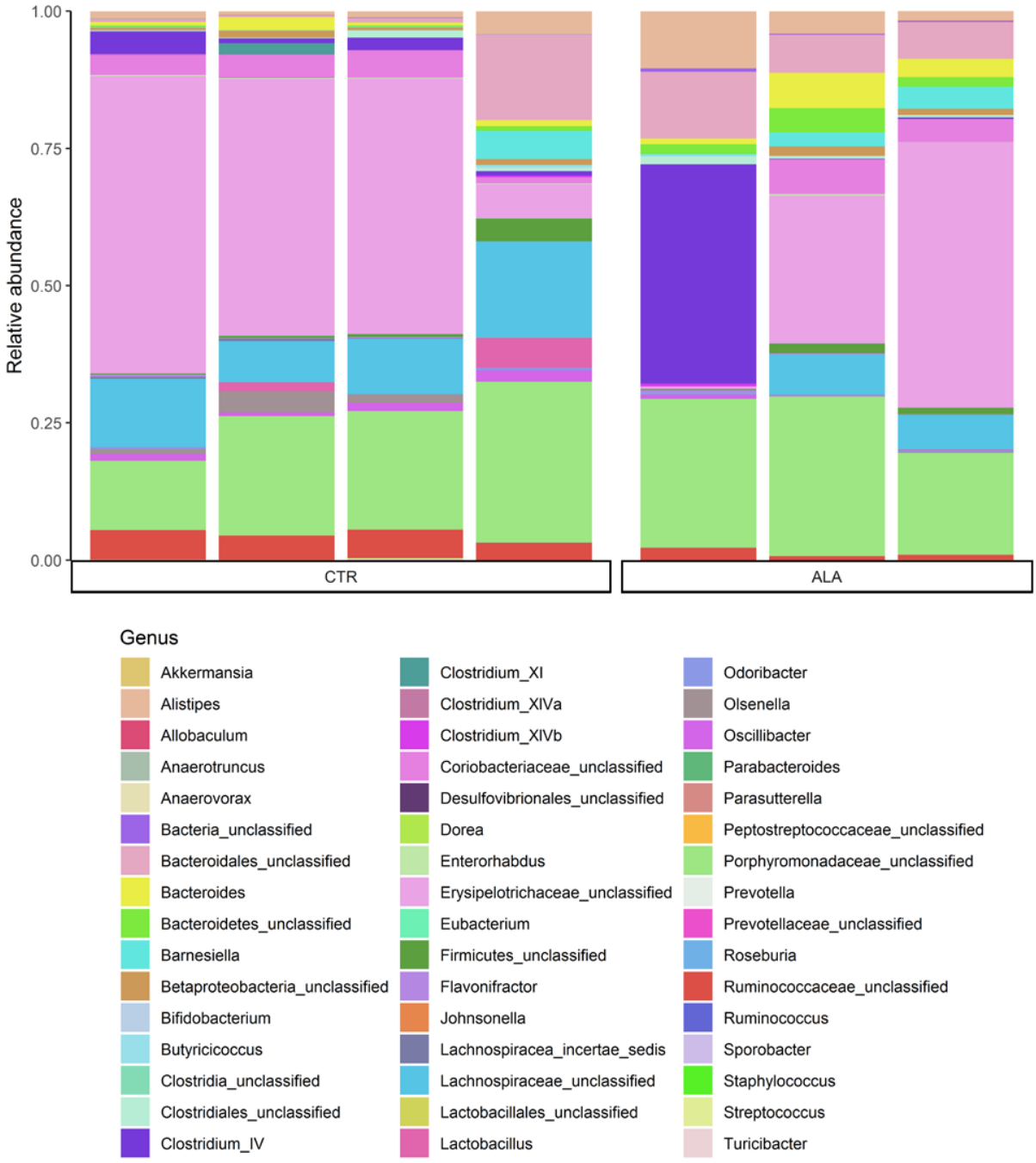

Figure S1. Composition of the small intestine microbiota at the genus level. Data are shown as relative abundance for each animal in the α-linolenic acid-rich diet group (ALA) or the control chow group (CTR).

References

1 Tian, Y. *et al.* Perilla oil has similar protective effects of fish oil on high-fat diet-induced nonalcoholic fatty liver disease and gut dysbiosis. *BioMed Research International* **2016**, 11, doi:10.1155/2016/9462571 (2016).

2 Wang, F. *et al.* Perilla Oil Supplementation Improves Hypertriglyceridemia and Gut Dysbiosis in Diabetic KKAy Mice. *Molecular nutrition & food research* **62**, e1800299-e1800299, doi:10.1002/mnfr.201800299 (2018).

3 Power, K. A. *et al.* Dietary flaxseed modulates the colonic microenvironment in healthy C57Bl/6 male mice which may alter susceptibility to gut-associated diseases. *The Journal of Nutritional Biochemistry* **28**, 61-69, doi:https://doi.org/10.1016/j.jnutbio.2015.09.028 (2016).

4 Patterson, E. *et al.* Impact of dietary fatty acids on metabolic activity and host intestinal microbiota composition in C57BL/6J mice. *British Journal of Nutrition* **111**, 1905-1917, doi:10.1017/S0007114514000117 (2014).

5 Pusceddu, M. M. *et al.* N-3 Polyunsaturated Fatty Acids (PUFAs) Reverse the Impact of Early-Life Stress on the Gut Microbiota. *PloS one* **10**, e0139721-e0139721, doi:10.1371/journal.pone.0139721 (2015).

6 Beilharz, J. E., Kaakoush, N. O., Maniam, J. & Morris, M. J. The effect of short-term exposure to energy-matched diets enriched in fat or sugar on memory, gut microbiota and markers of brain inflammation and plasticity. *Brain, Behavior, and Immunity* **57**, 304-313, doi:https://doi.org/10.1016/j.bbi.2016.07.151 (2016).

2.4 Impact of acute and chronic amyloid-β peptide exposure on gut microbial commensals in the mouse

Authors: Malena dos Santos Guilherme[#]; **Hristo Todorov**[#]; Carina Osterhof; Anton Möllerke; Kristina Cub; Thomas Hankeln; Susanne Gerber; Kristina Endres
This article is published in *Frontiers in Microbiology*, 2020, 11:1008.
doi: 10.3389/fmicb.2020.01008

# Authors contributed equally

My contributions to this article are listed in section 4.2 Contributions to individual publications.

frontiers in Microbiology

ORIGINAL RESEARCH
published: 20 May 2020
doi: 10.3389/fmicb.2020.01008

Impact of Acute and Chronic Amyloid-β Peptide Exposure on Gut Microbial Commensals in the Mouse

Malena dos Santos Guilherme[1†], Hristo Todorov[2,3,4†], Carina Osterhof[5], Anton Möllerke[1], Kristina Cub[1], Thomas Hankeln[5], Susanne Gerber[2,3] and Kristina Endres[1]*

[1] Department of Psychiatry and Psychotherapy, University Medical Center, Johannes Gutenberg University Mainz, Mainz, Germany, [2] Faculty of Biology, Institute for Developmental Biology and Neurobiology, Center of Computational Sciences Mainz, Johannes Gutenberg University Mainz, Mainz, Germany, [3] Institute for Human Genetics, University Medical Center, Johannes Gutenberg University Mainz, Mainz, Germany, [4] Fresenius Kabi Deutschland GmbH, Oberursel, Germany, [5] Institute of Organismic and Molecular Evolution, Molecular Genetics and Genome Analysis, Johannes Gutenberg University Mainz, Mainz, Germany

Alzheimer's disease (AD) is the most common form of dementia. Besides its cognitive phenotype, AD leads to crucial changes in gut microbiome composition in model mice and in patients, but the reported data are still highly inconsistent. Therefore, we investigated chronic effects of AD-characteristic neurotoxic amyloid-β (Aβ) peptides as provided by transgenic overexpression (5xFAD mouse model) and acute effects due to oral application of Aβ on gut microbes. Astonishingly, one-time feeding of wild type mice with $Aβ_{42}$ provoked immediate changes in gut microbiome composition (β diversity) as compared to controls. Such obvious changes were not observed when comparing 5xFAD mice with wild type littermates. However, acute as well as chronic exposure to Aβ significantly affected the abundance of numerous individual operational taxonomic units. This provides first evidence that acute *in vivo* exposure to Aβ results in a shift in the enteric microbiome. Furthermore, we suggest that chronic exposure to Aβ might trigger an adaptive response of gut microbiota which could thereby result in dysbiosis in model mice but also in human patients.

Keywords: Alzheimer's disease, microbiome, anti-microbial, Amyloid-β peptide, mouse model, 5xFAD

OPEN ACCESS

Edited by:
Amparo Latorre, University of Valencia, Spain

Reviewed by:
Ximo Pechuan Jorge, Genentech, Inc., United States
Chenyang Lu, Ningbo University, China

****Correspondence:***
Kristina Endres
kristina.endres@unimedizin-mainz.de

[†]These authors have contributed equally to this work

Specialty section:
This article was submitted to Microbial Symbioses, a section of the journal Frontiers in Microbiology

Received: *17 February 2020*
Accepted: *24 April 2020*
Published: *20 May 2020*

Citation:
dos Santos Guilherme M, Todorov H, Osterhof C, Möllerke A, Cub K, Hankeln T, Gerber S and Endres K (2020) Impact of Acute and Chronic Amyloid-β Peptide Exposure on Gut Microbial Commensals in the Mouse. Front. Microbiol. 11:1008. doi: 10.3389/fmicb.2020.01008

INTRODUCTION

Improvements in our healthcare system have led to a global increase in the percentage of elderly people. Currently, nine percent of the population in the world is aged 65 or older; in 2050 this number will increase approximately to 16 percent and the older people will outnumber adolescents aged 15 to 24 years (United Nations Department of Economic and Social Affairs, 2019). Currently, 50 million people suffer from dementia (Alzheimer Disease International, 2019). The most common form of these divergent disorders is Alzheimer's disease (AD) and age is the major risk factor for developing AD (Alzheimer Disease International, 2019). One of the characteristic hallmarks in the brain of AD patients are amyloid plaques derived from amyloid-β (Aβ) peptides – a cleavage product of the amyloid precursor protein (APP). APP can be processed in two different ways: (1) cleavage by α-secretase gives rise to non-amyloidogenic APPs-α and (2) cleavage by

Abbreviations: Aβ, amyloid-β peptide; AD, Alzheimer's disease; CFU, colony forming units; Sc, Scrambled; 5xFAD, Alzheimer's disease mouse model; OTU, operational taxonomic unit.

β-and γ-secretase generates neurotoxic Aβ peptides (for detailed reviews see Rossner et al., 2006; Endres and Deller, 2017). Imbalances of this processing or changes in Aβ degradation lead to oligomerization of neurotoxic Aβ peptides which are presumed to be the cause of sporadic AD (Hardy and Higgins, 1992; Yang et al., 2003; Roberts et al., 2017; Lane et al., 2018). Besides this, formation of neurofibrillary tangles of hyperphosphorylated tau protein and a loss of synapses as well as neurons are characteristics of the disease (Whitehouse et al., 1982; Kowall and Kosik, 1987; Shin et al., 1989). In sum, these pathological hallmarks are responsible for the observed decline in cognitive and general abilities in AD patients and finally lead to death. So far, there is no preventive or curative therapy. Treatment with, e.g., Rivastigmine, which acts as an acetylcholinesterase inhibitor, can help to ameliorate disease progression, but cannot stop it (Farlow et al., 2005). The etiology of sporadic AD is not yet fully understood; therefore a more systemic view – including other organs than CNS and also their microbiome – could provide new therapeutic targets.

Only recently, the interplay between brain and gut has gained more attention for researchers regarding neurodegenerative diseases (Quigley, 2017). However, investigations in the field of AD are still rare (for a detailed review see Endres, 2019). Research in the field of, e.g., Parkinson's disease (PD), a dementia with α-synuclein deposition in analogy to Aβ deposits in AD, is far more advanced and already gave insights into relevant gut-brain-connections. For example, differences in microbial composition of the gut, such as reduced Bacteroidetes and increased Enterobacteriaceae, were found when comparing fecal samples from PD patients with samples of healthy controls (Unger et al., 2016). Simultaneously, about 80% of PD patients suffer from gastrointestinal dysfunction (Poewe, 2008; Cersosimo and Benarroch, 2012). It has also been shown that gut microbiota can directly influence disease progression in PD model mice by regulating motor deficits and neuroinflammation (Sampson et al., 2016). Furthermore, α-synuclein, the main driver of the disease which was also found in gut tissue, is discussed as a biomarker for pre-motor PD by using colon biopsies (Shannon et al., 2012). These investigations give profound basis for the assumption that a neurodegenerative disease might derive from or be influenced by gastrointestinal properties. The avenues which are used for this are not fully understood so far.

Brain and gut are connected *via* the so-called gut-brain-axis which consists of the enteric nervous system (ENS), the *Nervus vagus*, immune cells and the microbiome (Mayer, 2011). The *Nervus vagus* allows bidirectional communication *via* efferent and afferent fibers (Quan and Banks, 2007). The connection between brain and gut enforces speculation if the microbiota and their metabolites may influence AD progression or vice versa if AD pathogenesis impacts the microbiome.

Joachim et al. (1989) already showed Aβ deposition in the gut of individual patients. Also, antimicrobial properties of Aβ on single microbial strains have been demonstrated (Soscia et al., 2010). Furthermore, different studies concluded, that transgenic AD model mice as well as AD patients present differences in microbiota composition in comparison to healthy controls (Brandscheid et al., 2017; Cattaneo et al., 2017; Harach et al., 2017; Shen et al., 2017; Vogt et al., 2017; Bauerl et al., 2018). The investigations of the role of microbiota in AD are still highly inconsistent. Harach et al. (2017), for example, showed an increase of Firmicutes, but a decrease of Bacteroidetes, in fecal samples of 1 month old AD model mice (APPPS1) as compared to wild type controls. The opposite result could be found in the same mouse strain at an age of 8 months. In a study using fecal samples of 9 week old 5xFAD mice, elevated amount of Firmicutes and less Bacteroidetes were detected as compared to wild type controls (Brandscheid et al., 2017). The investigated mouse strains represent genetic models, which can be used for observatory studies of chronic exposition of gut tissue with neurotoxic Aβ peptides especially because the peptide itself has also been detected in the gut (Brandscheid et al., 2017). However, acute effects have not been investigated so far *in vivo* and compared to the prolonged exposure.

The aim of our study was to investigate chronic as well as acute effects of Aβ exposition in the gut. 5xFAD mice were used as a model for AD, which express mutated human APP and PSEN1 transgenes with a total of five mutations and show Aβ deposition in the brain and gut tissue already at an age of 4 weeks (Oakley et al., 2006; Brandscheid et al., 2017). We analyzed gut bacteria of C57Bl/6J wild type mice in comparison to 5xFAD transgenic littermates by 16S-rDNA sequencing. Additionally, acute effects of Aβ were investigated *in vivo* after oral administration of Aβ peptides to wild type mice. As expected, differences in the gut microbiome could be observed by comparing 5xFAD mice with wild type controls but interestingly, also acute exposition of gut tissue for just 5 h with Aβ peptides (one complete gut passage) led to substantial differences in microbiota as compared to animals treated with a scrambled, non-active peptide.

MATERIALS AND METHODS

Peptides

For the incubation of feces bacteria and oral application to the mice, human $A\beta_{1-42}$ or scrambled, biologically inactive peptide (both AnaSpec, Seraing, Belgium) in 5 mM NH_4OH buffered in PBS was used. TAMRA-labeled peptide (AnaSpec, Seraing, Belgium) was used for detecting gut transition of Aβ.

Quantitation of Colony Forming Units and Bacterial Viability Assay

Anaerobic Cultivatable Community

Freshly collected fecal pellets were suspended in isotonic sodium chloride solution (0.9%, 100 µl/mg) using a hand-held electric stirrer (Xenox, Fähren, Germany). Aliquots of 50 µl were supplemented with 5 µl of peptide solution in 0.4 mM NH_4OH buffered in PBS. After 10 min incubation at room temperature under careful mixing for every 2 min, 20 µl of this suspension were added to 4 ml of thioglycollate bouillon (Becton Dickinson GmbH, Heidelberg, Germany) and kept for overnight at 4°C. The following day, 1 µl of the diluted fecal suspension was spread on Schaedler agar plates (Becton Dickinson GmbH, Heidelberg, Germany) and incubated for 48 h anaerobically (Anoxomat, Mart Microbiology B.V, Drachten, Netherlands). Lastly, colony

forming units (CFU) were counted and normalized to controls from the same donor mouse incubated with scrambled peptide.

Family-Specific Cultivation

For assessing toxic effects of Aβ on specific microbial families, freshly collected feces was suspended and incubated with 2 μM peptide solution as described above. Afterward, feces suspensions were diluted with 0.9% sodium chloride solution for plating 1 ml on 3M^{TM}-Petrifilm plates specific for Enterobacteriaceae and Lactobacillaceae (3M Deutschland GmbH, Neuss, Germany). Plates were incubated for 20 h at 37°C. CFU were counted and normalized to samples from the same donor mouse incubated with scrambled peptide.

Viability Assay

After incubation of diluted feces samples with Aβ peptide or scrambled control for plating (see above), additional 1:100 dilutions were prepared and viability measured by using the BacTiter Glo assay as indicated by the vendor (Promega, Mannheim, Germany). Relative luminescence was measured and normalized to controls from the same donor mouse incubated with scrambled peptide.

Animals

B6SJL-Tg(APPSwFlLon,PSEN1*M146L*L286V)6799Vas/Mmjax (5xFAD) mice (Jackson Lab, Bar Harbor, Maine, United States) were maintained by crossbreeding with C57BL/6J background as described in Reinhardt et al. (2018). Animals aged 9–10 weeks were used and non-transgenic offspring served as control and for acute treatment with peptides. All animals were group-housed with 3–5 animals per cage in a 12 h light/dark cycle with food (Ssniff Spezialdiäten GmbH, Soest, Germany) and water available *ad libitum*. At least one week before sampling of feces or chyme, animals were single-caged to avoid microbial transfer, e.g., by coprophagy. All procedures were performed in accordance with the European Communities Council Directive regarding care and use of animals for experimental procedures and were approved by local authorities (Landesuntersuchungsamt Rheinland-Pfalz; approval number G17-1-035).

Oral Peptide Application

Animals were lightly anesthetized with Isoflurane and 10 μg of peptide or solvent (10 mM NH_4OH) administered slowly into the oral cavity. Mice were kept in manual fixation up to ingestion of the fluid to prevent aspiration.

Collection of Chyme

Animals were deeply anesthetized with isoflurane and sacrificed by decapitation. For microbiome determination, feces pellets close to the rectum were taken. For assessing fluorescence after feeding of TAMRA-labeled Aβ, the whole gut was placed in ice cold isotonic sodium chloride to prevent further peristalsis movement. Segments of 2 cm length were then chopped starting from the stomach, the content collected by longitudinal opening and stored on ice until further use.

Western Blot and Fluorescence Detection

To measure the stability of TAMRA-labeled Aβ in the gastrointestinal milieu, chyme samples were collected as described before and diluted with 500 μl ice cold PBS. TAMRA-labeled Aβ (0.025 μM or 0.005 μM) was added to chyme or PBS as control and incubated for 2 h at 37°C with gently mixing every 20 min. Afterward, LDS NuPAGE buffer (1×, Life Technologies, Carlsbad, California, United States) and DTT (1 M, 10% v/v, Carl Roth GmbH & Co. KG, Karlsruhe, Germany) were added and the solution was heated for 10 min at 70°C. Proteins were separated on a 12%-SDS polyacrylamide gel and subsequently transferred to a nitrocellulose membrane (GE Healthcare, Chalfont, Great Britain). The membrane was blocked with I-block solution (0.2% in PBS/T, Thermo Fisher Scientific) for 1 h before incubation with primary antibody in a dilution of 1:1,000 overnight at 4°C. On the next day, the membrane was washed with PBS/T and incubated with the secondary antibody coupled with horse reddish peroxidase (Thermo Scientific, Chalfont, Great Britain). Chemiluminescent signals were detected after application of SuperSignal West Femto chemiluminescent substrate (Thermo Scientific, Chalfont, Great Britain) by using a CCD-camera (Stella 3200 Camera, Raytest, Straubenhardt, Germany). Fluorescence signal was detected by using the Storm Scanner 860 (Molecular Dynamics, Caesarea, Israel).

Assessment of Gut Transition Time of Peptides

After oral application of TAMRA-labeled Aβ or NH_4OH as control and sacrifice of the animals 2, 4, or 24 h later, chyme samples were diluted with 500 μl ice cold PBS, incubated for 5 min and centrifuged. Fluorescence was measured by using 50 μl of the supernatant in duplicates (Exc 540 nm and Em 580 nm, FLUOstar Optima, BMG Labtech GmbH, Ortenberg, Germany) at intervals of 1 min over a period of 1 h at 37°C with shaking before every measurement. The mean of the values of the measurements between 15 and 45 min was used to calculate the difference between the TAMRA-labeled Aβ-treated animals and solvent-treated control animals.

DNA Extraction From Fecal Samples

Fecal samples were stored at −80°C before DNA extraction was done by using the QIAmp Fast DNA Stool Mini Kit (Qiagen GmbH, Hilden, Germany) as recommended by the vendor.

Sequencing and Taxonomic Assignment of 16S rDNA Amplicons

Library preparation and Illumina sequencing was performed by StarSEQ GmbH (Mainz, Germany). For amplicon generation, the V3-V4 16S metagenomics sequencing system (Illumina) was used. Amplicons were paired-end sequenced (2 × 300 bp) on an Illumina MiSeq platform. De-multiplexed sequences were loaded into QIIME2 version 2018.6 (Caporaso et al., 2010) and de-noising was done using the DADA2 algorithm (Callahan et al., 2016). Due to a low quality of the reverse reads, neither read merging within QIIME nor external read merging with BBMerge

from the BBMap suite[1] retained a sufficient amount of reads, so we decided to exclude the reverse reads from downstream analysis. Forward reads were truncated to 255 bp after quality control. A naïve Bayes classifier was trained on Greengenes database 13_8 containing the V3–V4 region only with QIIME's internal implementation of scikit-learn. Taxonomic assignment was then done on 97% sequence identity. A multiple sequence alignment was done with MAFFT and a phylogenetic tree was calculated using the q2-phylogeny plugin.

Microbial Composition of Fecal Samples

We employed the *phyloseq* R package for downstream analysis of 16S data. Separate statistical comparisons were always performed between wild type vs 5xFAD and scrambled Aβ vs Aβ-fed animals, respectively. Alpha diversity was estimated using the Chao and Shannon index. In order to account for different library sizes, each sample was normalized to the smallest library size by random sampling with replacement. This process was repeated a 1,000 times and the average values from all runs were considered as final estimates for alpha diversity. Groups were compared statistically with an unpaired *t*-test. Differences in beta diversity were analyzed using canonical analysis of principal coordinates (CAP) (Anderson and Willis, 2003) as implemented in the *vegan* R package. Ordinations based on both the Bray–Curtis dissimilarity as well as the binary Jaccard distance were performed to investigate quantitative and qualitative differences in beta diversity. Community composition at the phylum and family level was compared based on relative abundance. Subsequently, we performed differential abundance analysis by estimating log2 fold changes (FC) of bacterial abundance with the DESeq2 package (Love et al., 2014). This method was chosen because DESeq2 was previously shown to offer increased sensitivity to detect differentially abundant operational taxonomic units (OTUs) while keeping false discovery rates below 0.05 with small sample sizes (Weiss et al., 2017). Briefly, absolute bacterial abundances were transformed to normalized counts using the median-of-ratios method implemented in DESeq2. FC of bacterial abundance were calculated using generalized linear models assuming a negative binomial distribution. The relationship between the mean and dispersion parameters was estimated using local regression. The significance of FC was evaluated with Wald *z* tests. Differences were considered statistically significant if the adjusted *p*-value of the respective FC was below 0.05. *p*-values are two-tailed and adjustment for multiple comparisons was performed by controlling the false discovery rate with the help of the Benjamini–Hochberg method.

Statistical Analysis

All statistical analyses were performed using GraphPad Prism 6 for Windows or R version 3.5. Data are graphically represented as mean + standard error of the mean (SEM) (**Figure 1**) or with boxplots and scatter plots showing individual values (**Figure 3**). Statistical analysis was performed with an unpaired two-tailed Student's *t*-test ($^{*}p < 0.05$, $^{**}p < 0.01$, and $^{***}p < 0.001$) if not stated otherwise.

[1]https://sourceforge.net/projects/bbmap/

RESULTS

Impact of Aβ on Viability of Murine Fecal Bacteria

An antimicrobial effect of $A\beta_{42}$ on single microbial species such as *Enterococcus faecalis* or *Candida albicans* has been shown before (Soscia et al., 2010). In order to ensure the toxic properties of Aβ peptides in complex microbiota mixtures, fecal samples from 5xFAD mice and wild type littermates were incubated with $A\beta_{42}$ or scrambled peptide as control (incubation with solvent only did not statistically deviate from scrambled control, data not shown). Ten minutes of incubation sufficed to significantly reduce viability of fecal microorganisms from wild type mice in comparison to scrambled peptide treated samples (**Figure 1A**). Interestingly, no such toxic effect of the active peptide could be shown within samples derived from transgenic AD model mice. Furthermore, samples derived from wild type mice treated with 2 or 10 μM $A\beta_{42}$ were plated on Schaedler agar plates to analyze the effect on all anaerobically cultivatable bacteria. Two different concentrations were selected to address a wider range of bacteria. CFU were counted after 48 h of incubation. At both concentrations, a significant reduction of about 30–40% of bacterial growth was observed (**Figure 1B**). To assess if differences in vulnerability due to Aβ exist in different bacterial families, diluted bacterial suspension from transgenic and wild type animals were subsequently plated on agar plates selective for Lactobacillaceae (**Figure 1C**) or Enterobacteriaceae (**Figure 1D**). Both families were significantly reduced after $A\beta_{42}$ treatment in comparison to scrambled peptide control when fecal material was derived from wild type mice. However, no significant effects could be observed for Lactobacillaceae from transgenic 5xFAD animals, and only a non-significant reduction of Enterobacteriaceae occurred ($p = 0.09$).

Gastro-Intestinal Passage of Orally Administered Aβ Peptides

Before oral treatment of the mice, the stability of the Aβ peptide in the gastro-intestinal milieu had to be proven. Therefore, TAMRA-labeled $A\beta_{42}$ was incubated with PBS-diluted content of the stomach of wild type mice or PBS as control for 2 h at 37°C (exponential decay constant of stomach emptying in mice: 74 min; Schwarz et al., 2002). Detection of Aβ-dependent signals by Western blotting using the antibody 6E10 showed similar patterns of Aβ monomer and oligomers incubated with gastric content or PBS, independent of Aβ concentration (**Figure 2A**, upper panel). Fluorescence detection supported a clear assignment of the TAMRA-labeled peptide as the same pattern could be obtained as with the antibody (**Figure 2A**, lower panel). In sum, this indicated that the peptide would at least be stable within a 2 h period of digestive passage. After the stability of the Aβ peptide in the gastrointestinal milieu

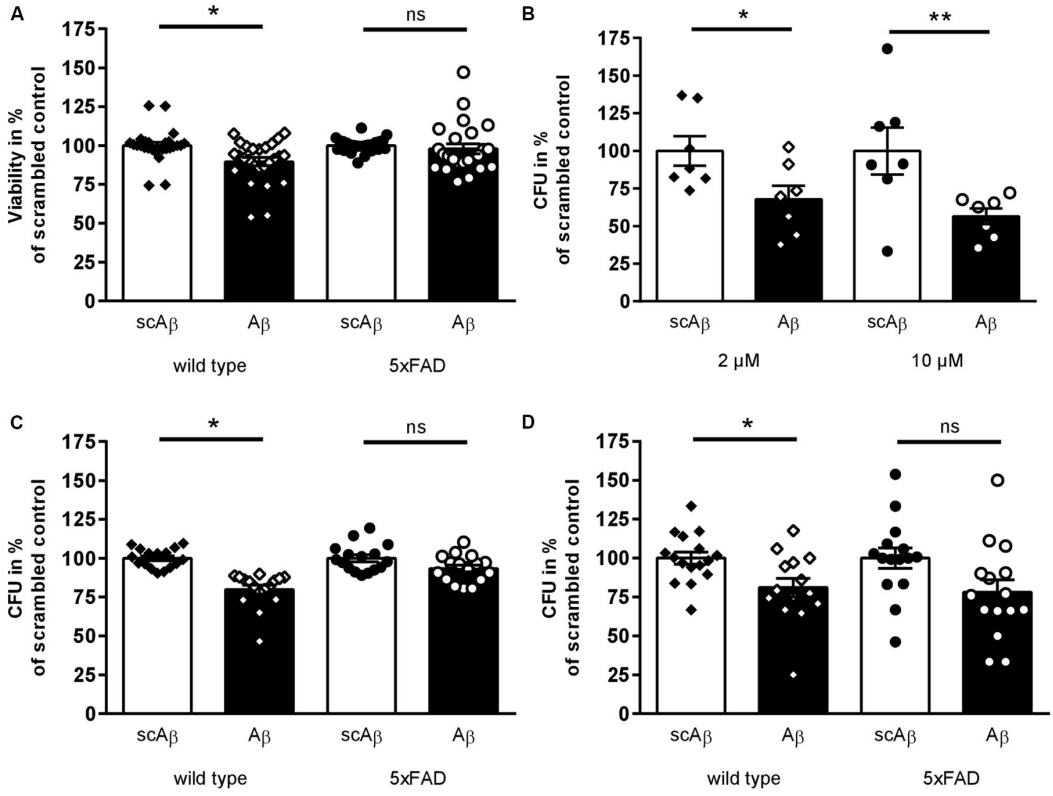

FIGURE 1 | Toxic effects of synthetic $A\beta_{42}$ on murine fecal microbial organisms. **(A)** Fecal samples of transgenic 5xFAD mice and wild type littermates were diluted and incubated with $A\beta_{42}$ peptide or scrambled control (2 µM) for 10 min. Viability was measured and calculated in percent of scrambled peptide treated samples (n = 13 animals per group, ♂ = 6–7, ♀ = 6–7). **(B)** Fecal material suspension from wild type mice were incubated with 2 or 10 µM $A\beta_{42}$ or the respective amount of scrambled peptide. Subsequently, aliquots of further diluted bacteria suspension were plated on Schaedler agar and incubated anaerobically for 48 h at 37°C. Number of colony forming units (CFU) of samples treated with scrambled peptide control were set to 100% (n = 7 animals per group; ♂ = 3, ♀ = 4). **(C, D)** After incubation of fecal samples from transgenic or wild type mice with 2 µM $A\beta_{42}$ or scrambled peptide, suspensions were spread on plates selective for Lactobacillaceae **(C)** and Enterobacteriaceae **(D)** (n = 10–11 per group, ♂ = 5–6, ♀ = 5). Datapoints for individual normalized measurements are shown in each graph (*$p < 0.05$; **$p < 0.01$).

could be ensured, mice were orally treated with the TAMRA-labeled peptide and sacrificed after 2, 4, and 24 h. To measure the transit time of the peptide, the gut was divided into 2 cm segments and fluorescence was measured within diluted chyme. Two hours after treatment, the TAMRA-labeled peptide could be detected in the 10th segment of the gut of the wild type animal (according to cecum) and in the 11th segment of the transgenic one (**Figure 2B**). Two hours later, in both animals the signal was measured in the 11th segment (cecum ampulla). No signal could be detected in any sample 24 h after the treatment. For further experiments, a complete gut passage was suspected after 5 h in mice of respective age and strain which fits to earlier reports on C57Bl/6 mice (Schwarz et al., 2002).

Diversity of the Gut Microbiome Under Chronic and Acute Exposure to Aβ Peptides

We employed high-throughput sequencing of the bacterial 16S rRNA gene in order to investigate the impact of acute or chronic exposure to the toxic Aβ peptide on the murine gut microbiome *in vivo*. Therefore, feces from 5xFAD mice and wild type littermates as well as feces from wild type mice treated with Aβ or scrambled Aβ were collected. Subsequently, DNA was purified and subjected to 16S rDNA sequencing. All animals used in these experiments were female.

In the first step of the analysis we compared the alpha and beta diversity of the negative control sample to all experimental groups as means of quality control. Estimates of species richness as well as evenness were considerably lower for the negative control sample as indicated by the Chao and Shannon index, respectively (**Supplementary Table S1**). Furthermore, unconstrained analysis of principal coordinates based both, the Bray-Curtis dissimilarity and Jaccard index, revealed that the negative control was distinctly separated from all experimental groups in reduced space (**Supplementary Figure S1**). This accounted for a large amount of the dispersion in sample scores, therefore the negative control was removed from the subsequent downstream analysis in order to better represent differences between experimental groups.

We did not observe differences in the alpha diversity estimates between wild type and 5xFAD animals in terms of species evenness (**Figure 3A**) and richness (**Figure 3B**). The comparison of mice fed with scrambled Aβ or the active form of the

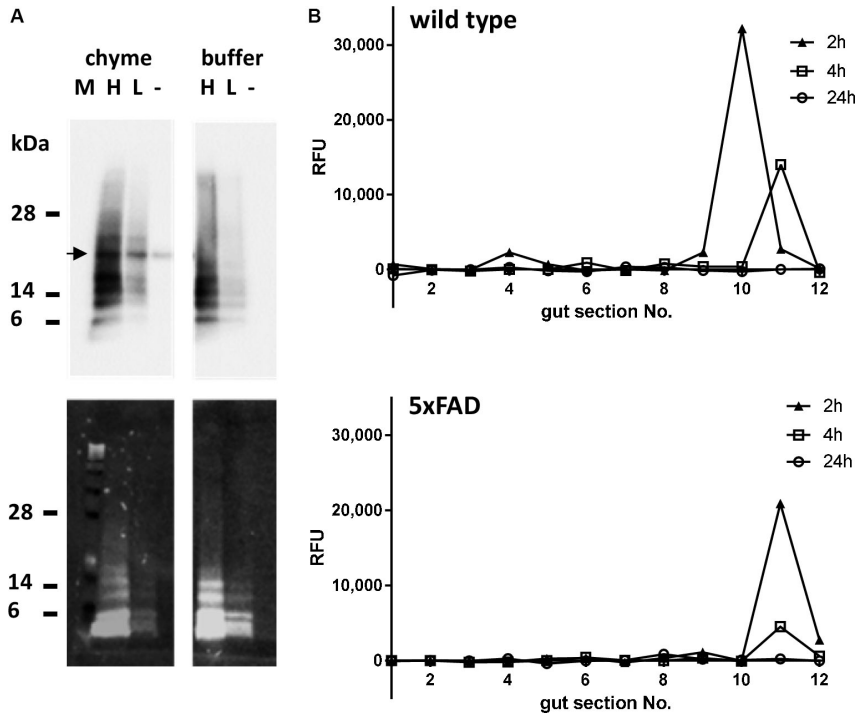

FIGURE 2 | Stability and time-dependent localization of *per os* administered Aβ peptides in the murine gastrointestinal tract. **(A)** TAMRA-labeled Aβ peptide was incubated in two different concentrations [high (H): 0.025 μM; low (L): 0.005 μM] with PBS-diluted gastric content of wild type mice for 2 h at 37°C. Solvent of the peptide was used as a negative control (–). Additionally, samples with PBS instead of chyme were incubated as described (buffer). Proteins were separated on PAA gel and transferred to nitrocellulose. Detection of Aβ-dependent signal was conducted by antibody 6E10 (upper panel) or by fluorescence (lower panel). The arrow indicates a cross reactivity only occurring in chyme. **(B)** To assess the passage of orally administered Aβ peptides, wild type or 5xFAD mice were fed with 10 μg of TAMRA-labeled Aβ peptides and sacrificed at indicated time points. TAMRA-dependent fluorescence was determined in the chyme of 2 cm gut sections numbered from 1 (oral end = stomach) to 12 (rectal section). Values are presented as measured difference between the TAMRA-Aβ-treated animals and solvent-treated control animals (one animal per time point, technical duplicates).

peptide yielded similar results with a very slight non-significant trend of reduced species richness in the Aβ group (mean Chao index = 423.4 vs 387.9 in scrambled Aβ compared to Aβ-fed animals, $p = 0.24$, **Figures 3C,D**).

Comparison of beta diversity of 5xFAD vs wild type mice using CAP resulted in better separation of experimental groups along the constrained dimension based on the Jaccard index (**Figures 3E,F**). Nevertheless, experimental group assignment only explained a small amount of the dispersion between samples and the grouping effect was not significant. In contrast, beta diversity significantly differed between Aβ- and scrambled Aβ-fed animals in the Jaccard distance based ordination. This was indicated by non-overlapping 95% confidence ellipses (**Figure 3H**). The difference was not significant when beta diversity was measured with the Bray–Curtis dissimilarity, implying that the shift in microbiota composition was qualitative in nature (**Figure 3G**).

Community Composition of Gut Microbiome

Community composition of the gut microbiome at the phylum level was highly similar in 5xFAD mice as compared to wild type littermates (**Figure 4A**). The most dominant phylum was Bacteroidetes with an average relative abundance around 60%, followed by Firmicutes with an average relative abundance of approximately 30% in both groups. Proteobacteria and Verrucomicrobia were the only remaining classified phyla with a relative abundance of above 1%. The phylum composition of Aβ- compared to scrambled Aβ-fed animals revealed similar trends (**Figure 4B**). The average relative abundance of Bacteroidetes was slightly lower in the Aβ group (53.9% compared to 59.5% in the scrambled Aβ group, $p = 0.463$). In contrast, Firmicutes average relative abundance of 25.4% in Aβ-fed animals was marginally higher than the scrambled peptide group (20.2%, $p = 0.102$). Nevertheless, differences in relative abundance at the phylum level were not statistically significant. The community composition at the family level is shown in **Supplementary Figure S2** for wild type and 5xFAD animals and **Supplementary Figure S3** for animals fed with Aβ or the scrambled peptide.

Differential Abundance Analysis

We performed a differential abundance analysis on the OTU level by calculating log2 FC of bacterial abundance using the DESeq2 package. Diagnostic plots from this analysis are shown in **Supplementary Figure S4**. This analysis revealed 109 phylotypes with a significantly different abundance in 5xFAD animals

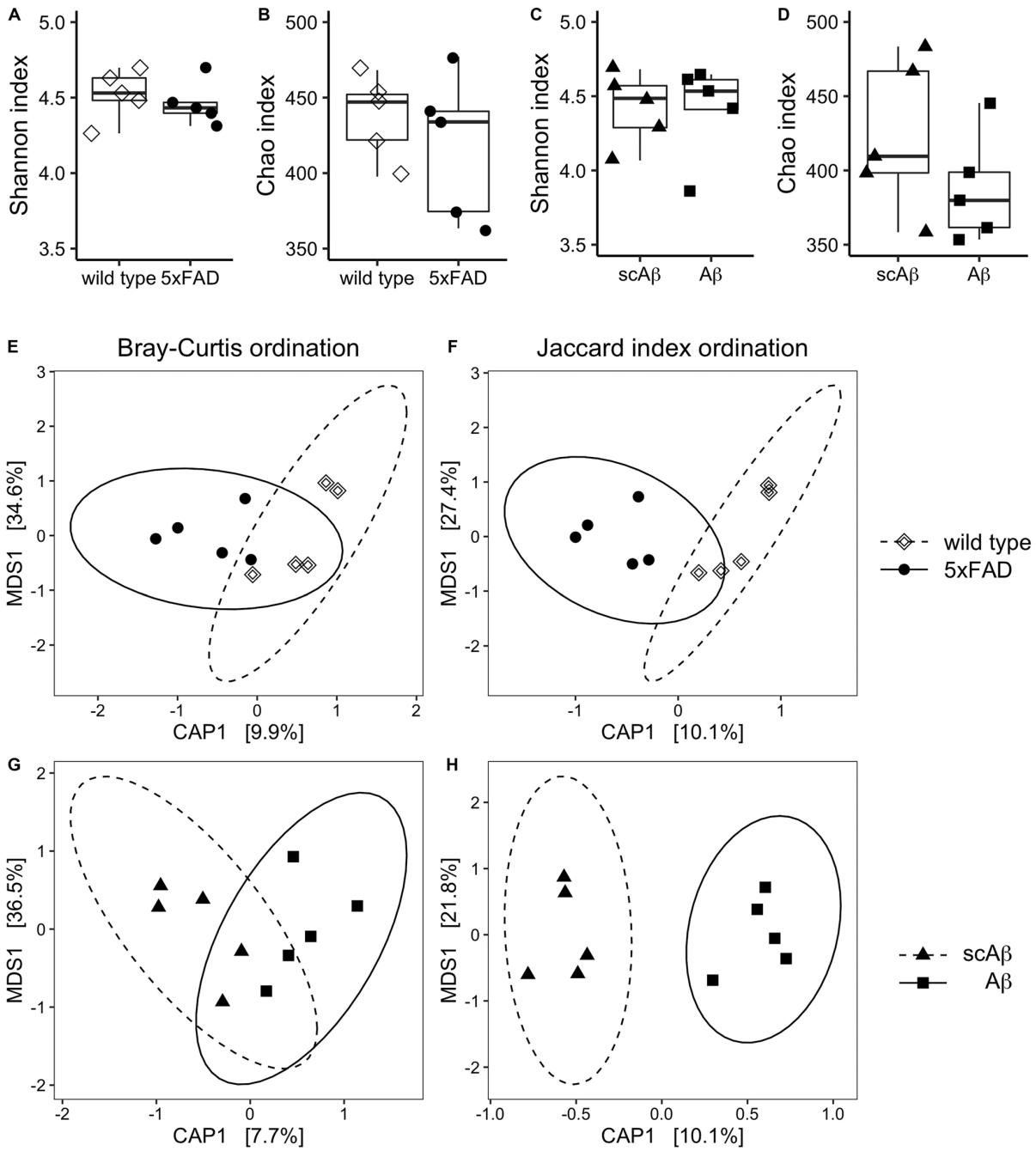

FIGURE 3 | Diversity measures of gut microbiota following chronic or acute exposure to Aβ. Species richness and evenness of each experimental group were evaluated by estimating the Chao index and Shannon index, respectively. Panels **(A)** and **(B)** show results for wild type compared to 5xFAD mice. Differences in alpha diversity between wild type animals receiving scrambled Aβ (scAβ) or Aβ are depicted in panels **(C)** and **(D)**. Data are shown as boxplots and individual values. Beta diversity was evaluated by calculating Bray–Curtis dissimilarity **(E, G)** and binary Jaccard distance **(F, H)**. Results were visualized using canonical analysis of principal coordinates (CAP) for each dissimilarity measure separately. Since there are two groups in each ordination analysis, only one constrained dimension is calculated (CAP1), which is shown on the *x*-axis. The *y*-axis corresponds to the first unconstrained dimension (MDS1). Confidence ellipses around the respective group centroid were drawn at the 95% confidence level. The percentage of total inertia captured by each axis is shown in brackets. MDS: Multi-dimensional scaling.

relative to the wild type group (**Figures 5A,B**). The majority of these OTUs were associated with the Clostridiales order within the Firmicutes phylum. A large amount of the differentially abundant OTUs could not be classified to a reference taxonomy beyond the order and family level. These taxonomic units included OTUs with either significantly increased or decreased abundance in 5xFAD animals which implies different influence of chronic Aβ exposure on the growth of bacteria at lower

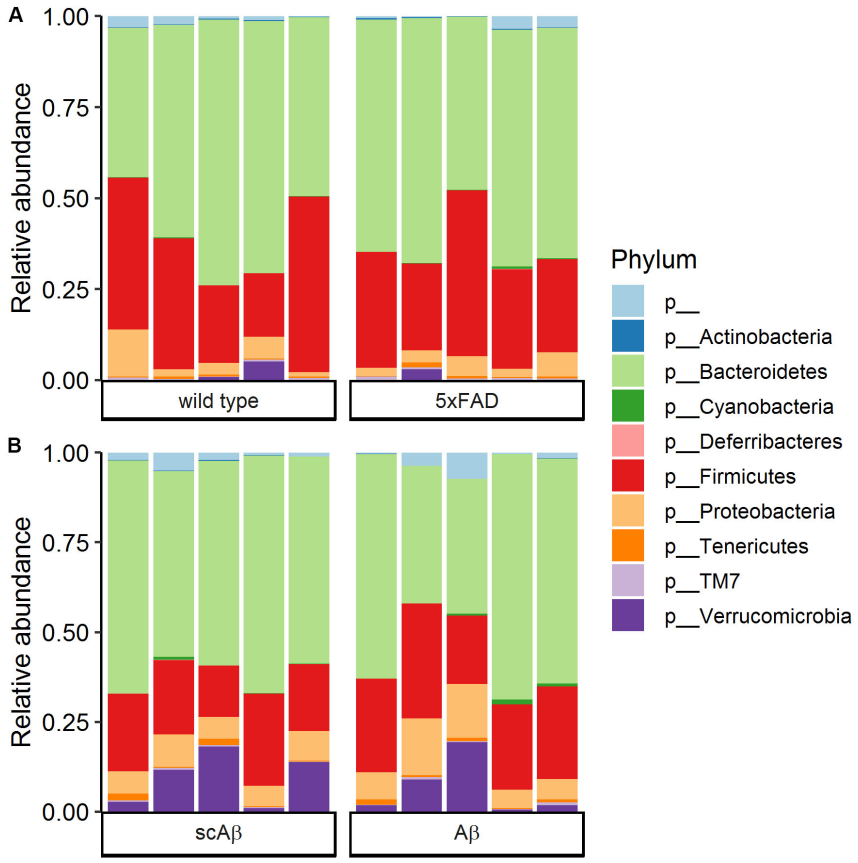

FIGURE 4 | Community composition at the phylum level. Bars show the relative abundance of bacterial phyla in **(A)** wild type compared to 5xFAD mice and **(B)** wild type animals fed with scrambled Aβ (scAβ) versus active Aβ. Phyla with a relative abundance below 0.05% were filtered out from the data set. The label "p__" corresponds to operational taxonomic units that could not be classified to a reference phylum.

taxonomic levels such as genera, species, or strains. At the genus level, we detected individual OTUs associated with *Allobaculum*, *Prevotella*, *Anaeroplasma*, *Bacteroides*, *SMB53*, and *Turicibacter*, respectively, all of which demonstrated significantly increased abundance in 5xFAD animals as compared to wild type littermates. At the species level, we observed an enhanced growth of individual OTUs belonging to *Bacteroides acidifaciens*, *Lactobacillus reuteri*, and *Ruminococcus gnavus* in the 5xFAD group. In contrast, abundance of *Helicobacter hepaticus* was significantly decreased relative to wild type animals whereas individual OTUs associated with *Alistipes massiliensis* demonstrated both, increased and decreased abundance in 5xFAD animals (for single fold changes and adjusted *p*-values see **Supplementary Table S2**).

Our comparison of the abundance of individual OTUs between Aβ- and scrambled Aβ-fed animals resulted in 55 differentially abundant OTUs (**Figures 5C,D**) most of which belonged to the Clostridiales order. Similarly to the previous analysis, multiple OTUs could not be classified beyond the order and family level. At the genus level, one OTU assigned to *Anaeroplasma* showed significantly decreased abundance in the Aβ group. In contrast, OTUs classified to *Oscillospira* and *Ruminococcus* were associated with instances of both, increased and decreased abundance, relative to the samples derived from scrambled Aβ-fed animals. At the species level, we identified one OTU associated with *Lactobacillus reuteri* and two OTUs belonging to *Ruminococcus gnavus* which demonstrated significantly reduced growth following feeding with Aβ (fold changes and adjusted *p*-values are given in **Supplementary Table S3**).

DISCUSSION

The link between AD and alterations in the gut microbiome composition has already been established in several experimental animal models (Brandscheid et al., 2017; Harach et al., 2017; Shen et al., 2017; Zhang et al., 2017; Bauerl et al., 2018; Peng et al., 2018; Zhan et al., 2018) and clinical studies (Cattaneo et al., 2017; Vogt et al., 2017; Zhuang et al., 2018). However, the exact causal mechanism is still not understood. On one hand, perturbations in gut bacterial homeostasis might lead to increased intestinal permeability, low grade inflammation or insulin resistance and obesity (Turnbaugh et al., 2006; Cani et al., 2008, 2009), the last two of which are risk factors for developing AD (e.g., Kivipelto et al., 2005; Fitzpatrick et al., 2009; Luchsinger et al., 2012;

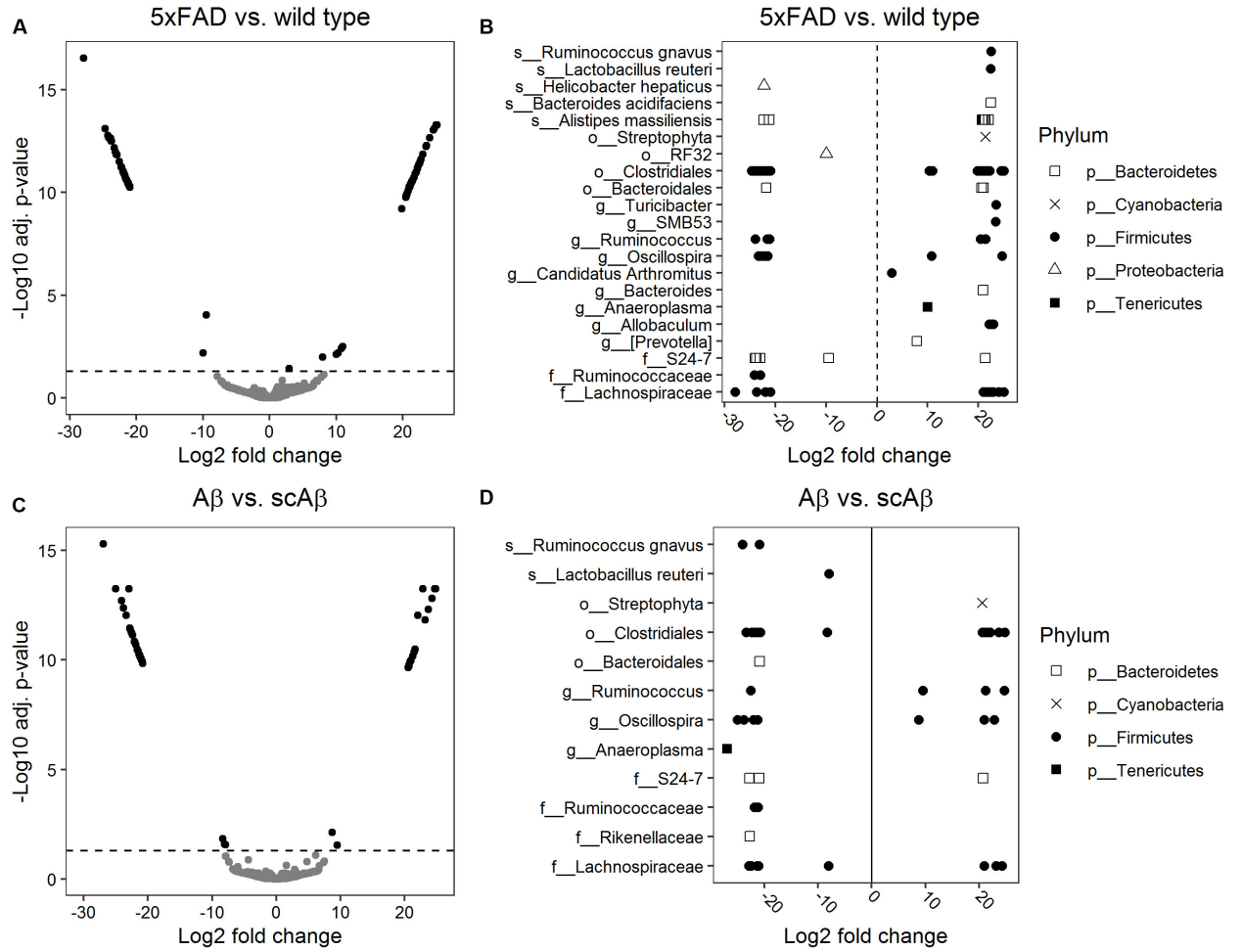

FIGURE 5 | Differential abundance analysis of bacterial operational taxonomic units (OTUs). Log2 fold changes of bacterial abundance were calculated using DESeq2. Volcano plots show the log2 fold changes versus –log10 adjusted *p*-values for 5xFAD relative to wild type mice **(A)** and animals fed with Aβ relative to mice receiving the scrambled peptide **(C)**. OTUs were considered to be differentially abundant if the adjusted *p*-value (Benjamini–Hochberg method) was below 0.05 (indicated by a dashed horizontal line). Significant log2 fold changes appear as black dots in panels **(A)** and **(C)**. The lowest level of taxonomy which could be assigned to the differentially abundant OTUs is depicted in panel **(B)** for 5xFAD mice relative to wild type littermates and in panel **(D)** for mice fed with Aβ relative to the scrambled peptide control group. Log2 fold changes greater than 0 correspond to OTUs significantly enriched in 5xFAD or Aβ-fed mice relative to the respective control group.

Ferreira et al., 2018). On the other hand, it is plausible that shifts in gut bacteria in AD patients might occur as a result of life style and dietary changes after onset of the disease. For instance, in a cross-sectional study, AD patients had an exacerbated nutritional status compared to age-matched controls (Saragat et al., 2012). An alternative mechanism of how the host affects microbiota in the context of AD has been hypothesized by us in a recent *in silico* study (Hewel et al., 2019). In this previous work, we demonstrated that host miRNAs differentially expressed in patients suffering from AD have the potential to bind on key regulatory sequences in commensal microbiota, thereby possibly regulating transcription in bacterial pathways.

Despite representing a major hallmark of AD pathology, the exact physiological function of the Aβ peptide is not known. However, both *in vitro* (Soscia et al., 2010; Kumar et al., 2016; Spitzer et al., 2016) and *in vivo* (Kumar et al., 2016) studies have demonstrated that Aβ exerts anti-microbial properties. Furthermore, oligomerization and fibrillization of the peptide, which are involved in the process of plaque deposition, are also characteristics shared with known anti-microbial peptides (Soscia et al., 2010; Kagan et al., 2012). This has led to the proposal of a new paradigm for the role of Aβ in AD pathogenesis referred to as the antimicrobial protection hypothesis of AD (reviewed in Moir et al., 2018). Considering the fact that Aβ depositions are also found in the intestine, we investigated if acute or chronic exposure to the toxic peptide modulates mouse gut microbiota composition *in vitro* and *in vivo*. Previous *in vitro* experiments on the anti-microbial properties of Aβ were performed under aerobic conditions (Soscia et al., 2010; Spitzer et al., 2016), which is not representative for the predominantly anaerobic environment of the intestine. Therefore, we incubated fecal samples from wild type and 5xFAD mice anaerobically in the

current study. Strikingly, Aβ inhibited bacterial growth in fecal samples originating from wild type animals. Only a tendency of bacterial growth reduction of Enterobacteriaceae of 5xFAD mice could be observed. This might suggest that prolonged exposure to the peptide in 5xFAD animals triggers an adaptive response in some gut microbiota, but individual species could still be affected. This assumption is corroborated by *in vitro* experiments showing that Aβ inhibited *E. faecalis* growth at early time points, whereas bacterial growth resumed at later time points (Soscia et al., 2010).

After observing the growth-inhibiting effects of Aβ on fecal bacteria *in vitro*, we also investigated how this translates to the *in vivo* situation. We did not detect any difference in alpha diversity measures between wild type and 5xFAD animals or between wild type mice fed with Aβ or scrambled peptide which is in line with previous reports in mice of similar age (Harach et al., 2017; Shen et al., 2017; Zhang et al., 2017). In contrast, conflicting results have been described regarding longitudinal changes of alpha diversity in mouse models of AD. For instance, Zhang et al. (2017) and Bauerl et al. (2018) observed a significant increase in alpha diversity in APP/PS1 transgenic mice over time whereas Shen et al. (2017) reported a significant decrease in older APP/PS1 mice. Differences were not gender-driven since the two studies showing an increase used male and female mice, respectively. Furthermore, APP/PS1 mice had significantly higher alpha-diversity compared to control animals at 8 months of age in a study by Harach et al. (2017). In the senescence accelerated mouse prone 8 (SAMP8) model of AD, alpha diversity was significantly lower in 7-month old SAMP8 mice as compared to age-matched controls (Zhan et al., 2018). While differences in the mouse models of AD and experimental designs might be partly responsible for these conflicting results, the true association between alpha diversity of the gut microbiome and AD still needs to be elucidated.

5xFAD animals did not significantly differ from wild type littermates in terms of beta diversity which is in agreement with existing studies in mice of comparable age (Harach et al., 2017; Zhang et al., 2017; Bauerl et al., 2018). Remarkably, wild type mice fed with Aβ were clearly separated from animals receiving the scrambled peptide on the ordination plot when beta diversity was measured with the Jaccard distance. This might again be an indication that intestinal bacteria in wild type mice are more susceptible to the acute effects of Aβ, whereas prolonged exposure in 5xFAD mice already led to compositional adaptation. However, longitudinal investigations or studies in older mice consistently reported a difference in beta diversity between mouse models of AD and controls at later times points such as 6, 7, 8, and 24 months of age (Harach et al., 2017; Bauerl et al., 2018; Peng et al., 2018; Zhan et al., 2018). Therefore, we hypothesize that increased Aβ burden might be an early driver of changes in the gut microbiome followed by an adaptive response to the direct anti-microbial effects of the peptide. This is also reflected by the lack of *in vitro* toxic effects of Aβ peptides administered to fecal samples derived from 5xFAD mice. However, the initial perturbations of gut homeostasis might trigger a larger cascade of subsequent events contributing to AD development and long-term alterations in microbiome composition. For instance, we previously described a significantly reduced body weight in male 5xFAD mice compared to wild type controls as early as 6 weeks of age (Brandscheid et al., 2017). Altered gut microbiome is well known in the context of obesity (Turnbaugh et al., 2006; Cani et al., 2008), therefore it is plausible to assume that body weight reduction might also be associated with shifts in fecal bacteria.

With regard to community composition of intestinal bacteria in female mice aged 10 weeks, we did not detect any significant changes at the phylum level. In an earlier study, we described a significantly increased relative abundance of Firmicutes accompanied by a significant decrease in Bacteroidetes in male 5xFAD mice compared to wild type littermates at the age of 9 weeks (Brandscheid et al., 2017). It is important to mention that we previously employed a targeted approach to only quantify a specific subset of phyla and species using qPCR. Here, we performed a more comprehensive microbiome characterization by high-throughput amplicon sequencing of the 16S rRNA gene. Therefore, methodological differences might in part account for the discrepancy in results. However, gender itself is also associated with differences in intestinal microbiota composition (Yurkovetskiy et al., 2013; Fransen et al., 2017; Elderman et al., 2018). Importantly, female mice were reported to have a higher diversity and richness which might be an indicator of a more robust microbiome (Yurkovetskiy et al., 2013; Elderman et al., 2018). Furthermore, male mice exhibited an altered gut bacterial composition at puberty and this was not observed in female animals (Yurkovetskiy et al., 2013). Therefore, shifts at the phylum level in the context of AD might take longer to develop in female mice as compared to males which might explain why we did not detect any changes in the current study. In line with this, Bauerl et al. (2018) described a significantly increased abundance of the phylum Proteobacteria in 6-month-old APP/PS1 female mice compared to controls. The difference was not present at 3 months of age.

Even though the composition of gut microbiota was not altered after acute or chronic exposure to Aβ at higher taxonomic levels, we detected numerous differentially abundant OTUs pointing to early perturbations in gut homeostasis at the species and strain level. In line with the *in vitro* growth inhibiting effect of Aβ on Lactobacillaceae family, we observed a significantly lower abundance of an OTU associated with *Lactobacillus reuteri* in animals fed with Aβ compared to scrambled peptide. Interestingly, abundance of *L. reuteri* was drastically decreased in the offspring of mice kept on a high fat diet compared to mothers on a regular diet in an autism mouse model (Buffington et al., 2016). Moreover, supplementation with this bacterium significantly improved deficits in social behavior in the offspring of the high-fat diet mice. However, we observed an increased abundance of this bacterium in 5xFAD mice compared to wild type littermates, which in theory may again point to a compensatory reaction after a prolonged exposure to the toxic Aβ peptide. However, the possible role of *L. reuteri* in AD needs to be further validated. Another potential target of interest could be *Ruminococcus gnavus* which belongs to the Lachnospiraceae family and has been linked to inflammatory bowel disease (Joossens et al., 2011; Hall et al., 2017; Henke et al., 2019). We identified two OTUs corresponding to this species with significantly lower abundance in mice fed with Aβ, however,

one OTU demonstrated an increased abundance in 5xFAD mice relative to wild type controls. Interestingly, OTUs associated with *R. gnavus* were identified to have an increased abundance in patients with clinically diagnosed AD dementia compared to age-matched individuals with normal cognitive function (Zhuang et al., 2018). In the same study, an OTU associated with *Prevotella* was more abundant in the AD group which is in line with our observation of enhanced growth of a *Prevotella* OTU in 5xFAD mice compared to controls. In contrast, a decreased abundance of *Prevotella* was described in AD mice as compared to controls (Shen et al., 2017; Peng et al., 2018), so results remain controversial. An OTU belonging to the *Bacteroides* genus demonstrated an enhanced growth in 5xFAD mice in our study. Increased abundance of this bacterial genus was also described in patients with AD by Vogt et al. (2017). Furthermore, *Bacteroides* abundance in the AD group was positively correlated with $A\beta_{42}/A\beta_{40}$ and p-tau/$A\beta_{42}$ in cerebrospinal fluid, both of which are biomarkers for exacerbated AD pathology.

Overall, the abundance of multiple other OTUs, which belong to the same higher taxonomic unit, was regulated in an opposite direction after acute or chronic exposure to Aβ. This demonstrates that species and strains react differently possibly even within the same genus. However, the majority of OTUs could not be classified to these lower taxonomic levels. This highlights the need for optimization of reference databases for taxonomic assignment especially if pre- or probiotic treatments should emerge as an option for ameliorating AD pathology. Namely, such therapies would have to target specific bacterial species or strains which would first have to be identified with high certainty in 16S marker-gene survey studies.

In conclusion, to the best of our knowledge, we provide first evidence that acute *in vivo* administration of Aβ is associated with a shift in gut microbiota composition. Our study does not answer the question if this is the factor that leads to long-term intestinal bacteria alterations in the context of AD. However, we suggest that increased exposure to the Aβ peptide might be an early trigger of a process that ends in a vicious circle of exacerbated AD pathology promoting impaired gut homeostasis and vice versa.

DATA AVAILABILITY STATEMENT

The raw sequencing data generated in this study have been deposited in the NCBI SRA data base under the accession number PRJNA627235.

ETHICS STATEMENT

The animal study was reviewed and approved by LUA Rhineland-Palatinate, Germany.

AUTHOR CONTRIBUTIONS

KE conceived the project and designed the experiments. MS, AM, and KC performed the experiments. HT and CO conducted bioinformatics data analysis. MS and HT wrote the manuscript. KE, TH, SG, MS, and HT edited the manuscript. KE and SG supervised the study. All authors have read and approved the final manuscript.

FUNDING

The work of HT was financed by Fresenius Kabi Deutschland GmbH, Oberursel, Germany. MS was supported by Boehringer Ingelheim Foundation and KE by Alfons Geib Stiftung. The funder, Fresenius Kabi Deutschland GmbH, was not involved in the study design, collection, analysis, interpretation of data, the writing of this article or the decision to submit it for publication.

SUPPLEMENTARY MATERIAL

The Supplementary Material for this article can be found online at: https://www.frontiersin.org/articles/10.3389/fmicb.2020.01008/full#supplementary-material

REFERENCES

Anderson, M. J., and Willis, T. J. (2003). Canonical analysis of principal coordinates: a useful method of constrained ordination for ecology. *Ecology* 84, 511–525. doi: 10.1890/0012-9658(2003)084%5B0511:caopca%5D2.0.co;2

Bauerl, C., Collado, M. C., Diaz Cuevas, A., Vina, J., and Perez Martinez, G. (2018). Shifts in gut microbiota composition in an APP/PSS1 transgenic mouse model of Alzheimer's disease during lifespan. *Lett. Appl. Microbiol.* 66, 464–471. doi: 10.1111/lam.12882

Brandscheid, C., Schuck, F., Reinhardt, S., Schafer, K. H., Pietrzik, C. U., Grimm, M., et al. (2017). Altered gut microbiome composition and tryptic activity of the 5xFAD Alzheimer's mouse model. *J. Alzheimers Dis.* 56, 775–788. doi: 10.3233/JAD-160926

Buffington, S. A., Di Prisco, G. V., Auchtung, T. A., Ajami, N. J., Petrosino, J. F., and Costa-Mattioli, M. (2016). Microbial Reconstitution reverses maternal diet-induced social and synaptic deficits in offspring. *Cell* 165, 1762–1775. doi: 10.1016/j.cell.2016.06.001

Callahan, B. J., McMurdie, P. J., Rosen, M. J., Han, A. W., Johnson, A. J. A., and Holmes, S. P. (2016). DADA2: high-resolution sample inference from Illumina amplicon data. *Nat. Methods* 13, 581–583. doi: 10.1038/nmeth.3869

Cani, P. D., Bibiloni, R., Knauf, C., Waget, A., Neyrinck, A. M., Delzenne, N. M., et al. (2008). Changes in Gut microbiota control metabolic endotoxemia-induced inflammation in High-Fat Diet–Induced obesity and diabetes in mice. *Diabetes* 57:1470. doi: 10.2337/db07-1403

Cani, P. D., Possemiers, S., Van de Wiele, T., Guiot, Y., Everard, A., Rottier, O., et al. (2009). Changes in gut microbiota control inflammation in obese mice through a mechanism involving GLP-2-driven improvement of gut permeability. *Gut* 58, 1091–1103. doi: 10.1136/gut.2008.165886

Caporaso, J. G., Kuczynski, J., Stombaugh, J., Bittinger, K., Bushman, F. D., Costello, E. K., et al. (2010). QIIME allows analysis of high-throughput community sequencing data. *Nat. Methods* 7:335. doi: 10.1038/nmeth.f.303

Cattaneo, A., Cattane, N., Galluzzi, S., Provasi, S., Lopizzo, N., Festari, C., et al. (2017). Association of brain amyloidosis with pro-inflammatory gut bacterial taxa and peripheral inflammation markers in cognitively impaired elderly. *Neurobiol. Aging* 49, 60–68. doi: 10.1016/j.neurobiolaging.2016.08.019

Cersosimo, M. G., and Benarroch, E. E. (2012). Pathological correlates of gastrointestinal dysfunction in Parkinson's disease. *Neurobiol. Dis.* 46, 559–564. doi: 10.1016/j.nbd.2011.10.014

Elderman, M., Hugenholtz, F., Belzer, C., Boekschoten, M., van Beek, A., de Haan, B., et al. (2018). Sex and strain dependent differences in mucosal immunology and microbiota composition in mice. *Biol. Sex Differ.* 9, 26–26. doi: 10.1186/s13293-018-0186-186

Endres, K. (2019). Retinoic acid and the gut microbiota in Alzheimer's disease: fighting back-to-Back? *Curr. Alzheimer Res.* 16, 405–417. doi: 10.2174/1567205016666190321163705

Endres, K., and Deller, T. (2017). Regulation of Alpha-Secretase ADAM10 in vitro and in vivo: genetic, epigenetic, and protein-based mechanisms. *Front. Mol. Neurosci.* 10:56. doi: 10.3389/fnmol.2017.00056

Farlow, M. R., Small, G. W., Quarg, P., and Krause, A. (2005). Efficacy of rivastigmine in Alzheimer's disease patients with rapid disease progression: results of a meta-analysis. *Dement. Geriatr. Cogn. Disord.* 20, 192–197. doi: 10.1159/000087301

Ferreira, L. S. S., Fernandes, C. S., Vieira, M. N. N., and De Felice, F. G. (2018). Insulin resistance in Alzheimer's disease. *Front. Neurosci.* 12:830. doi: 10.3389/fnins.2018.00830

Fitzpatrick, A. L., Kuller, L. H., Lopez, O. L., Diehr, P., O'Meara, E. S., Longstreth, W. T., et al. (2009). Midlife and late-life obesity and the risk of dementia: cardiovascular health study. *Arch. Neurol.* 66, 336–342. doi: 10.1001/archneurol.2008.582

Fransen, F., van Beek, A. A., Borghuis, T., Meijer, B., Hugenholtz, F., van der Gaast-de Jongh, C., et al. (2017). The impact of gut microbiota on gender-specific differences in immunity. *Front. Immunol.* 8:754. doi: 10.3389/fimmu.2017.00754

Hall, A. B., Yassour, M., Sauk, J., Garner, A., Jiang, X., Arthur, T., et al. (2017). A novel Ruminococcus gnavus clade enriched in inflammatory bowel disease patients. *Genome Med.* 9:103. doi: 10.1186/s13073-017-0490-495

Harach, T., Marungruang, N., Duthilleul, N., Cheatham, V., Mc Coy, K. D., Frisoni, G., et al. (2017). Reduction of Abeta amyloid pathology in APPPS1 transgenic mice in the absence of gut microbiota. *Sci. Rep.* 7:41802. doi: 10.1038/srep41802

Hardy, J. A., and Higgins, G. A. (1992). Alzheimer's disease: the amyloid cascade hypothesis. *Science* 256, 184–185. doi: 10.1126/science.1566067

Henke, M. T., Kenny, D. J., Cassilly, C. D., Vlamakis, H., Xavier, R. J., and Clardy, J. (2019). Ruminococcus gnavus, a member of the human gut microbiome associated with Crohn's disease, produces an inflammatory polysaccharide. *Proc. Natl. Acad. Sci. U.S.A.* 116:12672. doi: 10.1073/pnas.1904099116

Hewel, C., Kaiser, J., Wierczeiko, A., Linke, J., Reinhardt, C., Endres, K., et al. (2019). Common miRNA patterns of Alzheimer's disease and Parkinson's disease and their putative impact on commensal gut microbiota. *Front. Neurosci.* 13:113. doi: 10.3389/fnins.2019.00113

Alzheimer Disease International (2019). *World Alzheimer Report 2019: Attitudes to Dementia*. London: Alzheimer Disease International.

Joachim, C. L., Mori, H., and Selkoe, D. J. (1989). Amyloid beta-protein deposition in tissues other than brain in Alzheimer's disease. *Nature* 341, 226–230. doi: 10.1038/341226a0

Joossens, M., Huys, G., Cnockaert, M., De Preter, V., Verbeke, K., Rutgeerts, P., et al. (2011). Dysbiosis of the faecal microbiota in patients with Crohn's disease and their unaffected relatives. *Gut* 60:631. doi: 10.1136/gut.2010.223263

Kagan, B. L., Jang, H., Capone, R., Teran Arce, F., Ramachandran, S., Lal, R., et al. (2012). Antimicrobial properties of amyloid peptides. *Mol. Pharm.* 9, 708–717. doi: 10.1021/mp200419b

Kivipelto, M., Ngandu, T., Fratiglioni, L., Viitanen, M., Kåreholt, I., Winblad, B., et al. (2005). Obesity and vascular risk factors at midlife and the risk of Dementia and Alzheimer disease. *Arch. Neurol.* 62, 1556–1560. doi: 10.1001/archneur.62.10.1556

Kowall, N. W., and Kosik, K. S. (1987). Axonal disruption and aberrant localization of tau protein characterize the neuropil pathology of Alzheimer's disease. *Ann. Neurol.* 22, 639–643. doi: 10.1002/ana.410220514

Kumar, D. K. V., Choi, S. H., Washicosky, K. J., Eimer, W. A., Tucker, S., Ghofrani, J., et al. (2016). Amyloid-β peptide protects against microbial infection in mouse and worm models of Alzheimer's disease. *Sci. Transl. Med.* 8:340ra372. doi: 10.1126/scitranslmed.aaf1059

Lane, C. A., Hardy, J., and Schott, J. M. (2018). Alzheimer's disease. *Eur. J. Neurol.* 25, 59–70. doi: 10.1111/ene.13439

Love, M. I., Huber, W., and Anders, S. (2014). Moderated estimation of fold change and dispersion for RNA-seq data with DESeq2. *Genome Biol.* 15:550. doi: 10.1186/s13059-014-0550-558

Luchsinger, J. A., Cheng, D., Tang, M. X., Schupf, N., and Mayeux, R. (2012). Central obesity in the elderly is related to late-onset Alzheimer disease. *Alzheimer Dis. Assoc. Disord.* 26, 101–105. doi: 10.1097/WAD.0b013e318222f0d4

Mayer, E. A. (2011). Gut feelings: the emerging biology of gut-brain communication. *Nat. Rev. Neurosci.* 12, 453–466. doi: 10.1038/nrn3071

Moir, R. D., Lathe, R., and Tanzi, R. E. (2018). The antimicrobial protection hypothesis of Alzheimer's disease. *Alzheimer's Dementia* 14, 1602–1614. doi: 10.1016/j.jalz.2018.06.3040

Oakley, H., Cole, S. L., Logan, S., Maus, E., Shao, P., Craft, J., et al. (2006). Intraneuronal beta-amyloid aggregates, neurodegeneration, and neuron loss in transgenic mice with five familial Alzheimer's disease mutations: potential factors in amyloid plaque formation. *J. Neurosci.* 26, 10129–10140. doi: 10.1523/JNEUROSCI.1202-06.2006

Peng, W., Yi, P., Yang, J., Xu, P., Wang, Y., Zhang, Z., et al. (2018). Association of gut microbiota composition and function with a senescence-accelerated mouse model of Alzheimer's Disease using 16S rRNA gene and metagenomic sequencing analysis. *Aging* 10, 4054–4065. doi: 10.18632/aging.101693

Poewe, W. (2008). Non-motor symptoms in Parkinson's disease. *Eur. J. Neurol.* 15(Suppl. 1), 14–20. doi: 10.1111/j.1468-1331.2008.02056.x

Quan, N., and Banks, W. A. (2007). Brain-immune communication pathways. *Brain Behav. Immun.* 21, 727–735. doi: 10.1016/j.bbi.2007.05.005

Quigley, E. M. M. (2017). Microbiota-Brain-Gut Axis and Neurodegenerative diseases. *Curr. Neurol. Neurosci. Rep.* 17:94. doi: 10.1007/s11910-017-0802-806

Reinhardt, S., Stoye, N., Luderer, M., Kiefer, F., Schmitt, U., Lieb, K., et al. (2018). Identification of disulfiram as a secretase-modulating compound with beneficial effects on Alzheimer's disease hallmarks. *Sci. Rep.* 8:1329. doi: 10.1038/s41598-018-19577-19577

Roberts, B. R., Lind, M., Wagen, A. Z., Rembach, A., Frugier, T., Li, Q. X., et al. (2017). Biochemically-defined pools of amyloid-beta in sporadic Alzheimer's disease: correlation with amyloid PET. *Brain* 140, 1486–1498. doi: 10.1093/brain/awx057

Rossner, S., Sastre, M., Bourne, K., and Lichtenthaler, S. F. (2006). Transcriptional and translational regulation of BACE1 expression–implications for Alzheimer's disease. *Prog. Neurobiol.* 79, 95–111. doi: 10.1016/j.pneurobio.2006.06.001

Sampson, T. R., Debelius, J. W., Thron, T., Janssen, S., Shastri, G. G., Ilhan, Z. E., et al. (2016). Gut microbiota regulate motor deficits and neuroinflammation in a model of Parkinson's disease. *Cell* 167:1469-1480 e1412. doi: 10.1016/j.cell.2016.11.018

Saragat, B., Buffa, R., Mereu, E., Succa, V., Cabras, S., Mereu, R. M., et al. (2012). Nutritional and psycho-functional status in elderly patients with Alzheimer's disease. *J. Nutr. Health Aging* 16, 231–236. doi: 10.1007/s12603-011-0347-343

Schwarz, R., Kaspar, A., Seelig, J., and Kunnecke, B. (2002). Gastrointestinal transit times in mice and humans measured with 27Al and 19F nuclear magnetic resonance. *Magn. Reson. Med.* 48, 255–261. doi: 10.1002/mrm.10207

Shannon, K. M., Keshavarzian, A., Dodiya, H. B., Jakate, S., and Kordower, J. H. (2012). Is alpha-synuclein in the colon a biomarker for premotor Parkinson's disease? Evidence from 3 cases. *Mov. Disord.* 27, 716–719. doi: 10.1002/mds.25020

Shen, L., Liu, L., and Ji, H. F. (2017). Alzheimer's disease histological and behavioral manifestations in transgenic mice correlate with specific Gut microbiome State. *J. Alzheimers Dis.* 56, 385–390. doi: 10.3233/JAD-160884

Shin, R. W., Ogomori, K., Kitamoto, T., and Tateishi, J. (1989). Increased tau accumulation in senile plaques as a hallmark in Alzheimer's disease. *Am. J. Pathol.* 134, 1365–1371.

Soscia, S. J., Kirby, J. E., Washicosky, K. J., Tucker, S. M., Ingelsson, M., Hyman, B., et al. (2010). The Alzheimer's disease-associated amyloid beta-protein is an antimicrobial peptide. *PLoS One* 5:e9505. doi: 10.1371/journal.pone.0009505

Spitzer, P., Condic, M., Herrmann, M., Oberstein, T. J., Scharin-Mehlmann, M., Gilbert, D. F., et al. (2016). Amyloidogenic amyloid-β-peptide variants induce microbial agglutination and exert antimicrobial activity. *Sci. Rep.* 6:32228. doi: 10.1038/srep32228

Turnbaugh, P. J., Ley, R. E., Mahowald, M. A., Magrini, V., Mardis, E. R., and Gordon, J. I. (2006). An obesity-associated gut microbiome with increased capacity for energy harvest. *Nature* 444:1027. doi: 10.1038/nature05414

Unger, M. M., Spiegel, J., Dillmann, K. U., Grundmann, D., Philippeit, H., Burmann, J., et al. (2016). Short chain fatty acids and gut microbiota differ between patients with Parkinson's disease and age-matched controls. *Parkinson. Relat. Disord.* 32, 66–72. doi: 10.1016/j.parkreldis.2016.08.019

United Nations Department of Economic and Social Affairs. (2019). *World Population Prospects 2019*. Herndon, VA: United Nations Publications.

Vogt, N. M., Kerby, R. L., Dill-McFarland, K. A., Harding, S. J., Merluzzi, A. P., Johnson, S. C., et al. (2017). Gut microbiome alterations in Alzheimer's disease. *Sci. Rep.* 7:13537. doi: 10.1038/s41598-017-13601-y

Weiss, S., Xu, Z. Z., Peddada, S., Amir, A., Bittinger, K., Gonzalez, A., et al. (2017). Normalization and microbial differential abundance strategies depend upon data characteristics. *Microbiome* 5:27. doi: 10.1186/s40168-017-0237-y

Whitehouse, P. J., Price, D. L., Struble, R. G., Clark, A. W., Coyle, J. T., and Delon, M. R. (1982). Alzheimer's disease and senile dementia: loss of neurons in the basal forebrain. *Science* 215, 1237–1239. doi: 10.1126/science.7058341

Yang, L. B., Lindholm, K., Yan, R., Citron, M., Xia, W., Yang, X. L., et al. (2003). Elevated beta-secretase expression and enzymatic activity detected in sporadic Alzheimer disease. *Nat. Med.* 9, 3–4. doi: 10.1038/nm0103-3

Yurkovetskiy, L., Burrows, M., Khan, A. A., Graham, L., Volchkov, P., Becker, L., et al. (2013). Gender bias in autoimmunity is influenced by microbiota. *Immunity* 39, 400–412. doi: 10.1016/j.immuni.2013.08.013

Zhan, G., Yang, N., Li, S., Huang, N., Fang, X., Zhang, J., et al. (2018). Abnormal gut microbiota composition contributes to cognitive dysfunction in SAMP8 mice. *Aging* 10, 1257–1267. doi: 10.18632/aging.101464

Zhang, L., Wang, Y., Xiayu, X., Shi, C., Chen, W., Song, N., et al. (2017). Altered Gut microbiota in a mouse model of Alzheimer's disease. *J. Alzheimer's Dis.* 60, 1241–1257. doi: 10.3233/JAD-170020

Zhuang, Z.-Q., Shen, L.-L., Li, W.-W., Fu, X., Zeng, F., Gui, L., et al. (2018). Gut microbiota is altered in patients with Alzheimer's disease. *J. Alzheimer's Dis.* 63, 1337–1346. doi: 10.3233/JAD-180176

Conflict of Interest: HT was employed by Fresenius Kabi Deutschland GmbH at the time the research was conducted.

The remining authors declare that the research was conducted in the absence of any commercial or financial relationships that could be construed as a potential conflict of interest.

2.4.1 Supplementary material to publication 4

Table S1. Alpha diversity measures for the negative control sample

Shannon index	Chao index
3.38	113.87

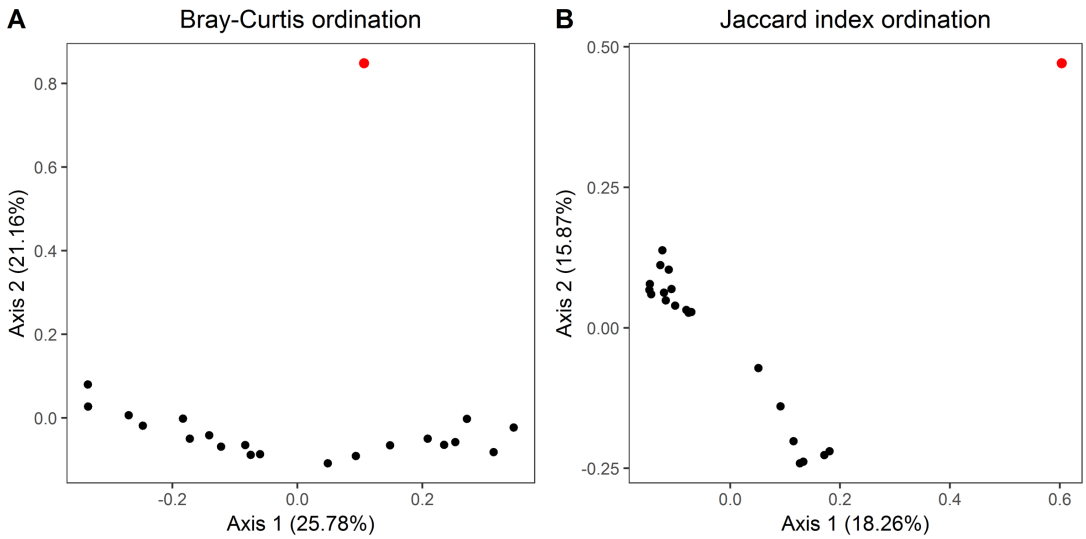

Figure S1. Unconstrained ordination analysis of all experimental groups including negative control. Ordination analysis was performed based on the **(A)** Bray-Cutis dissimilarity or **(B)** binary Jaccard distance. The negative control sample appears as a red dot on the plots. The amount of dispersion in sample scores (inertia) in percent captured by each multivariate dimension is given in brackets on the respective axis.

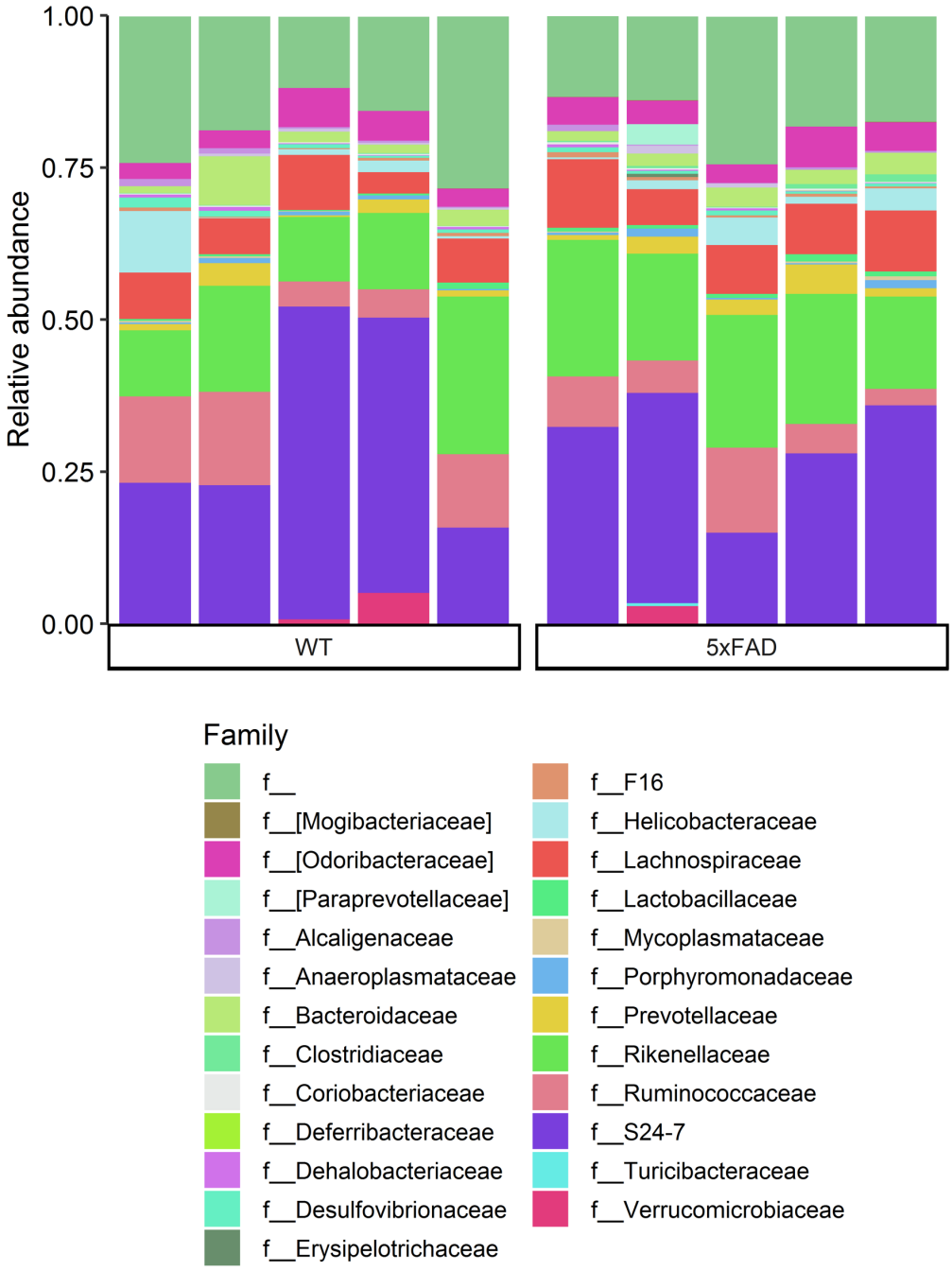

Figure S2. Community composition of wildtype and 5xFAD animals at the family level. Each bar shows the relative abundance of bacterial families for individual animals.

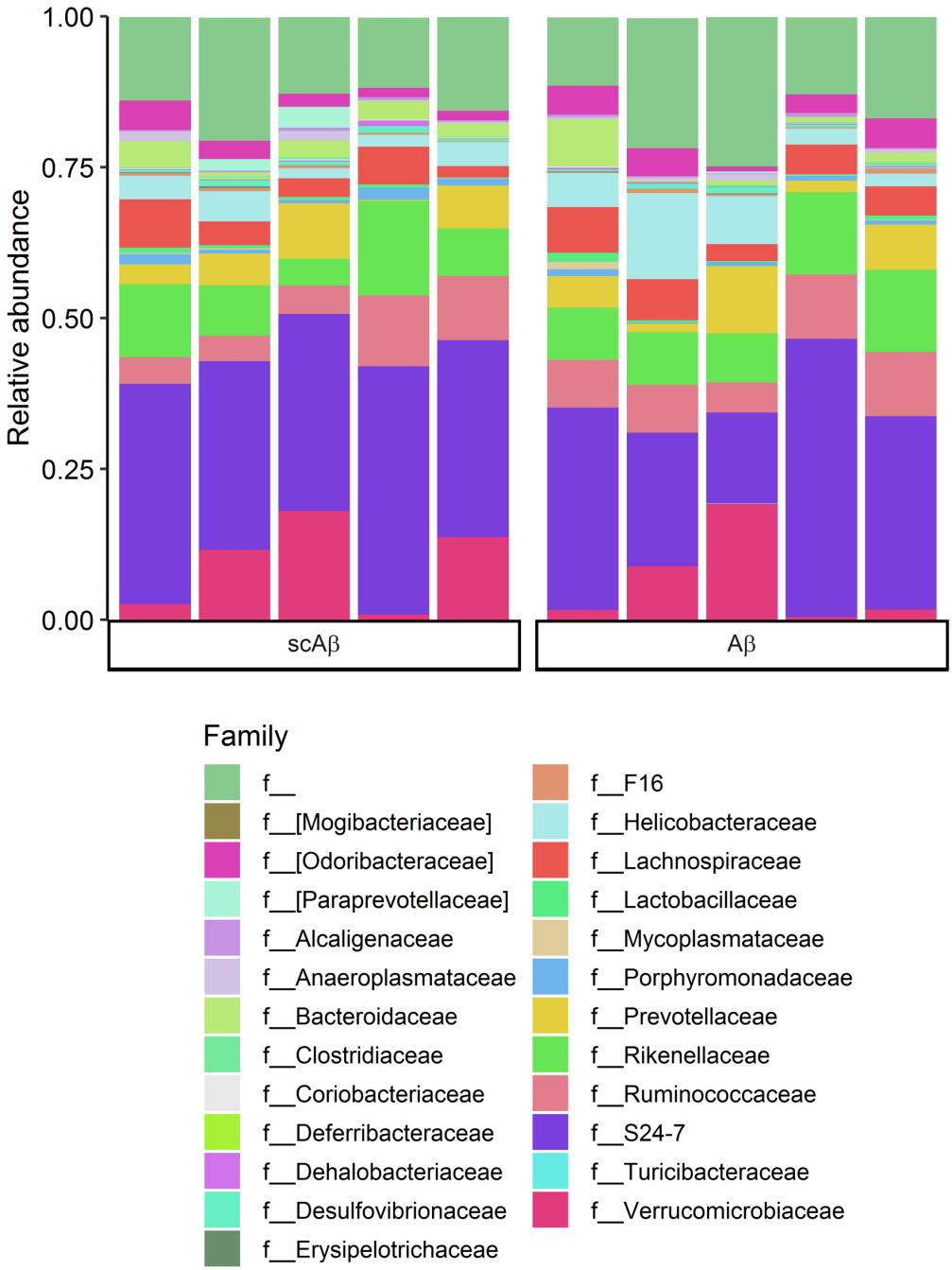

Figure S3. Community composition of scrambled Aβ or Aβ-fed animals at the family level. Each bar shows the relative abundance of bacterial families for individual animals.

Table S2 Differentially abundant operational taxonomic units (OTU) in 5xFAD animals relative to wildtype controls. The taxonomy classification for each OTU, the fold change (FC) together with the corresponding adjusted p-value (Benjamini-Hochberg method) are reported. FC values below 0 indicate OTUs with significantly lower abundance in 5xFAD animals whereas positive FC values correspond to enriched OTUs in the 5xFAD group.

Taxonomy	Log2 fold change	Adj. p-value
p__Firmicutes; c__Clostridia; o__Clostridiales; f__Lachnospiraceae	-27.93	2.96E-17
p__Firmicutes; c__Clostridia; o__Clostridiales; f__Lachnospiraceae	25.01	5.15E-14
p__Firmicutes; c__Clostridia; o__Clostridiales	25.09	5.15E-14
p__Firmicutes; c__Clostridia; o__Clostridiales	-24.67	7.96E-14
p__Firmicutes; c__Clostridia; o__Clostridiales; f__Ruminococcaceae; g__Oscillospira	24.73	7.96E-14
p__Firmicutes; c__Clostridia; o__Clostridiales	24.54	9.32E-14
p__Firmicutes; c__Clostridia; o__Clostridiales	-24.26	1.73E-13
p__Firmicutes; c__Clostridia; o__Clostridiales; f__Ruminococcaceae	-24.13	2.15E-13
p__Firmicutes; c__Clostridia; o__Clostridiales; f__Ruminococcaceae; g__Ruminococcus	-24	2.24E-13
p__Firmicutes; c__Clostridia; o__Clostridiales; f__Lachnospiraceae	24.04	2.24E-13
p__Bacteroidetes; c__Bacteroidia; o__Bacteroidales; f__S24-7	-24.02	2.24E-13
p__Firmicutes; c__Clostridia; o__Clostridiales	-23.91	2.38E-13
p__Bacteroidetes; c__Bacteroidia; o__Bacteroidales; f__S24-7	-23.77	3.16E-13
p__Firmicutes; c__Clostridia; o__Clostridiales; f__Lachnospiraceae	-23.74	3.23E-13
p__Firmicutes; c__Bacilli; o__Turicibacterales; f__Turicibacteraceae; g__Turicibacter	23.52	5.40E-13
p__Firmicutes; c__Clostridia; o__Clostridiales; f__Clostridiaceae; g__SMB53	23.46	5.95E-13
p__Firmicutes; c__Clostridia; o__Clostridiales; f__Ruminococcaceae; g__Oscillospira	-23.36	6.97E-13
p__Firmicutes; c__Clostridia; o__Clostridiales; o__Clostridiales; o__Clostridiales	-23.36	6.97E-13
p__Firmicutes; c__Clostridia; o__Clostridiales; f__Ruminococcaceae; g__Oscillospira	-23.19	1.01E-12
p__Bacteroidetes; c__Bacteroidia; o__Bacteroidales; f__S24-7	-23	1.38E-12
p__Firmicutes; c__Clostridia; o__Clostridiales; f__Ruminococcaceae; g__Oscillospira	-23.03	1.38E-12
p__Firmicutes; c__Clostridia; o__Clostridiales; f__Ruminococcaceae	-23.01	1.38E-12
p__Firmicutes; c__Clostridia; o__Clostridiales; f__Lachnospiraceae	23.02	1.38E-12
p__Firmicutes; c__Erysipelotrichi; o__Erysipelotrichales; f__Erysipelotrichaceae; g__Allobaculum	22.96	1.41E-12
p__Firmicutes; c__Clostridia; o__Clostridiales	-22.98	1.41E-12
p__Firmicutes; c__Clostridia; o__Clostridiales	-22.92	1.50E-12
p__Firmicutes; c__Erysipelotrichi; o__Erysipelotrichales; f__Erysipelotrichaceae; g__Allobaculum	22.71	2.46E-12
p__Firmicutes; c__Clostridia; o__Clostridiales; f__Lachnospiraceae	22.59	3.15E-12
p__Firmicutes; c__Clostridia; o__Clostridiales	-22.59	3.15E-12
p__Firmicutes; c__Clostridia; o__Clostridiales; f__Lachnospiraceae; g__[Ruminococcus]; s__Ruminococcus gnavus	22.49	3.89E-12
p__Bacteroidetes; c__Bacteroidia; o__Bacteroidales; f__Bacteroidaceae; g__Bacteroides; s__Bacteroides acidifaciens	22.46	4.08E-12
p__Firmicutes; c__Bacilli; o__Lactobacillales; f__Lactobacillaceae; g__Lactobacillus; s__Lactobacillus reuteri	22.41	4.50E-12
p__Bacteroidetes; c__Bacteroidia; o__Bacteroidales; f__Rikenellaceae; g__Alistipes; s__Alistipes massiliensis	-22.29	5.87E-12

p__Firmicutes; c__Clostridia; o__Clostridiales	-22.26	5.88E-12
p__Firmicutes; c__Clostridia; o__Clostridiales	22.27	5.88E-12
p__Proteobacteria; c__Epsilonproteobacteria; o__Campylobacterales; f__Helicobacteraceae; g__Helicobacter; s__Helicobacter hepaticus	-22.26	5.88E-12
p__Firmicutes; c__Clostridia; o__Clostridiales; f__Ruminococcaceae; g__Oscillospira	-22.23	6.05E-12
p__Firmicutes; c__Erysipelotrichi; o__Erysipelotrichales; f__Erysipelotrichaceae; g__Allobaculum	22.17	6.90E-12
p__Firmicutes; c__Clostridia; o__Clostridiales; f__Lachnospiraceae	22.14	7.22E-12
p__Firmicutes; c__Clostridia; o__Clostridiales	-22.06	8.80E-12
p__Bacteroidetes; c__Bacteroidia; o__Bacteroidales; f__Rikenellaceae; g__Alistipes; s__Alistipes massiliensis	22	9.66E-12
p__Firmicutes; c__Clostridia; o__Clostridiales; f__Ruminococcaceae; g__Oscillospira	-21.99	9.82E-12
p__Firmicutes; c__Clostridia; o__Clostridiales; f__Lachnospiraceae	-21.97	1.03E-11
p__Firmicutes; c__Clostridia; o__Clostridiales	-21.95	1.04E-11
p__Firmicutes; c__Clostridia; o__Clostridiales; f__Lachnospiraceae	21.93	1.06E-11
p__Firmicutes; c__Clostridia; o__Clostridiales	-21.88	1.18E-11
p__Firmicutes; c__Clostridia; o__Clostridiales	21.83	1.28E-11
p__Firmicutes; c__Clostridia; o__Clostridiales	-21.82	1.32E-11
p__Bacteroidetes; c__Bacteroidia; o__Bacteroidales	-21.81	1.33E-11
p__Firmicutes; c__Clostridia; o__Clostridiales	-21.75	1.50E-11
p__Firmicutes; c__Clostridia; o__Clostridiales	21.67	1.77E-11
p__Firmicutes; c__Clostridia; o__Clostridiales; f__Ruminococcaceae; g__Ruminococcus	-21.65	1.84E-11
p__Firmicutes; c__Clostridia; o__Clostridiales	-21.59	2.08E-11
p__Firmicutes; c__Clostridia; o__Clostridiales	-21.57	2.17E-11
p__Firmicutes; c__Clostridia; o__Clostridiales	21.55	2.18E-11
p__Firmicutes; c__Clostridia; o__Clostridiales; f__Ruminococcaceae; g__Oscillospira	-21.52	2.32E-11
p__Firmicutes; c__Clostridia; o__Clostridiales	-21.52	2.32E-11
p__Firmicutes; c__Clostridia; o__Clostridiales	-21.42	2.71E-11
p__Cyanobacteria; c__Chloroplast; o__Streptophyta	21.41	2.71E-11
p__Firmicutes; c__Clostridia; o__Clostridiales	21.43	2.71E-11
p__Bacteroidetes; c__Bacteroidia; o__Bacteroidales; f__S24-7	21.42	2.71E-11
p__Firmicutes; c__Clostridia; o__Clostridiales; f__Ruminococcaceae; g__Ruminococcus	21.42	2.71E-11
p__Bacteroidetes; c__Bacteroidia; o__Bacteroidales; f__Rikenellaceae; g__Alistipes; s__Alistipes massiliensis	21.38	2.91E-11
p__Firmicutes; c__Clostridia; o__Clostridiales	21.37	2.92E-11
p__Firmicutes; c__Clostridia; o__Clostridiales	-21.37	2.96E-11
p__Firmicutes; c__Clostridia; o__Clostridiales	21.35	3.01E-11
p__Firmicutes; c__Clostridia; o__Clostridiales	-21.35	3.02E-11
p__Firmicutes; c__Clostridia; o__Clostridiales; f__Ruminococcaceae; g__Ruminococcus	21.32	3.10E-11
p__Firmicutes; c__Clostridia; o__Clostridiales	21.28	3.33E-11
p__Firmicutes; c__Clostridia; o__Clostridiales	-21.28	3.41E-11
p__Firmicutes; c__Clostridia; o__Clostridiales	-21.24	3.63E-11
p__Firmicutes; c__Clostridia; o__Clostridiales; f__Lachnospiraceae	21.23	3.63E-11
p__Firmicutes; c__Clostridia; o__Clostridiales	21.22	3.63E-11
p__Firmicutes; c__Clostridia; o__Clostridiales; f__Lachnospiraceae	21.22	3.63E-11

p__Bacteroidetes; c__Bacteroidia; o__Bacteroidales; f__Rikenellaceae; g__Alistipes; s__Alistipes massiliensis	-21.22	3.67E-11
p__Firmicutes; c__Clostridia; o__Clostridiales	21.19	3.77E-11
p__Firmicutes; c__Clostridia; o__Clostridiales; f__Ruminococcaceae; g__Ruminococcus	-21.19	3.78E-11
p__Bacteroidetes; c__Bacteroidia; o__Bacteroidales; f__Rikenellaceae; g__Alistipes; s__Alistipes massiliensis	21.17	3.91E-11
p__Bacteroidetes; c__Bacteroidia; o__Bacteroidales; f__Rikenellaceae; g__Alistipes; s__Alistipes massiliensis	21.14	4.14E-11
p__Bacteroidetes; c__Bacteroidia; o__Bacteroidales	21.05	4.97E-11
p__Firmicutes; c__Clostridia; o__Clostridiales	-21.06	4.97E-11
p__Firmicutes; c__Clostridia; o__Clostridiales	21.04	5.03E-11
p__Firmicutes; c__Clostridia; o__Clostridiales	-21.04	5.09E-11
p__Firmicutes; c__Clostridia; o__Clostridiales	21.02	5.17E-11
p__Firmicutes; c__Clostridia; o__Clostridiales	-21.02	5.17E-11
p__Bacteroidetes; c__Bacteroidia; o__Bacteroidales; f__Bacteroidaceae; g__Bacteroides	20.98	5.48E-11
p__Firmicutes; c__Clostridia; o__Clostridiales; f__Lachnospiraceae	20.97	5.48E-11
p__Firmicutes; c__Clostridia; o__Clostridiales	-20.97	5.49E-11
p__Firmicutes; c__Clostridia; o__Clostridiales; f__Lachnospiraceae	-20.98	5.49E-11
p__Firmicutes; c__Clostridia; o__Clostridiales; f__Lachnospiraceae	20.95	5.59E-11
p__Bacteroidetes; c__Bacteroidia; o__Bacteroidales; f__Rikenellaceae; g__Alistipes; s__Alistipes massiliensis	20.9	6.18E-11
p__Firmicutes; c__Clostridia; o__Clostridiales	20.79	8.12E-11
p__Bacteroidetes; c__Bacteroidia; o__Bacteroidales; f__Rikenellaceae; g__Alistipes; s__Alistipes massiliensis	20.76	8.54E-11
p__Bacteroidetes; c__Bacteroidia; o__Bacteroidales	20.66	1.07E-10
p__Firmicutes; c__Clostridia; o__Clostridiales	20.58	1.27E-10
p__Firmicutes; c__Clostridia; o__Clostridiales	20.52	1.36E-10
p__Firmicutes; c__Clostridia; o__Clostridiales	20.5	1.50E-10
p__Firmicutes; c__Clostridia; o__Clostridiales; f__Ruminococcaceae; g__Ruminococcus	20.45	1.63E-10
p__Firmicutes; c__Clostridia; o__Clostridiales	20.45	1.63E-10
p__Firmicutes; c__Clostridia; o__Clostridiales	20.43	1.70E-10
p__Firmicutes; c__Clostridia; o__Clostridiales	19.82	6.26E-10
p__Bacteroidetes; c__Bacteroidia; o__Bacteroidales; f__S24-7	-9.49	9.01E-05
p__Firmicutes; c__Clostridia; o__Clostridiales	10.94	0.003137
p__Firmicutes; c__Clostridia; o__Clostridiales; f__Ruminococcaceae; g__Oscillospira;	10.77	0.003848
p__Proteobacteria; c__Alphaproteobacteria; o__RF32;;;	-10.01	0.00635
p__Firmicutes; c__Clostridia; o__Clostridiales;;;	10.31	0.00664
p__Tenericutes; c__Mollicutes; o__Anaeroplasmatales; f__Anaeroplasmataceae; g__Anaeroplasma	9.99	0.007711
p__Bacteroidetes; c__Bacteroidia; o__Bacteroidales; f__[Paraprevotellaceae]; g__[Prevotella]	7.91	0.010456
p__Firmicutes; c__Clostridia; o__Clostridiales; f__Clostridiaceae; g__Candidatus Arthromitus	2.91	0.03776

Table S3. Differentially abundant operational taxonomic units (OTU) in amyloid-β (Aβ) relative to scrambled amyloid beta (scAβ)-fed animals. The taxonomy classification for each OTU, the fold change (FC) together with the corresponding adjusted p-value (Benjamini-Hochberg method) are reported. FC below 0 indicate OTUs with significantly lower abundance in Aβ animals whereas positive FC values correspond to enriched OTUs in the Aβ group.

Taxonomy	Log2 fold change	Adj. p-value
p__Firmicutes; c__Clostridia; o__Clostridiales; f__Lachnospiraceae;	24.24	1.72E-16
p__Tenericutes; c__Mollicutes; o__Anaeroplasmatales; f__Anaeroplasmataceae; g__Anaeroplasma	-26.96	1.84E-16
p__Firmicutes; c__Clostridia; o__Clostridiales; f__Ruminococcaceae; g__Oscillospira	-24.99	3.50E-14
p__Firmicutes; c__Clostridia; o__Clostridiales	24.8	4.45E-14
p__Firmicutes; c__Clostridia; o__Clostridiales; f__Ruminococcaceae; g__Ruminococcus	24.68	4.98E-14
p__Firmicutes; c__Clostridia; o__Clostridiales; f__Lachnospiraceae; g__[Ruminococcus]; s__Ruminococcus gnavus	-24.11	5.89E-14
p__Firmicutes; c__Clostridia; o__Clostridiales	23.75	7.10E-14
p__Firmicutes; c__Clostridia; o__Clostridiales; f__Ruminococcaceae; g__Oscillospira	-23.78	7.10E-14
p__Firmicutes; c__Clostridia; o__Clostridiales; f__Lachnospiraceae	23.94	7.10E-14
p__Firmicutes; c__Clostridia; o__Clostridiales; f__Lachnospiraceae	-22.93	2.22E-13
p__Firmicutes; c__Clostridia; o__Clostridiales; f__Ruminococcaceae; g__Oscillospira	22.81	2.89E-13
p__Firmicutes; c__Clostridia; o__Clostridiales	-23.38	6.71E-13
p__Firmicutes; c__Clostridia; o__Clostridiales	22.02	1.22E-12
p__Bacteroidetes; c__Bacteroidia; o__Bacteroidales; f__S24-7	-22.79	2.60E-12
p__Bacteroidetes; c__Bacteroidia; o__Bacteroidales; f__Rikenellaceae	-22.71	2.99E-12
p__Firmicutes; c__Clostridia; o__Clostridiales; f__Lachnospiraceae	-22.58	3.83E-12
p__Firmicutes; c__Clostridia; o__Clostridiales; f__Ruminococcaceae; g__Ruminococcus	-22.55	3.94E-12
p__Firmicutes; c__Clostridia; o__Clostridiales; f__Lachnospiraceae	-22.48	4.45E-12
p__Firmicutes; c__Clostridia; o__Clostridiales	-22.38	5.50E-12
p__Firmicutes; c__Clostridia; o__Clostridiales	-22.09	1.07E-11
p__Firmicutes; c__Clostridia; o__Clostridiales	-22.06	1.10E-11
p__Firmicutes; c__Clostridia; o__Clostridiales; f__Ruminococcaceae; g__Oscillospira	-22.01	1.17E-11
p__Firmicutes; c__Clostridia; o__Clostridiales; f__Ruminococcaceae	-21.89	1.51E-11
p__Firmicutes; c__Clostridia; o__Clostridiales	-21.87	1.52E-11
p__Firmicutes; c__Clostridia; o__Clostridiales	-21.63	2.42E-11
p__Firmicutes; c__Clostridia; o__Clostridiales	21.64	2.42E-11
p__Firmicutes; c__Clostridia; o__Clostridiales	21.59	2.56E-11
p__Firmicutes; c__Clostridia; o__Clostridiales	-21.53	2.93E-11
p__Firmicutes; c__Clostridia; o__Clostridiales	21.46	3.27E-11
p__Firmicutes; c__Clostridia; o__Clostridiales; f__Lachnospiraceae	-21.36	4.14E-11
p__Firmicutes; c__Clostridia; o__Clostridiales; f__Ruminococcaceae	-21.34	4.16E-11
p__Firmicutes; c__Clostridia; o__Clostridiales; f__Ruminococcaceae	-21.32	4.27E-11
p__Firmicutes; c__Clostridia; o__Clostridiales; f__Ruminococcaceae; g__Ruminococcus	21.23	4.90E-11
p__Firmicutes; c__Clostridia; o__Clostridiales; f__Ruminococcaceae; g__Oscillospira	-21.24	4.90E-11
p__Firmicutes; c__Clostridia; o__Clostridiales; f__Ruminococcaceae	-21.2	5.19E-11

p__Firmicutes; c__Clostridia; o__Clostridiales; f__Lachnospiraceae	-21.1	6.11E-11
p__Firmicutes; c__Clostridia; o__Clostridiales;	-21.12	6.11E-11
p__Firmicutes; c__Clostridia; o__Clostridiales; f__Lachnospiraceae	-21.08	6.42E-11
p__Firmicutes; c__Clostridia; o__Clostridiales; f__Lachnospiraceae;	20.97	7.70E-11
p__Bacteroidetes; c__Bacteroidia; o__Bacteroidales; f__S24-7	-20.97	7.88E-11
p__Firmicutes; c__Clostridia; o__Clostridiales; f__Ruminococcaceae; g__Oscillospira	20.95	7.92E-11
p__Firmicutes; c__Clostridia; o__Clostridiales; f__Lachnospiraceae; g__[Ruminococcus]; s__Ruminococcus gnavus	-20.94	7.96E-11
p__Bacteroidetes; c__Bacteroidia; o__Bacteroidales	-20.89	8.55E-11
p__Firmicutes; c__Clostridia; o__Clostridiales	20.89	8.55E-11
p__Firmicutes; c__Clostridia; o__Clostridiales	20.85	9.09E-11
p__Firmicutes; c__Clostridia; o__Clostridiales	-20.77	1.07E-10
p__Bacteroidetes; c__Bacteroidia; o__Bacteroidales; f__S24-7	20.71	1.21E-10
p__Firmicutes; c__Clostridia; o__Clostridiales	20.66	1.33E-10
p__Firmicutes; c__Clostridia; o__Clostridiales	20.58	1.49E-10
p__Cyanobacteria; c__Chloroplast; o__Streptophyta	20.55	1.67E-10
p__Firmicutes; c__Clostridia; o__Clostridiales; f__Ruminococcaceae; g__Ruminococcus	9.5	0.003558
p__Firmicutes; c__Clostridia; o__Clostridiales; f__Ruminococcaceae; g__Oscillospira	8.73	0.009744
p__Firmicutes; c__Clostridia; o__Clostridiales	-8.32	0.01723
p__Firmicutes; c__Bacilli; o__Lactobacillales; f__Lactobacillaceae; g__Lactobacillus; s__Lactobacillus reuteri	-7.92	0.02619
p__Firmicutes; c__Clostridia; o__Clostridiales; f__Lachnospiraceae	-8.06	0.02619

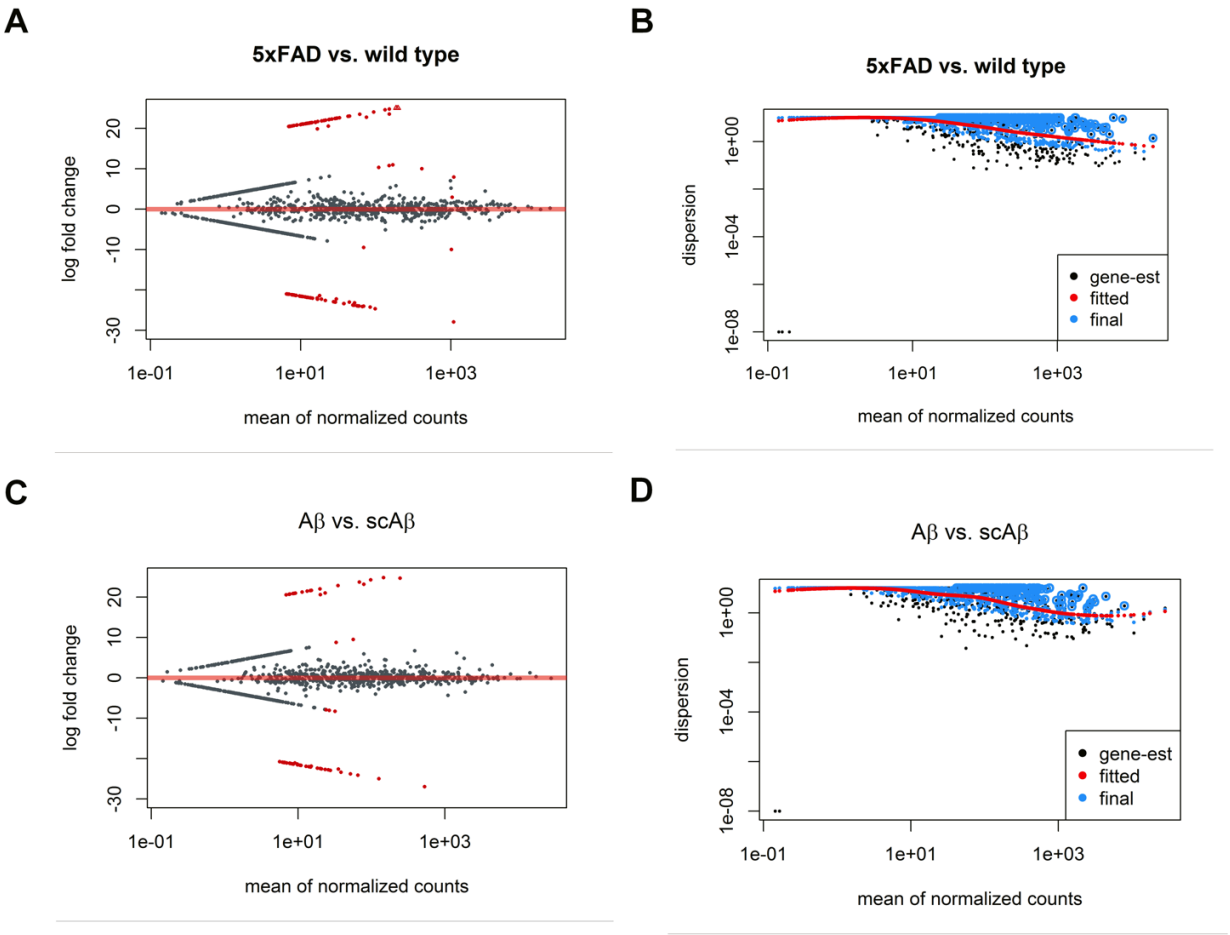

Figure S4. Diagnostic plots for the differential abundance analysis performed with DESeq2. The relationship between the mean normalized bacterial abundance and log2 fold change is shown in panel A for 5xFAD mice relative to wild type mice and panel C for Aβ-fed wild type mice relative to animals receiving scrambled Aβ (scAβ). Fold changes with an adjusted p-value less than 0.05 are colored red. The relationship between the dispersion and mean parameters of the negative binomial distributions used to estimate log2 fold changes is shown in panels B and D. Dispersions estimates directly obtained from the data appear as black dots, the red line corresponds to the fitted values using local regression. The blue dots correspond to the final estimates of dispersion after shrinkage.

Overall discussion and outlook

The current thesis addressed the issue of hypothesis testing and dimensionality reduction in the context of multidimensional data generated from animal studies with small sample sizes. The following points summarize the major findings of this research project:

- Multivariate hypothesis testing techniques do not offer an appreciable advantage over univariate methods in terms of power to detect treatment effects in animal studies with small group sizes.
- PLS-DA was associated with the highest sensitivity to detect treatment effect patterns compared to PCA and RDA for quantitative and semiquantitative variables.
- PCA is an appropriate and useful dimensionality reduction technique for omics data, however it does not take additional experimental information into account and no hypothesis testing can be performed directly.
- Microbiome studies require ordination techniques which can handle distance measures appropriate for ecological data.

Some important considerations which have not been addressed explicitly in the publications in sections 2.1 - 2.4 are discussed below.
The simulation study presented in section 2.2 demonstrated that LDA was associated with a high false positive rate for detecting group differences in multidimensional data sets with correlated variables. Similar to multiple regression analysis, LDA involves calculating the inverse of an empirical dispersion matrix, e.g. the covariance matrix S, during the classification process [Næs and Mevik, 2001]. In the presence of multicollinearity, some of the predictor variables are linear combinations of other predictors which results in a nearly singular dispersion matrix [Dormann et al., 2013]. This leads to unstable matrix inversion. In fact, classical LDA and multiple regression techniques cannot be applied to data sets where the number of variables p is larger than the number of observations n. In such cases, the empirical covariance matrix is singular

and therefore its inverse cannot be calculated [Ramey and Young, 2013, Dormann et al., 2013]. Near-singularity arising from collinearity and small sample sizes reduces performance of LDA since the classification function is proportional to the inverse of the covariance matrix, S^{-1}. The issue emerges in the spectral decomposition of this matrix: $S^{-1} = \sum_{j=1}^{p} v_j \frac{1}{\lambda_j} v_j^T$, where v denotes the eigenvectors of S and λ denotes the corresponding eigenvalues. This equation demonstrates that small eigenvalues and the respective eigenvectors have a stronger weight on the calculation of S^{-1} and thereby on the classification function. These eigenvalues are biased and less reliably estimated in the case of collinearity and small samples [Ramey and Young, 2013, Næs and Mevik, 2001]. One possible approach to address this issue is to only consider dimensions defined by eigenvectors with large corresponding eigenvalues in the classification procedure. Such a solution is provided if PCA is first applied to the set of continuous predictor variables and then only relevant components with large eigenvalues are used for the classification procedure in LDA. PLS-DA is a similar technique in the sense that is performs classification based on a subset of linear combinations of the predictor variables x while simultaneously maximizing the covariance with the grouping variable y [Barker and Rayens, 2003]. In fact, PLS-DA would provide identical results to LDA if all non-zero components are retained in the model [Brereton and Lloyd, 2014]. In practice, components with little explanatory power are discarded which is how PLS-DA overcomes the multicollinearity problem and can also be applied to data with more variables than observations.

A different strategy of dealing with multicollinearity and small sample sizes for regression and classification problems in multi-dimensional data sets, which has not been addressed in this thesis, is regularization of the dispersion matrix. This process includes introducing penalties in the estimation of the parameters of the regression or classification model with the trade-off of reducing variance in exchange for a certain amount of bias. The two most popular techniques are ridge [Hoerl and Kennard, 2000] and lasso regularization [Tibshirani, 1996]. The main difference between the two methods is that lasso penalizes the sum of absolute model coefficients whereas ridge regression penalizes the sum of their squared values. As a result, many model coefficients are set to 0 in lasso regularization which can be also used for feature selection [Melkumova and Shatskikh, 2017]. While multiple implementations of classification and regression methods with regularization exist (e.g. [Guo et al., 2006, Cao et al., 2011, Gschwandtner et al., 2012, Allen et al., 2012, Shen and Huang, 2008]), a detailed comparison of the methodology and their performance is beyond the scope of the current thesis.

In certain cases, the choice of the ordination and dimensionality-reduction technique is mainly driven by the nature of the input data. Ecological studies such as the analysis of microbiota composition of biological samples are one such example. Here, the ordination method has to be capable of handling distance/dissimilarity measures which are appropriate for the analysis of ecological data. In the case studies presented in sections 2.3 and 2.4, canonical analysis of principal coordinates was used in combination with either the Bray-Curtis dissimilarity or the binary Jaccard distance. Another popular distance measure which has not been considered here but would be appropriate for microbial data is the weighted or unweighted UniFrac distance, which incorporates phylogenetic information [Lozupone and Knight, 2005]. However, numerous other distance or dissimilarity measures could be applied. A detailed overview is provided by Legendre and Legendre [2003] and Borcard et al. [2011]. The impact of the experimental condition on the multivariate signature of the commensal microbiota was statistically evaluated using permutational analysis of variance. The null hypothesis for this test assumes that a constrained axis does not explain more variation in the data than expected by chance. The p-value of the test is derived by comparing the eigenvalue of the constrained axis against an F-distribution of eigenvalues obtained from random permutations of the data [Legendre et al., 2011].

While ordination techniques allow exploring and testing the effects of experimental factors on the overall microbial composition, shifts in the abundance of individual bacterial taxa are also often the focus of research. It is important to mention that the statistical model employed here for performing differential abundance analysis may not be the optimal strategy. While generally applicable to count data, the DESeq2 algorithm was developed for RNA-Seq analysis. DESeq2 uses the median of ratios method for library size normalization which is followed by log2 fold change estimation with generalized linear models assuming a negative binomial distribution [Love et al., 2014]. This approach offered an increased sensitivity with small sample sizes and acceptable type I error rates when library sizes were not extremely uneven in a study comparing different normalization and differential abundance analysis methods for microbiome sequencing data [Weiss et al., 2017]. These findings provided the main motivation for using the DESeq2 method in the microbiome case studies presented in the publications in sections 2.3 and 2.4. In preliminary analyses of the 16S rRNA sequencing data, the metagenomeSeq R package was tested [Paulson et al., 2013]. This method was specifically developed for microbial data. It employs a zero-inflated distribution to model zero counts which are the result of either a true biological effect or

technical issues such as under-sampling. The non-zero component of the abundance data is modeled by a log-normal distribution. However, applying this method to the 16S rRNA data presented in this thesis led to convergence problems. An alternative approach for differential abundance analysis is using non-parametric statistical tests on relative bacterial abundances. For instance, linear discriminant analysis effect size (LEfSe) is a popular tool for microbial data analysis which uses either a Kruskal-Wallis test (with more than two groups) or a Wilcoxon test (when only two groups are compared) to identify differentially abundant taxonomic units [Segata et al., 2011]. However, this step is followed by LDA to identify important features which are responsible for group separation in reduced multivariate space. In the simulation study presented in section 2.2, LDA was associated with increased false positive rate when group size was small, and multicollinearity was present. This consideration combined with the fact that non-parametric statistical methods generally offer reduced power with small samples motivated the decision not to use LEfSe in the case studies presented here. Altogether, these findings demonstrate that none of the currently existing strategies to analyze microbial data is optimal. Selecting the appropriate method remains a case-by-case decision which needs to carefully take the experimental specifics such as group sizes into account. Additionally, none of the statistical models discussed above explicitly take repeated measures into account which might limit the power of longitudinal microbial studies. The simulation study presented in section 2.2 demonstrated that linear mixed effects models are associated with increased power when applied to data with repeated measures. Such models could theoretically be used for differential abundance analysis of microbial data after appropriate normalization. Furthermore, random effects can be extended to generalized mixed models which are suitable for non-normal data [Faraway, 2016]. These considerations provide points of reference for future efforts to optimize analysis strategies for microbiome sequencing data.

Conclusion

The current thesis focused on alternative strategies for hypothesis testing and dimensionality reduction in the challenging set-up of multidimensional data from animal studies having small group sizes. The results demonstrated that no gold-standard approach can be defined, and the choice of statistical method is influenced by the specific research question and the nature of the generated data. While multivariate statistics did not offer an advantage for hypothesis testing, dimensionality reduction techniques are still very useful for detecting patterns in the data and identifying important variables which may be used for targeted statistical testing. However, a detailed understanding of the theoretical background of alternative methods is needed to identify the optimal analysis strategy and subsequently obtain robust inferences from the data.

References

G. I. Allen, C. Peterson, M. Vannucci, and M. Maletić-Savatić. Regularized partial least squares with an application to NMR spectroscopy. *Statistical Analysis and Data Mining*, 6(4):302–314, Nov. 2012. doi: 10.1002/sam.11169.

M. Barker and W. Rayens. Partial least squares for discrimination. *Journal of Chemometrics*, 17(3):166–173, 2003. doi: 10.1002/cem.785.

R. Bender and S. Lange. Adjusting for multiple testing—when and how? *Journal of Clinical Epidemiology*, 54(4):343–349, Apr. 2001. doi: 10.1016/s0895-4356(00)00314-0.

D. Borcard, F. Gillet, and P. Legendre. *Numerical ecology with R*. Springer, 2011.

C. J. F. T. Braak. Canonical correspondence analysis: A new eigenvector technique for multivariate direct gradient analysis. *Ecology*, 67(5):1167–1179, 1986.

R. G. Brereton and G. R. Lloyd. Partial least squares discriminant analysis: taking the magic away. *Journal of Chemometrics*, 28(4):213–225, 2014. doi: 10.1002/cem.2609.

S. A. Buffington, G. V. D. Prisco, T. A. Auchtung, N. J. Ajami, J. F. Petrosino, and M. Costa-Mattioli. Microbial reconstitution reverses maternal diet-induced social and synaptic deficits in offspring. *Cell*, 165(7):1762–1775, June 2016. doi: 10.1016/j.cell.2016.06.001.

K. S. Button, J. P. A. Ioannidis, C. Mokrysz, B. A. Nosek, J. Flint, E. S. J. Robinson, and M. R. Munafò. Power failure: why small sample size undermines the reliability of neuroscience. *Nature Reviews Neuroscience*, 14(5):365–376, Apr. 2013. doi: 10.1038/nrn3475.

P. D. Cani, R. Bibiloni, C. Knauf, A. Waget, A. M. Neyrinck, N. M. Delzenne, and R. Burcelin. Changes in gut microbiota control metabolic endotoxemia-induced inflammation in high-fat diet-induced obesity and diabetes in mice. *Diabetes*, 57(6):1470–1481, Feb. 2008. doi: 10.2337/db07-1403.

P. D. Cani, S. Possemiers, T. V. de Wiele, Y. Guiot, A. Everard, O. Rottier, L. Geurts, D. Naslain, A. Neyrinck, D. M. Lambert, G. G. Muccioli, and N. M. Delzenne. Changes in gut microbiota control inflammation in obese mice through a mechanism involving GLP-2-driven improvement of gut permeability. *Gut*, 58(8):1091–1103, Feb. 2009. doi: 10.1136/gut.2008.165886.

K.-A. L. Cao, S. Boitard, and P. Besse. Sparse PLS discriminant analysis: biologically relevant feature selection and graphical displays for multiclass problems. *BMC Bioinformatics*, 12(1), June 2011. doi: 10.1186/1471-2105-12-253.

S.-Y. Chen, Z. Feng, and X. Yi. A general introduction to adjustment for multiple comparisons. *Journal of Thoracic Disease*, 9(6):1725–1729, June 2017. doi: 10.21037/jtd.2017.05.34.

C. F. Dormann, J. Elith, S. Bacher, C. Buchmann, G. Carl, G. Carré, J. R. G. Marquéz, B. Gruber, B. Lafourcade, P. J. Leitão, T. Münkemüller, C. McClean, P. E. Osborne, B. Reineking, B. Schröder, A. K. Skidmore, D. Zurell, and S. Lautenbach. Collinearity: a review of methods to deal with it and a simulation study evaluating their performance. *Ecography*, 36(1):27–46, 2013. doi: 10.1111/j.1600-0587.2012.07348.x.

J. J. Faraway. *Extending the linear model with R.* CRC Press, 2016.

A. R. Ferguson, E. D. Stück, and J. L. Nielson. Syndromics: A bioinformatics approach for neurotrauma research. *Translational Stroke Research*, 2(4):438–454, Nov. 2011. doi: 10.1007/s12975-011-0121-1.

A. R. Ferguson, K.-A. Irvine, J. C. Gensel, J. L. Nielson, A. Lin, J. Ly, M. R. Segal, R. R. Ratan, J. C. Bresnahan, and M. S. Beattie. Derivation of multivariate syndromic outcome metrics for consistent testing across multiple models of cervical spinal cord injury in rats. *PLOS ONE*, 8:1–13, 03 2013. doi: 10.1371/journal.pone.0059712.

M. Gschwandtner, P. Filzmoser, C. Croux, and G. Haesbroeck. *rrlda: Robust Regularized Linear Discriminant Analysis*, 2012. URL `https://CRAN.R-project.org/package=rrlda`. R package version 1.1.

Y. Guo, T. Hastie, and R. Tibshirani. Regularized linear discriminant analysis and its application in microarrays. *Biostatistics*, 8(1):86–100, 2006. doi: 10.1093/biostatistics/kxj035.

A. B. Hall, M. Yassour, J. Sauk, A. Garner, X. Jiang, T. Arthur, G. K. Lagoudas, T. Vatanen, N. Fornelos, R. Wilson, M. Bertha, M. Cohen, J. Garber, H. Khalili, D. Gevers, A. N. Ananthakrishnan, S. Kugathasan, E. S. Lander, P. Blainey,

H. Vlamakis, R. J. Xavier, and C. Huttenhower. A novel ruminococcus gnavus clade enriched in inflammatory bowel disease patients. *Genome Medicine*, 9(1), Nov. 2017. doi: 10.1186/s13073-017-0490-5.

M. T. Henke, D. J. Kenny, C. D. Cassilly, H. Vlamakis, R. J. Xavier, and J. Clardy. Ruminococcus gnavus, a member of the human gut microbiome associated with crohn's disease, produces an inflammatory polysaccharide. *Proceedings of the National Academy of Sciences*, 116(26):12672–12677, June 2019. doi: 10.1073/pnas.1904099116.

A. E. Hoerl and R. W. Kennard. Ridge regression: Biased estimation for nonorthogonal problems. *Technometrics*, 42(1):80–86, 2000.

M. Joossens, G. Huys, M. Cnockaert, V. D. Preter, K. Verbeke, P. Rutgeerts, P. Vandamme, and S. Vermeire. Dysbiosis of the faecal microbiota in patients with crohn's disease and their unaffected relatives. *Gut*, 60(5):631–637, Jan. . doi: 10.1136/gut.2010.223263.

P. Legendre and L. Legendre. *Numerical Ecology*. Elsevier, second edition, 2003.

P. Legendre, J. Oksanen, and C. J. F. ter Braak. Testing the significance of canonical axes in redundancy analysis. *Methods in Ecology and Evolution*, 2(3):269–277, 2011. doi: 10.1111/j.2041-210X.2010.00078.x.

M. I. Love, W. Huber, and S. Anders. Moderated estimation of fold change and dispersion for RNA-seq data with DESeq2. *Genome Biology*, 15(12), Dec. 2014. doi: 10.1186/s13059-014-0550-8.

C. Lozupone and R. Knight. UniFrac: a new phylogenetic method for comparing microbial communities. *Applied and Environmental Microbiology*, 71(12):8228–8235, Dec. 2005. doi: 10.1128/aem.71.12.8228-8235.2005.

C. Manzoni, D. A. Kia, J. Vandrovcova, J. Hardy, N. W. Wood, P. A. Lewis, and R. Ferrari. Genome, transcriptome and proteome: the rise of omics data and their integration in biomedical sciences. *Briefings in Bioinformatics*, 19(2):286–302, Nov. 2016. doi: 10.1093/bib/bbw114.

L. Melkumova and S. Shatskikh. Comparing ridge and lasso estimators for data analysis. *Procedia Engineering*, 201:746 – 755, 2017. doi: https://doi.org/10.1016/j.proeng.2017.09.615.

C. Meng, O. A. Zeleznik, G. G. Thallinger, B. Kuster, A. M. Gholami, and A. C. Culhane. Dimension reduction techniques for the integrative analysis of multi-omics

data. *Briefings in Bioinformatics*, 17(4):628–641, 2016. ISSN 1467-5463. doi: 10.1093/bib/bbv108.

X. C. Morgan and C. Huttenhower. Chapter 12: Human microbiome analysis. *PLOS Computational Biology*, 8:1–14, 12 2012. doi: 10.1371/journal.pcbi.1002808.

J. L. Nielson, J. Haefeli, E. A. Salegio, A. W. Liu, C. F. Guandique, E. D. Stück, S. Hawbecker, R. Moseanko, S. C. Strand, S. Zdunowski, J. H. Brock, R. R. Roy, E. S. Rosenzweig, Y. S. Nout-Lomas, G. Courtine, L. A. Havton, O. Steward, V. R. Edgerton, M. H. Tuszynski, M. S. Beattie, J. C. Bresnahan, and A. R. Ferguson. Leveraging biomedical informatics for assessing plasticity and repair in primate spinal cord injury. *Brain Research*, 1619:124–138, Sept. 2015. doi: 10.1016/j.brainres.2014.10.048.

T. Næs and B.-H. Mevik. Understanding the collinearity problem in regression and discriminant analysis. *Journal of Chemometrics*, 15(4):413–426, 2001. doi: 10.1002/cem.676.

J. N. Paulson, O. C. Stine, H. C. Bravo, and M. Pop. Differential abundance analysis for microbial marker-gene surveys. *Nature Methods*, 10(12):1200–1202, Sept. 2013. doi: 10.1038/nmeth.2658.

S. Pavoine, A.-B. Dufour, and D. Chessel. From dissimilarities among species to dissimilarities among communities: a double principal coordinate analysis. *Journal of Theoretical Biology*, 228(4):523 – 537, 2004. ISSN 0022-5193. doi: https://doi.org/10.1016/j.jtbi.2004.02.014.

J. A. Ramey and P. D. Young. A comparison of regularization methods applied to the linear discriminant function with high-dimensional microarray data. *Journal of Statistical Computation and Simulation*, 83(3):581–596, 2013. doi: 10.1080/00949655.2011.625946.

M. Ringnér. What is principal component analysis? *Nature Biotechnology*, 26(3):303–304, Mar. 2008. doi: 10.1038/nbt0308-303.

N. Segata, J. Izard, L. Waldron, D. Gevers, L. Miropolsky, W. S. Garrett, and C. Huttenhower. Metagenomic biomarker discovery and explanation. *Genome Biology*, 12(6):R60, 2011. doi: 10.1186/gb-2011-12-6-r60.

E. S. Sena, H. B. van der Worp, P. M. W. Bath, D. W. Howells, and M. R. Macleod. Publication bias in reports of animal stroke studies leads to major overstatement of efficacy. *PLoS Biology*, 8(3):e1000344, Mar. 2010. doi: 10.1371/journal.pbio.1000344.

H. Shen and J. Z. Huang. Sparse principal component analysis via regularized low rank matrix approximation. *Journal of Multivariate Analysis*, 99(6):1015 – 1034, 2008. ISSN 0047-259X. doi: https://doi.org/10.1016/j.jmva.2007.06.007.

B. G. Tabachnik and L. S. Fidell. *Using multivariate statistics*. Pearson Education Ltd., sixth edition, 2014.

R. Tibshirani. Regression shrinkage and selection via the lasso. *Journal of the Royal Statistical Society. Series B (Methodological)*, 58(1):267–288, 1996.

P. J. Turnbaugh, R. E. Ley, M. A. Mahowald, V. Magrini, E. R. Mardis, and J. I. Gordon. An obesity-associated gut microbiome with increased capacity for energy harvest. *Nature*, 444(7122):1027–1031, Dec. 2006. doi: 10.1038/nature05414.

M. M. Unger, J. Spiegel, K.-U. Dillmann, D. Grundmann, H. Philippeit, J. Bürmann, K. Faßbender, A. Schwiertz, and K.-H. Schäfer. Short chain fatty acids and gut microbiota differ between patients with parkinson's disease and age-matched controls. *Parkinsonism & Related Disorders*, 32:66–72, Nov. 2016. doi: 10.1016/j.parkreldis.2016.08.019.

N. M. Vogt, R. L. Kerby, K. A. Dill-McFarland, S. J. Harding, A. P. Merluzzi, S. C. Johnson, C. M. Carlsson, S. Asthana, H. Zetterberg, K. Blennow, B. B. Bendlin, and F. E. Rey. Gut microbiome alterations in alzheimer's disease. *Scientific Reports*, 7(1), Oct. 2017. doi: 10.1038/s41598-017-13601-y.

S. Weiss, Z. Z. Xu, S. Peddada, A. Amir, K. Bittinger, A. Gonzalez, C. Lozupone, J. R. Zaneveld, Y. Vázquez-Baeza, A. Birmingham, E. R. Hyde, and R. Knight. Normalization and microbial differential abundance strategies depend upon data characteristics. *Microbiome*, 5(1), Mar. 2017. doi: 10.1186/s40168-017-0237-y.

Z.-Q. Zhuang, L.-L. Shen, W.-W. Li, X. Fu, F. Zeng, L. Gui, Y. Lü, M. Cai, C. Zhu, Y.-L. Tan, and et al. Gut microbiota is altered in patients with alzheimer's disease. *Journal of Alzheimer's Disease*, 63(4):1337–1346, May 2018. ISSN 1387-2877. doi: 10.3233/JAD-180176.

Appendices

4.1 List of abbreviations

5xFAD	Alzheimer's disease genetic mouse model
ALA	α-Linolenic acid
ANOVA	Analysis of variance
CA	Correspondence analysis
CAP	Constrained analysis of principal coordinates
CCA	Canonical correspondence analysis
DA	Discriminant analysis
DCA	Detrended correspondence analysis
DCCA	Detrended canonical correspondence analysis
dbRDA	Distance-based redundancy analysis
LDA	Linear discriminant analysis
LEfSe	Linear discriminant analysis effect size
MANOVA	Multivariate analysis of variance
MDS	Multidimensional scaling
NMDS	Non-metric multidimensional scaling
PCA	Principal component analysis
PCoA	Principal coordinate analysis
PLS-DA	Partial least squares discriminant analysis
RDA	Redundancy analysis

4.2 Contributions to individual publications

The contributions to individual publications are given in percent from all authors' contributions according to the CRediT Taxonomy

Contributor role	**Publication 1**	**Publication 2**	**Publication 3**	**Publication 4**
Conceptualization: Ideas; formulation or evolution of overarching research goals and aims.	80	90	40	20
Data curation: Management activities to annotate (produce metadata), scrub data and maintain research data (including software code, where it is necessary for interpreting the data itself) for initial use and later re-use.	100	100	50	50
Formal analysis: Application of statistical, mathematical, computational, or other formal techniques to analyze or synthesize study data.	100	100	80	70
Funding acquisition: Acquisition of the financial support for the project leading to this publication.	0	0	0	0
Investigation: Conducting a research and investigation process, specifically performing the experiments, or data/evidence collection.	90	100	0	0
Methodology: Development or design of methodology; creation of models.	100	100	60	50
Project administration: Management and coordination responsibility for the research activity planning and execution.	80	80	30	30
Resources: Provision of study materials, reagents, materials, patients, laboratory samples, animals, instrumentation, computing resources, or other analysis tools.	0	0	0	0

Software: Programming, software development; designing computer programs; implementation of the computer code and supporting algorithms; testing of existing code components.	100	100	90	80
Supervision: Oversight and leadership responsibility for the research activity planning and execution, including mentorship external to the core team.	0	0	0	0
Validation: Verification, whether as a part of the activity or separate, of the overall replication/reproducibility of results/experiments and other research outputs.	90	100	20	20
Visualization: Preparation, creation and/or presentation of the published work, specifically visualization/data presentation.	90	100	90	60
Writing - original draft: Preparation, creation and/or presentation of the published work, specifically writing the initial draft (including substantive translation).	100	100	70	50
Writing - review & editing: Preparation, creation and/or presentation of the published work by those from the original research group, specifically critical review, commentary or revision - including pre- or post-publication stages.	60	80	50	25